

**DEVELOPMENT OF DIAGNOSTIC AND THERAPEUTIC
RADIOTRACERS FOR TARGETING TUMORS USING
DIFFERENT APPROACHES**

By

MOHINI GULERIA

CHEM01201004013

Bhabha Atomic Research Centre, Mumbai

*A thesis submitted to the
Board of Studies in Chemical Sciences*

*In partial fulfillment of requirements
for the Degree of*

DOCTOR OF PHILOSOPHY

of

HOMI BHABHA NATIONAL INSTITUTE



August, 2015

Homi Bhabha National Institute

Recommendations of the Viva Voce Committee

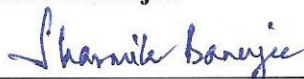
As members of the Viva Voce Committee, we certify that we have read the dissertation prepared by **Mohini Guleria** entitled “Development of diagnostic and therapeutic radiotracers for targeting tumors using different approaches” and recommend that it may be accepted as fulfilling the thesis requirement for the award of Degree of Doctor of Philosophy.

Chairman – Dr. K. L. Ramakumar



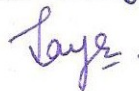
Date: 04/2/16

Guide/Convener – Dr. (Smt.) Sharmila Banerjee



Date: 5/4/2016

External Examiner – Dr. Jaya Shukla



Date: 5.4.2016

Member 1 – Dr. S. K. Nayak



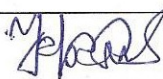
Date: 5-4-2016
5.4.16

Member 2 – Dr. S. Kannan



Date:

Member 3 – Dr. Tapas Das




Date: 05.04.2016

Final approval and acceptance of this thesis is contingent upon the candidate's submission of the final copies of the thesis to HBNI.

I/We hereby certify that I/we have read this thesis prepared under my/our direction and recommend that it may be accepted as fulfilling the thesis requirement.

Date: April 5, 2016

Place: BARC


Dr. (Smt.) Sharmila Banerjee
(Guide)

STATEMENT BY AUTHOR

This dissertation has been submitted in partial fulfillment of requirements for an advanced degree at Homi Bhabha National Institute (HBNI) and is deposited in the Library to be made available to borrowers under rules of the HBNI.

Brief quotations from this dissertation are allowable without special permission, provided that accurate acknowledgement of source is made. Requests for permission for extended quotation from or reproduction of this manuscript in whole or in part may be granted by the Competent Authority of HBNI when in his or her judgment the proposed use of the material is in the interests of scholarship. In all other instances, however, permission must be obtained from the author.

Mohini Guleria

DECLARATION

I, hereby declare that the investigation presented in the thesis has been carried out by me.

The work is original and has not been submitted earlier as a whole or in part for a degree/diploma at this or any other Institution / University.

Mohini Guleria

List of Publications arising from the thesis

Journal

1. Synthesis and bio-evaluation of a ^{177}Lu -labeled unsymmetrical cationic porphyrin derivative as a tumor targeting agent. **Mohini Guleria**, Tapas Das, Haladhar Dev Sarma, Sharmila Banerjee. *Journal of Radioanalytical and Nuclear Chemistry*, 307, 1537-1544 (2016).
2. Neutral $^{99\text{m}}\text{Tc}(\text{CO})_3$ complexes of “clicked” nitroimidazoles for the detection of tumor hypoxia. **Mohini Bhadwal**, Madhava B Mallia, Haladhar Dev Sarma, Sharmila Banerjee. *Journal of Radioanalytical and Nuclear Chemistry*, 307, 69-77 (2016).
3. Radiosynthesis and bioevaluation of ^{68}Ga -labeled 5,10,15,20-tetra(4-methylpyridyl)-porphyrin for possible application as a PET Radiotracer for tumor imaging. **Mohini Bhadwal**, Tapas Das, Haladhar Dev Sarma, Sharmila Banerjee. *Molecular Imaging and Biology*, 17, 111-118 (2015).
4. Synthesis and biological evaluation of ^{177}Lu -DOTA-porphyrin conjugate as a potential agent for targeted tumor radiotherapy. **Mohini Bhadwal**, Sweety Mittal, Tapas Das, Haladhar Dev Sarma, Sudipta Chakraborty, Sharmila Banerjee, M. R. A. Pillai. *Quarterly Journal of Nuclear Medicine and Molecular Imaging*, 58, 224-233 (2014).
5. Synthesis and bioevaluation of a $^{99\text{m}}\text{Tc}$ labeled cyclic RGD peptide derivative using $[\text{}^{99\text{m}}\text{TcN}]^{+2}$ core: A novel concept of synthesizing a potential radiotracer for tumor imaging. Sweety Mittal, **Mohini Bhadwal**, Sudipta Chakraborty, Haladhar Dev Sarma, Sharmila Banerjee. *Bioorganic and Medicinal Chemistry Letters*, 23, 1808–1812 (2013).
6. Synthesis and biological evaluation of ^{90}Y labeled porphyrin-DOTA conjugate for targeted tumor therapy. Sweety Mittal, **Mohini Bhadwal**, Tapas Das, Haladhar Dev Sarma, Rubel Chakravarty, Ashutosh Dash, Sharmila Banerjee, M. R. A. Pillai. *Cancer Biotherapy and Radiopharmaceuticals*, 28, 651-656 (2013).

Others

1. Preparation of $^{99m}\text{Tc}(\text{CO})_3$ -carboxymethylthioethyl iminodiacetic acid and evaluation as a potential renal imaging agent. **Mohini Bhadwal**, Drishty Satpati, Sweetly Singhal, Haladhar Dev Sarma, Meera Venkatesh, Sharmila Banerjee. *Current Radiopharmaceuticals*, 5, 65-70 (2012).
2. Preparation of DOTA-TATE and DOTA-NOC freeze-dried kits for formulation of patient doses of ^{177}Lu -labeled agents and their comparison for peptide receptor radionuclide therapy application. Tapas Das, **Mohini Bhadwal**, Sharmila Banerjee, Haladhar Dev Sarma, Ajit Shinto, K.K. Kamaleshwaran. *Journal of Radioanalytical and Nuclear Chemistry*, 299, 1389–1398 (2014).
3. Formulation and radiochemical evaluation of a freeze-dried mixed peptide kit for the preparation of ^{68}Ga -labeled peptides for PET imaging of somatostatin receptor positive neuroendocrine cancers. Tapas Das, **Mohini Bhadwal**, Haladhar Dev Sarma, Sharmila Banerjee. *Journal of Radioanalytical and Nuclear Chemistry*, 302, 1259-1264 (2014).
4. Preparation and bioevaluation of $[^{99m}\text{TcN}]^{2+}$ -labeled tetrameric complex of E-c(RGDfK)₂ as a radiotracer for imaging $\alpha v \beta 3$ integrins in tumors. **Mohini Guleria**, Subhajit Ghosh, Tapas Das, Haladhar Dev Sarma, Sharmila Banerjee. *Journal of Radioanalytical and Nuclear Chemistry*, DOI: 10.1007/s10967-015-4680-6 (2016).
5. Clinical translation of ^{177}Lu -labeled PSMA-617: Initial experience in prostate cancer patients. Tapas Das, **Mohini Guleria**, Anil Parab, Chanchala Kale, Hina J Shah, Haladhar Dev Sarma, Vikram R Lele, Sharmila Banerjee. *Nuclear Medicine and Biology*, DOI: 10.1016/j.nucmedbio.2016.02.002

Mohini Guleria

DEDICATIONS

To my respected Teachers and loving Parents.....

ACKNOWLEDGEMENTS

At the outset, I wish to express my deepest and sincere gratitude to my guide, Dr. (Smt.) Sharmila Banerjee, Head, Radiopharmaceuticals Chemistry Section for her invaluable guidance, constant encouragement and persistent motivation. Her wide knowledge and logical way of thinking and reasoning on scientific problems greatly helped me during the course of work. I am thankful to her for sharing her knowledge and scientific understanding during the fruitful discussions with me throughout the work.

I am privileged to thank Dr. Tapas Das, my immediate superior, for his unstinted support and encouragement. His advice and comments have been priceless and played a significant role in documenting my experimental work.

I am grateful to my colleague Dr. (Smt.) Drishti Satpati, with whom I started my first scientific endeavor after joining BARC, for sharing her work experience and scientific knowledge with me.

I take this opportunity to express my sincere regards and deepest appreciation to Dr. Madhava B. Mallia. His invaluable constructive criticisms and suggestions on academic level have always been extremely helpful to me.

It gives me a great pleasure to acknowledge to Dr. Haladhar D. Sarma, Head, Experimental Animal Facility and Radioisotope Laboratory, Radiation Biology and Health Sciences Division for his kind help in carrying out biological evaluations of the compounds reported in this thesis.

I would take this opportunity to thank the respected members of my doctoral committee Dr. K. L. Ramakumar (Chairman), Dr. S. K. Nayak (member), Dr. S. Kannan (member) and Dr. Tapas Das (member) for their critical reviews and invaluable suggestions during the annual progress reviews and pre-synopsis presentation.

I would also like to thank my colleague Dr. (Smt.) Sweety Mittal, for sharing her experimental expertise and scientific knowledge with me.

I am thankful to Dr. Chandan Kumar and colleagues from RPES, IP&AD for carrying out in-vitro cell binding studies for radiolabeled antibody conjugates.

I would also like to thank my colleagues of Isotope Production and Applications Division for regularly supplying ^{99}Mo and ^{177}Lu activity for carrying out the radiolabeling studies reported in this thesis.

My sincere thanks are due to all of my colleagues from Radiopharmaceuticals Chemistry Section for their help, suggestion and encouragement. I sincerely acknowledge all my colleagues from Isotope Production and Applications Division for their help and support. I am thankful to all my friends for their encouragement and support. I greatly value their friendship and deeply appreciate their belief in me.

It is my pleasant duty to acknowledge the help and technical assistance received from Mr. Umesh Kumar and Mr. G. Gandhale throughout the course of work.

I would like to express my sincere gratitude to Dr. K. L. Ramakumar once again for his constant support and encouragement as Director, Radiochemistry and Isotope Group (RC&IG).

I cannot imagine my current position without the blessings of my teachers and will always be indebted to them.

Most importantly, I owe my heartfelt gratitude to my parents for their constant encouragement, care and never fading love. Their blessings and good wishes have helped me to achieve what I am today.

Finally, I would like to express my endless thanks and appreciations to my husband for his support and care.

August, 2015

Mohini Guleria

RPhCS, BARC, Mumbai

CONTENTS

	Page No.
SYNOPSIS	xvii
LIST OF FIGURES	xxx
LIST OF TABLES	xxxiv
Chapter 1: General introduction	
1.1 Nuclear medicine	3
1.2. Molecular imaging	5
1.3. Radiopharmaceuticals	6
1.3.1. Diagnostic radiopharmaceuticals	7
1.3.1.1. SPECT (single photon emission computed tomography)	7
1.3.1.2. PET (positron emission tomography)	8
1.3.2. Therapeutic radiopharmaceuticals	9
1.4. Radiopharmaceutical design	11
1.5. Tumor targeting mechanism	12
1.6. Brief overview of radioisotopes used in the present work	14
1.6.1. Technetium-99m	14
1.6.1.1. [^{99m} TcN] ²⁺ core	16
1.6.1.2. [^{99m} Tc(CO) ₃ (H ₂ O) ₃] ⁺ core	17
1.6.2. Gallium-68	18
1.6.3. Yttrium-90	20
1.6.4. Lutetium-177	22
1.7. Biomolecules used in the present work	23
1.8. BFCA (bi-functional chelating agent)	24
1.9. Quality control of radiotracers	25
1.9.1. Physicochemical tests	26
1.9.1.1. Chemical purity	26
1.9.1.1.1. Spectral techniques used for characterization of unlabeled precursors	27

1.9.1.2. Radionuclidic purity	27
1.9.1.3. Radiochemical purity	27
1.9.1.3.1. Determination of radiochemical purity of $[^{99m}\text{Tc}(\text{CO})_3]^+$, $[^{99m}\text{TcN}]^{2+}$ and various ^{177}Lu , ^{90}Y , ^{68}Ga and $[^{99m}\text{Tc}(\text{CO})_3]^+$, $[^{99m}\text{TcN}]^{2+}$, ^{177}Lu , ^{90}Y and ^{68}Ga complexes	28
1.9.2. Biological quality control tests	29
1.9.2.1. Serum stability and binding studies	29
1.9.2.2. Biological evaluation in animal models	30
1.10. Determination of partition coefficient ($\text{LogP}_{o/w}$) of radiolabeled complexes	31
1.11. Radioactive counting	31
1.12. Work carried out in the present thesis	32
Chapter 2: Preparation of radiolabeled (^{68}Ga, ^{177}Lu and ^{90}Y) porphyrin derivatives for targeting tumor	
2.1. Introduction	35
2.2. Preparation and preliminary bio-evaluation of $^{177}\text{Lu}/^{90}\text{Y}$ -labeled- <i>p</i> -NCS-benzyl-DOTA coupled 5-(<i>p</i> -aminopropyleneoxyphenyl)-10,15,20-tri(<i>p</i> -carboxymethyleneoxyphenyl)porphyrin	39
2.2.1. Experimental	41
2.2.1.1. Materials and methods	41
2.2.1.2. Production of ^{177}Lu	41
2.2.1.3. Source of ^{90}Y	42
2.2.1.4. Synthesis	43
2.2.1.5. Radiolabeling of compound 2f with ^{177}Lu and ^{90}Y	47
2.2.1.6. Quality control studies	48
2.2.1.7. Stability studies	48
2.2.1.8. Biodistribution studies	48
2.2.1.9. Scintigraphy studies	49
2.2.2. Results and discussion	50

2.2.2.1. Production of ^{177}Lu	50
2.2.2.2. Production of ^{90}Y	50
2.2.2.3. Synthesis of 5-(<i>p</i> -aminopropyleneoxyphenyl)-10,15,20-tri(<i>p</i> -carboxymethyleneoxyphenyl)porphyrin and porphyrin- <i>p</i> -NCS-benzyl-DOTA conjugate	50
2.2.2.4. Radiolabeling of porphyrin- <i>p</i> -NCS-benzyl-DOTA conjugate with ^{177}Lu	54
2.2.2.5. <i>In-vitro</i> stability studies	57
2.2.2.6. Biodistribution studies	57
2.2.2.7. Scintigraphy studies	60
2.2.3. Conclusions	61
2.3. Radiosynthesis and bioevaluation of ^{68}Ga -labeled 5,10,15,20-tetra(4-methylpyridyl)porphyrin for possible application as a PET radiotracer for tumor imaging	62
2.3.1. Experimental	64
2.3.1.1. Materials and methods	64
2.3.1.2. Synthesis	65
2.3.1.3. Elution and purification of ^{68}Ga	67
2.3.1.4. Preparation of ^{68}Ga -labeled 5,10,15,20-tetra(4-methylpyridyl)porphyrin	68
2.3.1.5. Characterization of ^{68}Ga -labeled 5,10,15,20-tetra(4-methylpyridyl)porphyrin	68
2.3.1.6. Preparation of ^{68}Ga -labeled 5,10,15,20-tetra(4-methylpyridyl)porphyrin (2k)	69
2.3.1.7. Determination of partition coefficient ($\text{LogP}_{\text{o/w}}$) of ^{68}Ga -labeled 5,10,15,20-tetra(4-methylpyridyl)porphyrin	69
2.3.1.8. Stability of ^{68}Ga -labeled 5,10,15,20-tetra(4-methylpyridyl)porphyrin	70
2.3.1.9. Biodistribution studies	70

2.3.2. Results and discussion	70
2.3.2.1. Synthesis and characterization of 5,10,15,20-tetra(4-methylpyridyl)porphyrin (2j)	70
2.3.2.2. Preparation and characterization of ⁶⁸Ga-labeled 5,10,15,20-tetra(4-methylpyridyl)porphyrin	72
2.3.2.3. Preparation and characterization of Ga-labeled 5,10,15,20-tetra(4-methylpyridyl)porphyrin (2k)	74
2.3.2.4. Stability of ⁶⁸Ga-labeled 5,10,15,20-tetra(4-methylpyridyl)porphyrin	75
2.3.2.5. Determination of partition coefficient (LogP_{o/w}) of ⁶⁸Ga-labeled 5,10,15,20-tetra(4-methylpyridyl)porphyrin	76
2.3.2.6. Biological studies	76
2.3.3. Conclusions	79
2.4. Synthesis and bio-evaluation of a ¹⁷⁷Lu-labeled unsymmetrical cationic porphyrin derivative as a tumor targeting agent	79
2.4.1. Experimental	80
2.4.1.1. Materials and methods	80
2.4.1.2. Synthesis	81
2.4.1.3. Radiolabeling of UPTMPyA-<i>p</i>-NH₂-benzyl-DOTA with ¹⁷⁷LuCl₃	84
2.4.1.4. Characterization of ¹⁷⁷Lu-labeled UPTMPyA-<i>p</i>-NH₂-benzyl-DOTA complex	84
2.4.1.5. Preparation of Lu complex of UPTMPyA-<i>p</i>-NH₂-benzyl-DOTA	85
2.4.1.6. Determination of partition coefficient (LogP_{o/w})	85
2.4.1.7. <i>In-vitro</i> serum binding and stability studies	85
2.4.1.8. Biodistribution studies	85
2.4.2. Results and discussion	86
2.4.2.1. Production of ¹⁷⁷Lu	86

2.4.2.2. Synthesis and characterization of 5-carboxymethyleneoxyphenyl-10,15,20-tri(<i>p</i> -N-methylpyridyl)porphyrin	86
2.4.2.3. Radiolabeling of porphyrin- <i>p</i> -NH ₂ -benzyl-DOTA with ¹⁷⁷ LuCl ₃	89
2.4.2.4. Preparation of Lu complex of UPTMPyA- <i>p</i> -NH ₂ -benzyl-DOTA	90
2.4.2.5. Determination of partition coefficient (LogP _{o/w})	92
2.4.2.6. Determination of <i>in-vitro</i> serum binding and stability studies	92
2.4.2.7. Biodistribution studies	92
2.4.3. Conclusions	94

Chapter 3: Preparation of radiolabeled monoclonal antibodies and peptides as receptor specific tumor targeting agents

3(a) Preparation of ¹⁷⁷ Lu-labeled monoclonal antibodies rituximab and trastuzumab and their preclinical evaluation	97
3a.1. Antibodies	98
3a.2. Immunotherapy and radioimmunotherapy	104
3a.3. Experimental	104
3a.3.1. Material and methods	105
3a.3.2. Preparation of ¹⁷⁷ Lu-labeled-Rituximab and Trastuzumab	105
3a.3.2.1. Preparation and purification of <i>p</i> -NCS-benzyl-DOTA coupled IgG	106
3a.3.2.2. Preparation of <i>p</i> -NCS-benzyl-DOTA-Rituximab	106
3a.3.2.3. Preparation of <i>p</i> -NCS-benzyl-Trastuzumab	106
3a.3.2.4. Radiolabeling of <i>p</i> -NCS-benzyl-DOTA-IgG conjugate	106
3a.3.2.5. Radiolabeling of <i>p</i> -NCS-benzyl-DOTA-Rituximab	107
3a.3.2.6. Radiolabeling of <i>p</i> -NCS-benzyl-DOTA-Trastuzumab	107
3a.3.2.7. Determination of average number of BFCAs attached per antibody molecule	107
3a.3.3. Quality control	108

3a.3.4. <i>In vitro</i> stability studies	108
3a.3.5. <i>In vitro</i> cell binding studies	108
3a.3.6. Biodistribution studies	108
3a.4. Results and discussion	109
3a.4.1. Preparation of ¹⁷⁷Lu-labeled-<i>p</i>-NCS-benzyl-DOTA-Rituximab and ¹⁷⁷Lu-labeled-<i>p</i>-NCS-benzyl-DOTA-Trastuzumab	109
3a.4.2. Determination of average number of BFCAs per antibody molecule	111
3a.4.3. <i>In vitro</i> stability studies	111
3a.4.4. <i>In vitro</i> cell binding studies	111
3a.4.5. Biodistribution studies	112
3a.5. Conclusions	114
3(b) Preparation of ^{99m}TcN-labeled RGD derivative for tumor imaging	115
3b.1. Peptides and radionuclidic imaging of tumors	115
3b.2. $\alpha_v\beta_3$ integrin receptors as angiogenesis marker	116
3b.3. Radiolabeled RGDs for imaging $\alpha_v\beta_3$ overexpression	118
3b.4. Experimental	120
3b.4.1. Materials and method	120
3b.4.2. Synthesis of dithiocarbamate derivative of RGD monomer	121
3b.4.3. Radiolabeling studies	122
3b.4.3.1. Preparation of the [^{99m}TcN]²⁺ core	123
3b.4.3.2. Preparation of ^{99m}TcN-[G₃-c(RGDfK)]₂	123
3b.4.4. Quality control techniques	124
3b.4.5. Determination of partition coefficient (Log P_{o/w})	125
3b.4.6. Stability studies	125
3b.4.7. Biological studies	126
3b.5. Results and discussion	127
3b.5.1. Synthesis and characterization	127
3b.5.2. Radiochemistry	127
3b.5.3. <i>In vitro</i> stability studies	128

3b.5.4. Biological studies	128
3b.6. Conclusions	132
 Chapter 4: Preparation of neutral $^{99m}\text{Tc}(\text{CO}_3\text{-complexes})$ of “clicked”nitroimidazole ligands for imaging of tumor hypoxia	
4.1. Introduction	137
4.1.1. Hypoxia	137
4.1.2. Nitroimidazoles as the targeting vectors for tumor hypoxia	139
4.1.3. Radiopharmaceuticals for hypoxia	140
4.1.4. Choice of ^{99m}Tc as the radioisotope	141
4.2. Experimental	144
4.2.1. Materials and methods	144
4.2.2. Synthesis	145
4.2.2.1. Synthesis of 1-(3-bromopropyl)-2-nitro-1H-imidazole (4a)	145
4.2.2.2. Synthesis of 1-(3-bromopropyl)-4-nitro-1H-imidazole and 1-(3-bromopropyl)-5-nitro-1H-imidazole (4b & 4c)	145
4.2.2.3. General procedure for synthesis of nitroimidazole azides	146
4.2.2.4. Synthesis of 1-(3-azidopropyl)-2-nitro-1H-imidazole (4d)	147
4.2.2.5. Synthesis of 1-(3-azidopropyl)-4-nitro-1H-imidazole (4e)	147
4.2.2.6. Synthesis of 1-(3-azidopropyl)-5-nitro-1H-imidazole (4f)	147
4.2.2.7. General procedure for synthesis of triazole from azide	148
4.2.2.8. Synthesis of 2-amino-3-(1-(3-(2-nitro-1H-imidazol-1-yl)propyl)-1H-1,2,3-triazol-4-yl)propanoic acid (4g)	148
4.2.2.9. Synthesis of 2-amino-3-(1-(3-(4-nitro-1H-imidazol-1-yl)propyl)-1H-1,2,3-triazol-4-yl)propanoic acid (4h)	148
4.2.2.10. Synthesis of 2-amino-3-(1-(3-(5-nitro-1H-imidazol-1-yl)propyl)-1H-1,2,3-triazol-4-yl)propanoic acid (4i)	149
4.2.2.11. Preparation of 4-nitroimidazole-triazole-Re(CO)₃ complex (4m)	149
4.2.3. Radiolabeling	153

4.2.3.1. Preparation of [$^{99\text{m}}\text{Tc}(\text{CO})_3(\text{H}_2\text{O})_3$] $^+$ precursor complex	153
4.2.3.2. General procedure for the radiolabeling of nitroimidazole triazole derivatives (4g , 4h & 4i) with [$^{99\text{m}}\text{Tc}(\text{CO})_3(\text{H}_2\text{O})_3$] $^+$ precursor to prepare $^{99\text{m}}\text{Tc}(\text{CO})_3$ complexes of 2-, 4- and 5-nitroimidazoles (4j , 4k , 4l)	154
4.2.4. Quality control	154
4.2.4.1. HPLC	154
4.2.4.2. Determination of octanol-water partition coefficient (Log $P_{\text{o/w}}$)	155
4.2.4.3. In vitro serum stability and protein binding studies	155
4.2.5. Biological studies	155
4.2.6. Statistical analysis	156
4.3. Results and discussion	157
4.4. Conclusions	166
Summary	171
References	179

Synopsis

Cancer is one of the most dreaded challenges in modern medical science. Diagnosis and treatment of this disease at early stages is of utmost importance for a positive outcome of the treatment regime [1]. A variety of techniques both independent as well as in combination with other modalities are essential for early detection as well as for the treatment of cancer. Of the various modalities employed, chemotherapy, surgery, radionuclidic therapy, radiation therapy, photodynamic therapy etc. are the predominantly used ones for the treatment of cancer [2,4]. On the other hand, MRI (magnetic resonance imaging), CT (computed tomography), radionuclidic imaging etc. are the major ones used for the diagnosis [3,5]. In recent years, imaging and therapy of cancers involving systemic administration of radiolabeled agents viz. radiopharmaceuticals have not only gained eminence worldwide, but has become the only modality in some specific cases of cancer management [6-8]. As a result, research in the area of molecular imaging and therapy involving radiolabeled agents is on the increase, leading to introduction of newer agents for a variety of applications in nuclear medicine. Radiopharmaceuticals are radiolabeled drugs or molecules with a constant composition and can be administered either orally or intravenously with adequate safety, for the purpose of carrying out diagnosis or treatment of a diseased condition, particularly of cancerous origin.

Radiopharmaceuticals can be broadly categorized as diagnostic and therapeutic radiopharmaceuticals depending upon the selection of radionuclide used. The nuclear decay characteristics of the radionuclides determine whether they can be categorized as diagnostic or therapeutic ones. Diagnostic radionuclides are those which exhibit gamma

(γ) photons or positron (β^+) emission whereas therapeutic radionuclides are generally particulate emitters and emit particulate radiation viz. alpha (α), beta (β^-), Auger electron and conversion electron. In both diagnosis and therapy employing radiopharmaceuticals, one of the most important criteria which govern the success of the modality is the ability to accurately target the tumor lesions/cancer site with the radiolabeled agent, while sparing the major vital organs.

The targeting of radiopharmaceuticals to a tumor lesion can be achieved via various pathways. While targeting the cancer site, the carrier molecules which serve as molecular vectors in the radiolabeled agents, need to be carefully chosen. The tumors to be targeted are of varied origin and have different characteristic features such as specific receptor over expression, hypoxic condition etc. which are guiding factors towards the choice of the carrier molecules in the radiolabeled agent. Accordingly the targeting approaches or methodologies also differ. An example to illustrate this is the well known modality of peptide receptor radionuclide therapy (PRRT) wherein, tumors which have over expression of somatostatin receptors on their surface can be targeted using peptide based ligands, radiolabeled with an appropriate radionuclide. The other strategies that can be envisaged are by using antigen receptor specific antibodies and also molecules with inherent avidity for localization in tumor. In the present thesis, an attempt has been made to design radiolabeled molecular vectors with unique properties and potential for specific targeting of different types of tumors. The thesis is divided into four chapters. The contents of each chapter are briefly outlined below.

CHAPTER 1: INTRODUCTION

This chapter gives a brief overview of radiopharmaceuticals and their usage in nuclear medicine. General methods of production of radioisotopes with their advantages and disadvantages are described with an emphasis on the generator-produced radioisotopes viz. ^{99m}Tc , ^{68}Ga , ^{90}Y and reactor produced isotope viz. ^{177}Lu which are used in the present work described in the subsequent chapters. The coinage of the term “radiopharmaceutical” along with its usage is given. Radiopharmaceuticals have been classified according to their medical applications as ‘diagnostic’ and ‘therapeutic’ and ‘target-specific’ on the basis of their biodistribution. The physical properties and nuclear decay characteristics of the radionuclide, which govern its use in preparation of either diagnostic or therapeutic radiopharmaceuticals, have been dealt with. The purpose and criterion for choosing a radionuclide for designing of these radiopharmaceuticals are listed. Amongst the therapeutic radionuclides, the physical and nuclear properties of Lutetium-177 and Yttrium-90, which have been used in the preparation of therapeutic agents, have been provided. The administration of radiopharmaceuticals in the human body requires high purity and therefore, various physiochemical and biological parameters to be tested for proper quality control are described. Brief descriptions of the various mechanisms by which radiopharmaceuticals are metabolized in the body have been presented. The pathways of targeting the radiolabeled agent to the tumor site are varied. These considerations which provide the necessary guidelines in designing a radiopharmaceutical are discussed in this chapter. An introduction to bi-functional chelating agents (BFCA), their importance in preparation of stable radiometal complexes

as well as their role in improving the pharmacokinetic behaviour of resultant radiopharmaceutical has also been discussed. Radiolabeling methodologies for preparation of ^{99m}Tc -labeled radiotracers and the advantages of using preformed ^{99m}Tc cores/radiosynthons viz. $[\text{}^{99m}\text{TcN}]^{2+}$, $[\text{}^{99m}\text{Tc}(\text{CO})_3]^+$ etc. are discussed briefly whereas necessity for using substituted macrocyclic ligands as BFCA for achieving radiolabeling with radiolanthanides viz. ^{177}Lu and ^{90}Y has also been described in this chapter.

CHAPTER 2: PREPARATION OF RADIOLABELED (^{68}Ga , ^{177}Lu AND ^{90}Y) PORPHYRIN DERIVATIVES FOR TARGETING TUMOR

Porphyrin and its derivatives exhibit inherent affinity for localization in tumors [9-12]. This property provides the insight in envisaging radiolabeled porphyrins as molecular vectors to target the radioisotope to the tumor site. Depending on the nuclear decay characteristics of the radioisotope, the radiolabeled tracer can either act as a potential imaging agent for diagnostic application or can deliver the particulate radiation to the tumor site as a therapeutic agent. The macrocyclic tetrapyrrolic ring of the porphyrin is lipophilic which leads to their accumulation in non-target organs viz. liver, GIT etc. Various mechanisms which govern the uptake of porphyrins in tumor lesions have been discussed briefly in this chapter. It has been reported that substituents on the meso- and the peripheral positions of the porphyrin ring drastically change its physical, chemical, and biological properties. Therefore, careful selection of the peripheral substituents of the porphyrin is of importance for selective tumor targeting, while sparing the non-target tissues.

Taking this fact into account, an attempt was made to synthesize three different porphyrin derivatives with variable lipophilicities (c/o LogP_{o/w}). The first one is a novel, unsymmetrically substituted water soluble porphyrin viz. 5-(*p*-aminopropyleneoxyphenyl)-10,15,20-tris(*p*-carboxymethyleneoxyphenyl)porphyrin (**I**). Radiolabeling of this porphyrin derivative with radiolanthanides viz. ¹⁷⁷Lu and ⁹⁰Y was attempted via macrocyclic bifunctional chelating agent (BFCA) namely, *p*-NCS-benzyl-DOTA (*p*-isothiocyanatobenzyl-1,4,7,10-tetraazacyclododecane-1,4,7,10-tetraacetic acid) in the peripheral position of the porphyrin derivative (Fig. 1). It is pertinent to note that direct radiolabeling in the porphyrin core is not feasible while envisaging the radiolanthanides ¹⁷⁷Lu⁺³ and ⁹⁰Y⁺³ due to the mismatch of the porphyrin core size and that of the ionic radii of these radiometals. The nuclear decay characteristics of ¹⁷⁷Lu and ⁹⁰Y as well as their potential as therapeutic isotopes in tumor therapy have been discussed in this chapter. The porphyrin-*p*-NCS-benzyl-DOTA conjugate (**II**) was radiolabeled with ⁹⁰Y as well as ¹⁷⁷Lu in good radiolabeling yield. Biodistribution studies performed in Swiss mice bearing fibrosarcoma tumors revealed high tumor uptake. The complexes exhibited favorable tumor to blood and tumor to muscle ratios at various post-administration time points. Scintigraphic imaging studies performed in Swiss mice bearing fibrosarcoma tumors after intravenous administration of ¹⁷⁷Lu-labeled-compound **II** also corroborated the results obtained in biodistribution studies indicating the selective accumulation of activity in the tumor.

The modulation of lipophilicity of the porphyrin derivative has been addressed either by the use of hydrophilic substituents e.g. –COOH group as used in compound **I** or

by introduction of charge. The porphyrin derivatives belonging to latter type are readily water soluble and hydrophilic.

In this context a cationic porphyrin viz., 5,10,15,20-tetra(4-methylpyridyl)porphyrin (**III**) was synthesized in-house following a two-step procedure and subsequently radiolabeled with ^{68}Ga . Radiolabeling of compound **III** with ^{68}Ga was carried out directly in the porphyrin core owing to the suitable ionic radius (62 pm) of ^{68}Ga (**III**). Sourcing of ^{68}Ga from the ^{68}Ge - ^{68}Ga generator and its amenability as a diagnostic isotope has been discussed in this chapter. Tumor targeting potential of the ^{68}Ga labeled compound **III** was evaluated by biodistribution studies in Swiss mice bearing fibrosarcoma tumor. The studies revealed high uptake of the radiotracer in the tumor within 30 min post-injection (6.47 ± 0.87 % of the injected activity) and retention therein till 2 h post-administration (4.48 ± 1.11 % of the injected activity) up to which the study was continued.

An attempt was also made to synthesize another cationic porphyrin derivative namely, 5-carboethoxymethyleneoxyphenyl-10, 15, 20-tri(*p*-N-methylpyridyl)porphyrin (**IV**) which, in turn, was coupled with *p*-NH₂-benzyl-DOTA (*p*-aminobenzyl-1,4,7,10-tetraazacyclododecane-1,4,7,10-tetraacetic acid) (Fig. 1). The resultant conjugate was radiolabeled with ^{177}Lu . Bioevaluation of ^{177}Lu -labeled-compound (**V**) was carried out in Swiss mice bearing fibrosarcoma. Bio-distribution studies revealed early accumulation of the radiolabeled agent in the tumor (2.14 ± 0.48 % IA/g at 30 min p.i.). Non-accumulated activity exhibited major clearance through renal pathway (80.46 ± 3.40). The initially accumulated activity in the non-target organs was observed to completely clear away at

24 h p.i. However, the tumor uptake was also observed to be substantially reduced at this time point (0.05 ± 0.00 %IA/g at 24 h p. i.).

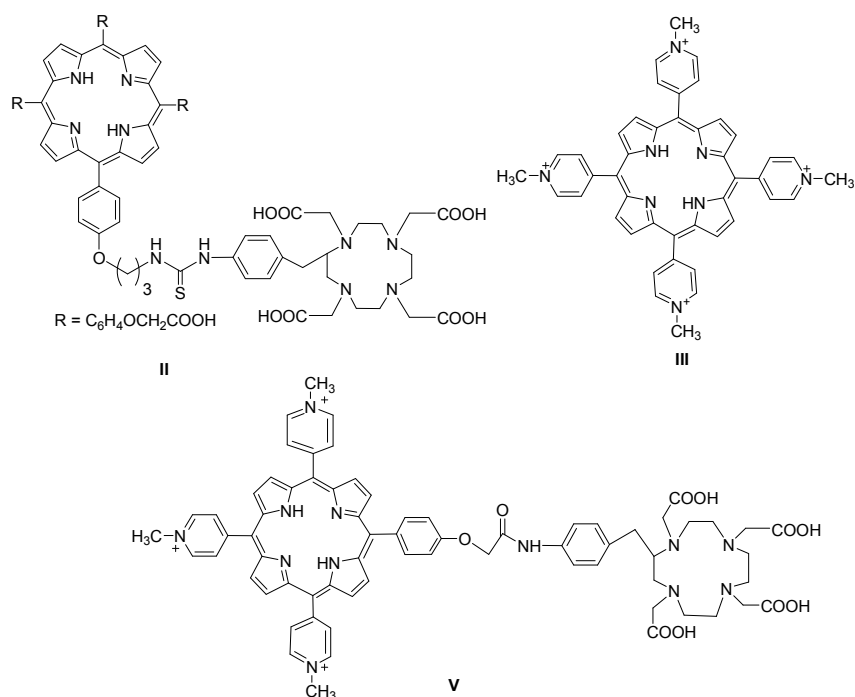


Fig. 1. Porphyrin derivatives synthesized for radiolabeling with isotopes viz. ^{177}Lu , ^{90}Y and ^{68}Ga .

CHAPTER 3: PREPARATION OF RADIOLABELED MONOCLONAL ANTIBODIES AND PEPTIDE AS RECEPTOR SPECIFIC TUMOR TARGETING AGENTS.

In this chapter, targeting receptor overexpression on specific tumor, using two different types of molecular vectors such as monoclonal antibodies and RGD peptide is discussed under two sub-headings.

3(a) PREPARATION OF ^{177}Lu -LABELED MONOCLONAL ANTIBODIES RITUXIMAB AND TRASTUZUMAB AND THEIR PRECLINICAL EVALUATION

Antibodies (Ab), also known as an immunoglobulin (Ig), are proteins produced by B-cells and are used by the immune system to identify foreign objects called antigens. Monoclonal antibodies (mAbs) are the antibodies prepared from same B-cell clone and are specific towards binding with same epitope (i.e. binding site on an antigen). Based on the high degree of affinity of mAb with the specific antigen expression of specific tumors, radiolabeled mAb can be envisaged as a guided vehicle for delivering adequate radiation dosages to the tumor site. This kind of therapy involving the use of radiolabeled mAbs is known as radioimmunotherapy (RIT). Various clinically approved mAbs used in RIT have been listed in chapter one of the thesis.

The present chapter gives the brief discussion about preparation of ^{177}Lu -labeled-monoclonal antibodies. Two antibodies chosen for present study are namely, Rituximab and Trastuzumab. Rituximab is chimeric mAb having specificity towards CD20 antigen receptors and is a FDA (Food Drug and Administration) approved drug for the treatment of Non-Hodgkins' Lymphoma [13]. On the other hand, Trastuzumab is a humanized IgG1 monoclonal antibody and is also FDA approved drug for the treatment of breast cancer where the targets on the cancer are HER2 receptors [14].

General procedure used for preparation of radiolabeled mAb involved three steps. As ^{177}Lu cannot be introduced directly in the antibody structure, mAb is first conjugated with a BFCA namely, *p*-NCS-benzyl-DOTA for complexation with ^{177}Lu . The second

step involves the purification of the antibody-BFCA conjugate, by separation of the free BFCA and the third step is the radiolabeling of the purified antibody-BFCA conjugate with ^{177}Lu . The radiochemical purity (RCP) of the radiolabeled mAbs was evaluated by HPLC indicating the formation of ^{177}Lu -labeled Rituximab and Trastuzumab with radiochemical purities of > 99%. Initial studies for optimising the conjugation method and also the radiolabeling parameters were carried out with a readily available mAb namely, immunoglobulin G (IgG) owing to its ready availability and low cost. In subsequent efforts, the radiolabeled mAbs i.e. Rituximab as well as Trastuzumab were prepared and evaluated *in vitro* using cell lines viz. Raji and BT 474 respectively known to over express antigen receptors, CD20 and HER2 respectively. This study indicated the specificity and binding of the radiolabeled mAb conjugates with these antigen receptors. Efforts to arrive at a freeze-dried kit formulation of Rituximab for radiolabeling with ^{177}Lu is also being pursued.

3 (b) PREPARATION OF $^{99\text{m}}\text{TcN}$ -LABELED RGD DERIVATIVE FOR TUMOR IMAGING

Targeting tumor by utilizing the ability of a ligand to bind with particular type of receptors over expressed by the tumor is one of the widely used tumor targeting techniques in the field of nuclear medicine. Arginine-Glycine-Aspartic acid (RGD) is one such peptide-based ligand which shows high specificity towards integrin $\alpha_v\beta_3$ receptors. Integrin $\alpha_v\beta_3$ plays a significant role in tumor angiogenesis and considered to be an important target for molecular imaging as well as *in vivo* targeted therapy using radiolabeled agents [15]. Therefore, there is a growing interest in developing suitable

radiolabeled RGD peptides that can be used for non-invasive imaging of $\alpha_v\beta_3$ expression. Efficacy of cyclic RGD dimer in targeting more number of receptors as compared to the corresponding monomer has been reported [16]. Taking this into account, an attempt was made to radiolabel a cyclic RGD monomer with ^{99m}Tc using $[\text{}^{99m}\text{TcN}]^{2+}$ core whereby the resultant complex can be envisaged to possess two monomeric units and could possibly mimic as dimeric species of RGD. The work outlined in this chapter is preparation of a dimeric $^{99m}\text{TcN}-[\text{G}_3\text{-c(RGDfk)}]_2$ complex and its bioevaluation as a potential agent for early detection of malignant tumor by SPECT imaging. The dithiocarbamate derivative of cyclic RGD monomer $\text{G}_3\text{-c(RGDfk)}$ was prepared as two such dithiocarbamate units are required for complexation with $[\text{}^{99m}\text{TcN}]^{2+}$ core of ^{99m}Tc to form the $^{99m}\text{TcN}-[\text{G}_3\text{-c(RGDfk)}]_2$ dimeric complex in high yield (Fig. 2). The radiochemical purity of the complex was more than 98% as determined by high performance liquid chromatography (HPLC). Results of biodistribution studies carried out in C57BL/6 mice bearing melanoma tumors showed good tumor uptake accompanied by favorable tumor/blood and tumor/muscle ratios. In order to support the biodistribution results, imaging studies in tumor bearing mice were also carried out and visible accumulation of activity in the tumor was observed with appreciable target to background ratio.

potential to detect hypoxia in tumor are evaluated *in vivo*. Triazole derivatives of 2-, 4-, and 5-nitroimidazole were synthesized via ‘click chemistry’ route (Fig. 3).

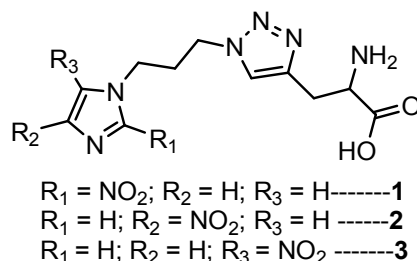


Fig. 3. Three different derivatives of 2-, 4- and 5-nitroimidazole prepared by click chemistry route.

The ligands synthesized were characterized and subsequently radiolabeled using $[\text{}^{99\text{m}}\text{Tc}(\text{CO})_3(\text{H}_2\text{O})_3]^+$ precursor complex to obtain corresponding neutral $^{99\text{m}}\text{Tc}(\text{CO})_3$ complexes. The labile water molecules in the $[\text{}^{99\text{m}}\text{Tc}(\text{CO})_3(\text{H}_2\text{O})_3]^+$ core can be replaced easily by a tridentate ligand. Radiolabeling using this core can be achieved at low ligand concentration, however heating is required for obtaining sufficient radiolabeling yields. The complexes obtained exhibit high thermodynamic stability and are kinetically inert which provides long term stability in serum or *in vivo*. All the complexes could be prepared in >90% radio chemical purity (RCP). The complexes were subsequently evaluated in Swiss mice bearing fibrosarcoma tumor. Biodistribution studies showed uptake and retention of all the complexes in tumor. However, contrary to usual expectations, the 5-nitroimidazole complex showed relatively better tumor uptake than the 2-nitroimidazole counterpart. A notable observation in the present study was the atypical tumor uptake of a 5-nitroimidazole complex. Though a conclusive evidence for

this observation could not be obtained, it underlines the importance of evaluating nitroimidazole radiotracers other than 2-nitroimidazole for detecting tissue hypoxia.

REFERENCES

1. Velikyan I. *Theranostics*, **2014**, 4, 47-80.
2. Saif MW, Tzannou I, Makrilia N, et al. *Yale J Biol Med*, **2010**, 83, 53–65.
3. Brřiza T, Kralova J, Cigler P, et al. *Bioorg Med Chem Lett*, **2012**, 22, 82–84.
4. Akudugu JM, Neti PVSV, Howell RW. *J Nucl Med*, **2011**, 52, 642–664.
5. Eggenspiller A, Michelin C, Desbois N, et al. *Eur J Org Chem*, **2013**, 2013, 6629–6643.
6. Vinjamuri S, Gilbert TM, Banks M, et al. *Brit J Cancer*, **2013**, 108, 1440–1448.
7. Volkert WA, Hoffman TJ. *Chem Rev*, **1999**, 99, 2269–2292.
8. Srivastava S. C., Dadachova E. *Semin Nucl Med*, **2001**, 31, 330–341.
9. Hamblin MR, Newman ELJ. *Photochem Photobiol B: Biol*, **1994**, 23, 3-8.
10. Moan J, Berg K. *Photochem Photobiol*, **1992**, 55, 931-948.
11. Gianferrara T, Bergamo A, Bratos I, et al. *J Med Chem*, **2010**, 53, 4678-4690.
12. Vicente MGH. *Curr Med Chem*, **2001**, 1, 175-194.
13. Forrer F, Chen J, Fani M, et al. *Eur J Nucl Med Mol I*, **2009**, 36, 1443–1452.
14. Rasaneha S, Hossein Rajabia H, Babaeib MH, et al. *Nucl Med Biol*, **2010**, 37, 949–955.
15. Liu Z, Jia B, Jiyun Shi J, et al. *Bioconjug Chem*, **2010**, 21, 548–555.
16. Liu Z, Niu G, Shi J, et al. *Eur J Nucl Med Mol I*, **2009**, 36, 947–957.
17. Krohn KA, Link JM, Mason RP. *J Nucl Med*, **2008**, Suppl 2, 129S.

LIST OF FIGURES

	Page No.
Fig.1.1. Structural representation of a typical radiopharmaceutical	12
Fig.1.2. Simplified ^{99}Mo decay scheme	15
Fig.1.3. Typical structures of (a) $[\text{}^{99\text{m}}\text{TcN}]^{2+}$ and (b) $[\text{}^{99\text{m}}\text{Tc}(\text{CO})_3(\text{H}_2\text{O})_3]^{1+}$ precursor complexes	18
Fig.1.4. Simplified decay scheme of ^{68}Ge	20
Fig.1.5. Simplified decay scheme of ^{90}Sr	22
Fig.1.6. Simplified decay scheme of ^{177}Lu	22
Fig.1.7. Structures of <i>p</i> -NH ₂ -benzyl-DOTA and <i>p</i> -NCS-benzyl-DOTA	25
Fig.2.1. Structures for simplest porphyrin molecule (I), lipophilic porphyrin (II) negatively charged porphyrin (III) and positively charged porphyrin (IV)	37
Fig. 2.2. Scheme for synthesis of porphyrin- <i>p</i> -NCS-benzyl-DOTA conjugate	54
Fig.2.3. Typical HPLC profiles of (a) $^{177}\text{LuCl}_3$ (b) ^{177}Lu -labeled porphyrin- <i>p</i> -NCS-benzyl-DOTA complex (c) $^{90}\text{YCl}_3$ (d) ^{90}Y -labeled porphyrin- <i>p</i> -NCS-benzyl-DOTA complex without purification (e) ^{90}Y -labeled porphyrin- <i>p</i> -NCS-benzyl-DOTA complex after purification	56
Fig.2.4. Whole-body scintigraphic images of the Swiss mice bearing fibrosarcoma tumors (in right thigh) injected with 7.4 MBq (200 μCi) of ^{177}Lu -labeled porphyrin- <i>p</i> -NCS-benzyl-DOTA conjugate, recorded at (a) 16 h (b) 48 h and (c) 72 h post-administration.	61
Fig.2.5. ^1H -NMR spectrum of 5,10,15,20-tetra(pyridyl)porphyrin (2i)	66

Fig. 2.6. ¹ H-NMR spectrum of 5,10,15,20-tetra(4-methylpyridyl)porphyrin (2j)	67
Fig.2.7. Scheme for synthesis of 5,10,15,20-tetra(4-methylpyridyl)porphyrin	72
Fig.2.8. Typical hplc elution profiles of (a) ⁶⁸ GaCl ₃ (b) ⁶⁸ Ga-labeled 5,10,15,20-tetra(4-methylpyridyl)porphyrin, before purification and (c) after purification	74
Fig. 2.9. Overlaid UV-visible profiles of 5,10,15,20-tetra(pyridyl)porphyrin, 5,10,15,20-tetra(4-methylpyridyl)porphyrin and Ga-labeled 5,10,15,20-tetra(4-methylpyridyl)porphyrin	75
Fig. 2.10. Synthesis of <i>p</i> -NH ₂ -benzyl-DOTA conjugated 5-carboxymethyleneoxyphenyl-10,15,20-tri(<i>p</i> -N-methylpyridyl)porphyrin (a) ethylbromoacetate, dry acetone, K ₂ CO ₃ , reflux 8 h (b) nitrobenzene, propionic acid, reflux, 2 h (c) CH ₃ I, r.t. stirring, 48 h (d) 2 N NaOH, r.t. stirring, 48 h (e) <i>p</i> -NH ₂ -benzyl-DOTA, 2 N NaOH, r.t. stirring 24 h	88
Fig.2.11. HPLC profiles of (a) ¹⁷⁷ LuCl ₃ (b) ¹⁷⁷ Lu-labeled-UPTMPyA- <i>p</i> -NH ₂ -benzyl-DOTA complex (c) Lu-labeled-UPTMPyA- <i>p</i> -NH ₂ -benzyl-DOTA	90
Fig.2.12. Overlaid UV-visible profile of (i) UPTMPyA- <i>p</i> -NH ₂ -benzyl-DOTA and (ii) Lu-labeled-UPTMPyA- <i>p</i> -NH ₂ -benzyl-DOTA complex	91
Fig.3a.1. Schematic representation of antibody-antigen interaction	97
Fig.3a.2. HPLC profiles of (a) ¹⁷⁷ Lu-labeled-Rituximab and (b) ¹⁷⁷ Lu-labeled Trastuzumab	110
Fig.3a.3. Percent cell binding versus varying amounts of ¹⁷⁷ Lu-Rituximab complex and effect of excess of cold (100 µg) on % cell binding	112

corresponding to 7.45 ng of ^{177}Lu -Rituximab complex.	
Fig.3b.1. Schematic representation of conversion of $\text{G}_3\text{-c(RGDfK)}$ to corresponding dithiocarbamate derivative	122
Fig.3b.2. Mass spectrum of dithiocarbamate derivative of $\text{G}_3\text{-c(RGDfK)}$	122
Fig.3b.3. Proposed structure of $^{99\text{m}}\text{TcN}[\text{G}_3\text{-c(RGDfK)}]_2$	124
Fig.3b.4. HPLC elution profile of $^{99\text{m}}\text{TcN}[\text{G}_3\text{-c(RGDfK)}]_2$	125
Fig.3b.5. Comparison of uptake of $^{99\text{m}}\text{TcN}[\text{G}_3\text{-c(RGDfK)}]_2$ in various organ/tissue of C57BL/6 mice bearing melanoma tumors at 30 min p.i. in the absence/presence of excess $\text{G}_3\text{-c(RGDfK)}$	131
Fig.3b.6. Whole-body scintigraphic images of C57BL/6 mice bearing melanoma tumors recorded at (a) 30 min and (b) 60 min post-administration of $^{99\text{m}}\text{TcN}[\text{G}_3\text{-c(RGDfK)}]_2$	132
Fig.4.1. Schematic representation of reduction of nitroimidazole	139
Fig.4.2. Structures of two clinically evaluated $^{99\text{m}}\text{Tc}$ -labeled nitroimidazole based hypoxia imaging agents	142
Fig.4.3. Structural representation of 2-, 4- and 5-nitroimidazoles with respective SERP values	144
Fig.4.4. ^1H -NMR of 1-(3-bromopropyl)-4-nitro-1H-imidazole (4b)	150
Fig.4.5. ^1H -NMR of 1-(3-azidopropyl)-4-nitro-1H-imidazole (4e)	151
Fig.4.6. ESI-MS of 2-amino-3-(1-(3-(4-nitro-1H-imidazol-1-yl)propyl)-1H-1,2,3-triazol-4-yl)propanoic acid (4h)	152
Fig.4.7. ESI-MS of Re(CO)_3 complex of compound 4h (4m)	153
Fig. 4.8. Synthesis of triazole derivatives of 2-, 4- and 5-nitroimidazoles	157

Fig. 4.9. Radiolabeling of 2-, 4- and 5-nitroimidazole triazole derivatives with $[^{99m}\text{Tc}(\text{CO})_3(\text{H}_2\text{O})_3]^+$ precursor complex	158
Fig.4.10. HPLC elution profile of (a) $[^{99m}\text{Tc}(\text{CO})_3(\text{H}_2\text{O})_3]^+$ precursor complex and (b) 2- nitroimidazole triazole- $^{99m}\text{Tc}(\text{CO})_3$ complex (c) 4-nitroimidazole triazole- $^{99m}\text{Tc}(\text{CO})_3$ complex (d) 5-nitroimidazole triazole- $^{99m}\text{Tc}(\text{CO})_3$ complex	159

LIST OF TABLES

	Page No.
Table 1.1. List of few radionuclides useful for SPECT imaging	8
Table 1.2. List of few radionuclides useful for PET imaging	9
Table 1.3. List of few radionuclides useful for therapy	10
Table 2.1. Biodistribution pattern of ^{177}Lu -labeled porphyrin- <i>p</i> -NCS-benzyl-DOTA conjugate in Swiss mice bearing fibrosarcoma tumors	59
Table 2.2. Biodistribution pattern of ^{90}Y -labeled porphyrin- <i>p</i> -NCS-benzyl-DOTA complex in Swiss mice bearing fibrosarcoma tumor	60
Table 2.3. Biodistribution pattern of ^{68}Ga -labeled 5,10,15,20-tetra(4-methylpyridyl)porphyrin complex in Swiss mice bearing fibrosarcoma tumors	78
Table 2.4. Bio distribution table for ^{177}Lu -labeled-UPTMPyA- <i>p</i> -NH ₂ -benzyl-DOTA complex in Swiss mice (n=5) at different time points.	93
Table 3a.1. Examples of ^{177}Lu -labeled mAbs studied for radioimmunotherapy	102
Table 3a.2. Biodistribution pattern of ^{177}Lu -Rituximab in normal Swiss mice at different time points (n=3).	113
Table 3b.1. List of few radiolabeled peptides and the corresponding target receptors	116
Table 3b.2. Biodistribution pattern of $^{99\text{m}}\text{TcN}$ -[G ₃ -c(RGDfK)] ₂ conjugate in C57BL/6 mice (n=5) bearing melanoma tumor	129
Table 4.1. LogP _{o/w} values and other quality control parameters of different nitroimidazole triazole- $^{99\text{m}}\text{Tc}(\text{CO})_3$ complexes	160
Table 4.2. Activity of different nitroimidazole-triazole- $^{99\text{m}}\text{Tc}(\text{CO})_3$ complexes and [^{18}F]FMISO observed in tumor and blood at different time points (n=5)	162

Table 4.3. Biodistribution of various nitroimidazole triazole-^{99m}Tc(CO)₃ complexes (**4j**, **4k** & **4l**) (% IA/gram) in Swiss mice bearing fibrosarcoma tumor (n=5) at three different time points 166

Chapter 1

GENERAL INTRODUCTION

Chapter 1

1.1. Nuclear Medicine

‘Nuclear medicine’ employs the nuclear decay properties of radioactive nuclides or radioisotopes in diagnosis, therapy and evaluation of metabolic, physiologic and pathologic conditions in human patients. Nuclear medicine is presently used in the diagnosis, management, treatment and prevention of many serious diseases and is immensely helpful in medical management ranging from oncology to cardiology to neurology. Nuclear medicine imaging procedures often identify abnormalities at the very early stage of the progression of the disease, long before it can be detected by other alternative diagnostic modalities and therefore allows the disease to be treated early in its course of progression [1,2]. However, the real strength of nuclear medicine lies in its ability to monitor both biochemical and physiological functions *in-vivo*, which is not possible by the other imaging modalities, such as, magnetic resonance imaging (MRI) and ultrasound imaging [3-8]. Although these imaging modalities are able to delineate anatomical features with better resolution, they provide only limited information on real-time biological function. Nuclear medicine offers the options of both diagnosis, by far the more widely used and therapy which include treatment of a wide range of cancers in cases where the other modalities do not have much promise.

Cancer is one of the most dreaded challenges in modern medical science. Diagnosis and treatment of this disease at early stages is of utmost importance for a positive outcome of the treatment regime [5]. A variety of techniques both independent as well as in combination with other modalities are essential for early detection as well as for the treatment of cancer. Of the various modalities employed, chemotherapy, surgery,

Chapter 1

radionuclidic therapy, radiation therapy, photodynamic therapy etc. are the predominantly used ones for the treatment of cancer [4,8]. On the other hand, MRI (magnetic resonance imaging), CT (computed tomography), radionuclidic imaging etc. are the major ones used for the diagnosis [1,3]. In recent years, imaging and therapy of cancers involving systemic administration of radiolabeled agents viz. radiopharmaceuticals have not only gained eminence worldwide, but has become the only modality in some specific cases of cancer management [4-6]. As a result, research in the area of molecular imaging and therapy involving radiolabeled agents is on the increase, leading to introduction of newer agents for a variety of applications in nuclear medicine.

The recent advances of nuclear medicine is attributable to the major developments viz. (i) development of appropriate radiolabeled molecular vectors which are designed to accumulate in a particular organ/tissue with high specificity and thereby exhibiting high target to non-target ratio after being radiolabeled to become a radiopharmaceutical, (ii) identification of the ideal radioisotope for a particular target, and (iii) development of sophisticated instrumentation for acquiring excellent quality dynamic images of the morphology and function of virtually every major organ of the body. Nuclear medicine technique can be used to monitor both biochemical and physiological functions *in vivo*, which is not possible by the other advanced imaging techniques viz. computed tomography (CT), nuclear magnetic resonance imaging (MRI) and ultrasound imaging [9,10]. By the end of the 20th century, nuclear medicine has become a very useful tool for both diagnosis and treatment of many serious diseases.

Chapter 1

1.2. Molecular Imaging

Molecular imaging is a type of medical imaging that provides detailed pictures of the real-time physiological processes in vivo at the molecular and cellular level [10]. It enables the visualization of the cellular function and the follow-up of the molecular process in living organisms in a non-invasive manner. Molecular imaging differs from traditional imaging in that probes known as biomarkers or molecular vectors are used to help image particular targets or pathways. Biomarkers interact chemically with their surroundings and, in turn, alter the image according to molecular changes occurring within the area of interest. This process is markedly different from other imaging modalities which primarily image the differences in qualities such as density or water content. This ability to image fine molecular changes opens up an incredible number of exciting possibilities for medical application, including early detection and treatment of disease and provides the necessary insights towards basic pharmaceutical development. While other diagnostic imaging procedures such as X-rays, computed tomography (CT), MRI and ultrasound offer information of anatomical structure, molecular imaging allows physicians an window to view the in vivo functioning of the chemical and biological processes [9,10] occurring at the cellular level.

Molecular imaging in nuclear medicine, uses very small amounts of radioactive species (radiolabeled molecules, inorganic ions or gases collectively called as radiopharmaceuticals) to diagnose and treat disease. In nuclear medicine imaging, the radiopharmaceuticals are detected by special types of cameras that work with computers to provide very precise pictures of the area of the body being imaged. In Nuclear medicine, radiolabeled molecular vectors/radiolabeled agents known as

Chapter 1

radiopharmaceuticals are used for obtaining images and depending upon the type of emission by the radionuclide, imaging technique can be categorized as SPECT (single photon emission tomography) and PET (positron emission tomography). SPECT and PET have been discussed briefly in later sections of this chapter [11].

1.3. Radiopharmaceuticals

Radiopharmaceuticals are radiochemical formulations or radiolabeled drugs with a constant composition and can be administered either orally or intravenously with adequate safety, for the purpose of carrying out diagnosis or treatment of a diseased condition, particularly of cancerous origin.

Some radiopharmaceuticals are used for the determination of the localisation of the tumor whereas others are used for its treatment. Apart from the diagnosis and treatment of the tumor, some radiopharmaceutical preparations are even used for evaluating the functioning of various organs including brain, kidney, heart etc. [1-4]. The ability of radiopharmaceuticals to take part in metabolic functions of the body unlike other modalities which give information about physical morphology and anatomy of human body imparts a special status to them [1,8]. Radiopharmaceuticals can be either metal essential or non metal essential. In metal essential radiopharmaceuticals the metal complex decides the biological distribution whereas in the latter case the carrier molecule is held responsible for the resultant biological distribution [1]. Radiopharmaceuticals can be broadly categorized as diagnostic and therapeutic radiopharmaceuticals. Segregation of a particular radiopharmaceutical in either category depends upon the type of radionuclide

Chapter 1

used for the preparation of the radiopharmaceutical. A brief description about diagnostic and therapeutic radiopharmaceuticals is presented below.

1.3.1. Diagnostic radiopharmaceuticals:

Diagnostic radiopharmaceuticals are the ones in which radioisotope used is either a gamma emitter or a positron emitter. In the former case, the radiopharmaceutical is used for SPECT (Single Photon Emission Computed Tomography) imaging, while in the latter the diagnostic radiopharmaceutical is used for PET (Positron Emission Tomography) imaging [1,8].

1.3.1.1. SPECT (Single Photon Emission Computed Tomography):

SPECT is an imaging modality where diagnosis of the disease/tumor lesion is carried out using radiopharmaceuticals containing gamma emitting radionuclides. The general SPECT system uses more than one NaI(Tl) detector heads mounted in a gantry, an on-line computer for acquisition and processing of data and display system. The scintillation camera depicts images of three dimensional distribution of activity in site of lesion in two-dimensional display. This 2D data is then reconstructed into three dimensional images by means of a technique called as computed tomography. Computed tomography or CT is a technique based on rigorous mathematical algorithms which is capable of reconstructing three dimensional images from the scans of recorded two-dimensional slices. A few SPECT radioisotopes are listed in **Table 1.1**.

Chapter 1

Table 1.1. List of few radionuclides useful for SPECT imaging [5,6]

Radionuclide	Half-life	Mode of decay	Principal gamma component E in keV (% abundance)
^{67}Ga	3.26 d	EC	93.31 (38.30)
^{123}I	13.27 h	EC	158.97 (82.80)
^{131}I	8.02 d	β^- & γ	364.48 (81.20)
^{111}In	2.81 d	EC	245.39 (94.17)
$^{99\text{m}}\text{Tc}$	6.02 h	IT	140.47 (88.97)
^{201}Tl	72.91h	EC	167.43 (10.00)

1.3.1.2. PET (positron emission tomography):

PET is an imaging modality where diagnosis of the disease/tumor lesion is carried out using radiopharmaceuticals containing positron (β^+) emitting radionuclides (**Table 1.2**) [1]. The principle of imaging here is based on the measurement of two coincident gamma rays emitted as a post-event of positron and electron annihilation. The detector used in this modality is BGO (bismuth germanate or $\text{Bi}_4\text{Ge}_3\text{O}_{12}$) for efficient detection of high energy gamma rays [11]. PET scans have some advantages over corresponding SPECT scans. PET scans are more sensitive as there is no need of physical collimators as in SPECT cameras as is taken care of by coincidence measurement [12]. The important implications of the high sensitivity are better quality images due to enhanced signal to noise ratio, possibility of performing shorter scans, high temporal resolution etc. However, advances being made in SPECT hardware and image reconstruction algorithms has significantly improved the spatial resolution of the images obtained with SPECT [12].

Table 1.2. List of few radionuclides useful for PET imaging [5, 6]

Radionuclide	Half-life	Mode of decay	Principal gamma component E in keV (% abundance)
^{11}C	20.39 min	β^+	511.00 (199.5)
^{18}F	109.77 min	β^+	511.00 (200)
^{68}Ga	68 min	β^+	511.00 (94.17)
^{13}N	9.97 min	β^+	511.00 (199.64)
^{15}O	2.03 min	β^+	511.00 (199.77)

1.3.2. Therapeutic radiopharmaceuticals

Therapeutic radiopharmaceuticals constitute those radiopharmaceuticals where the isotope of choice is a particulate emitter viz. Alpha (α), beta (β) and conversion electron (e^-). Therapeutic radiopharmaceuticals are intended to deliver the therapeutic doses at the target site and since they are particulate emitters damage to the healthy tissues is also expected to be more. So, in order to avoid this, the biomolecule of choice should have high specificity towards the disease site apart from that the pharmacokinetics should also be such so as to spare healthy organs and rapid clearance if any from non-target organs. A few therapeutic isotopes are listed in table 1.3.

Chapter 1

Table 1.3. List of few radionuclides useful for therapy [5,6].

Radionuclide	Half-life	Mode of decay	Energy in keV	Principal gamma component E in keV (% abundance)
^{225}Ac	10.00 d	α & γ	5935.1	99.70 (3.50)
^{111}Ag	7.45 d	β^- & γ	1036.8	342.13 (6.70)
^{77}As	38.83 h	β^- & γ	682.9	239.00 (1.60)
^{212}Bi	60.55 min	α & γ	6207.1	727.17 (11.80)
^{213}Bi	45.59 min	α & γ	5982.0	439.70 (27.30)
^{67}Cu	61.83 h	β^- & γ	577.0	184.58 (48.70)
^{159}Gd	18.48 h	β^- & γ	970.6	58.00 (26.25)
^{131}I	8.02 d	β^- & γ	970.8	81.00 (37.10)
^{32}P	14.26 d	β^-	1710.6	NIL
^{109}Pd	13.70 h	β^- & γ	1115.9	88.04 (3.60)
^{177}Lu	6.73 d	β^- & γ	498.2	208.36 (11.00)
^{223}Ra	11.44 d	α & γ	5979.3	269.41 (13.60)
^{186}Re	90.64 h	β^- & γ	1069.5	137.16 (8.60)
^{188}Re	16.98 h	β^- & γ	2120.4	155.04 (14.90)
^{105}Rh	35.36 h	β^- & γ	567.0	318.90 (19.20)
^{153}Sm	46.27 h	β^- & γ	808.4	103.18 (28.30)
^{89}Sr	50.53 d	β^-	1496.6	NIL
^{90}Y	64.10 h	β^-	2282.0	NIL

Chapter 1

1.4. Radiopharmaceutical design

The basic constituents of a typical radiopharmaceutical are a biomolecule (BM), a linker, bi-functional chelating agent (BFCA) and radionuclide (RN). A biomolecule is the main constituent of a radiopharmaceutical as it acts as a guiding vehicle for the whole radiopharmaceutical and binds with the target tissue or cells by following a mechanism which again depends upon the nature of the biomolecule. There are various mechanisms by which BM can get attached to the target cells, some of these will be discussed in latter parts of this chapter. A linker can be a polyamino acid sequence, an aliphatic chain or a polyether chain [13]. Its use in preparation of radiopharmaceutical is optional. The use of linker serves two purposes, the first being the introduction of a spacer between the radionuclide metal complex and BM so as to protect the bio-affinity of BM. Secondly, a linker is used in certain cases to improve the pharmacokinetics of radiopharmaceutical as it helps to provide better target to background ratio [13]. A bi-functional chelating agent (BFCA) as the name suggests can bind to the BM at one end and at other end it can form a complex with the radionuclide. Selection of BFCA depends upon the radionuclide to be used and the prime requirement being that the BFCA-RN complex should be highly stable in vivo, since instability can lead to the dissociation the complex wherein the RN can give undue dose burden to the non-target organs. The schematic representation of radiopharmaceutical structure is shown in **Fig. 1.1**.

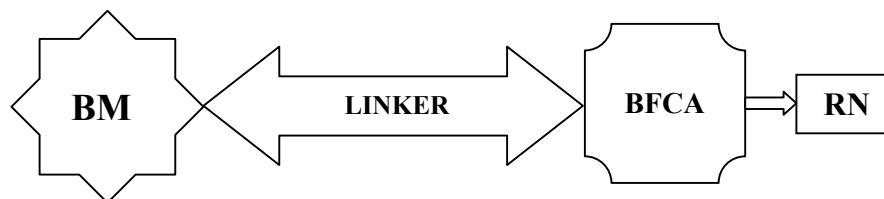


Fig. 1.1. Structural representation of a typical radiopharmaceutical

1.5. Tumor targeting mechanism

The mechanism by which a radiopharmaceutical targets a particular organ or cell gives rise to two type of agents viz. ‘radionuclide essential’ and ‘radionuclide non essential’. In cases where the target affinity and localization is acquired post complexation with the radionuclide, the radiopharmaceutical comes under the first category [4]. On the other hand, in the second type, the target affinity is dictated by the biomolecule acting as a specific vector. The work outlined in the thesis deals with radiolabeled agents which of the second type. Hence, in the present chapter, the mechanisms which are generally borne in mind while designing agents for targeting cancer or other diseased sites include metabolic perfusion, receptor binding, antigen-antibody complex formation, passive diffusion, active transport etc. In the present thesis, receptor binding, antigen-antibody complex formation, passive diffusion are the mechanisms which have been utilized in envisaging the radiopharmaceuticals to be discussed in the present thesis. A brief description of these mechanisms is given below.

Passive diffusion: In passive diffusion, entry of drugs or biomolecules into the cells is driven by the concentration gradient. In the process, these molecules move from the blood

Chapter 1

pool where their concentration is higher, into the cells wherein there is a lower concentration [14]. Lipophilicity as well as charge of the biomolecules play important role while deciding this mode of entry into tumor cells. Lipophilic molecules viz. non charged porphyrins, nitroimidazoles which have been used as molecular vectors in present thesis, undergo preferential accumulation in tumor cells via passive diffusion.

Receptor binding: Receptors are proteins present on cell surface and exhibit high specificity towards binding with certain ligands. This mechanism involves the binding of the receptor protein and a ligand specific towards binding with this receptor. Normal cells express various kinds of receptors and in tumor cells one or other of these receptors are over expressed. Targeting overexpressed receptors on the tumors with specific vectors, form the basis of the preferential accumulation of the ligands/biomolecules in the tumor cells. The receptor binding ligands are mostly peptides and due to their selective targeting of tumor cells are they are given the name of bio-markers [13]. This principle has been used in development of both peptide based imaging and therapeutic agents. In nuclear medicine field the peptide-based radiopharmaceuticals are by far the most effective and widely used ones used in diagnosis and therapy of cancer. Various peptide based radiopharmaceuticals which have been developed for imaging of different kinds of tumor include ^{99m}Tc -Hynic-TOC, ^{111}In -DOTA-TATE, ^{68}Ga -DOTA-NOC, ^{68}Ga -DOTA-TOC, ^{18}F -galacto-RGD, $^{68}\text{Ga}/^{111}\text{In}$ -DOTA-RGD etc [15]. In the present thesis, this strategy was utilized for targeting $\alpha_v\beta_3$ receptor overexpression by various metastatic tumors using a ^{99m}Tc -labeled peptide derivative i.e. [^{99m}Tc -N- $\{\text{G}_3\text{-c(RGDfK)}\}_2$].

Antigen-antibody complex formation: Antibodies are immunoglobulin proteins produced in the body in response to a foreign substance called as antigen. An antibody-antigen binding is unique and this phenomenon is used to selectively target tumor lesions over expressing particular antigen receptors [16]. The treatment involving antibodies is termed as immunotherapy. Apart from immunotherapy an another area of treatment has emerged known as radioimmunotherapy (RIT) which uses radiolabeled antibodies for specifically targeting tumor cells and deliver requisite radiation dose at the site of disease. Various radiolabeled antibodies have been approved for treatment of different kinds of cancers. In the present thesis two different antibodies viz. Rituximab and Trastuzumab were radiolabeled with ^{177}Lu for targeting CD20 antigens (non Hodgkins' lymphomas) and HER2 antigens (metastatic breast cancer) respectively.

1.6. Brief overview of radioisotopes used in the present work

1.6.1. Technetium-99m

Technetium belongs to group VIIB of the periodic table ($Z = 43$, $[\text{Kr}] 4d^5 5s^2$). Technetium-99m is a SPECT isotope the use of which amounts to approximately 80% of diagnostic radiopharmaceuticals in nuclear medicine. The source of $^{99\text{m}}\text{Tc}$ is ^{99}Mo - $^{99\text{m}}\text{Tc}$ generator system where $^{99\text{m}}\text{Tc}$ is in a transient equilibrium with parent ^{99}Mo isotope [13].

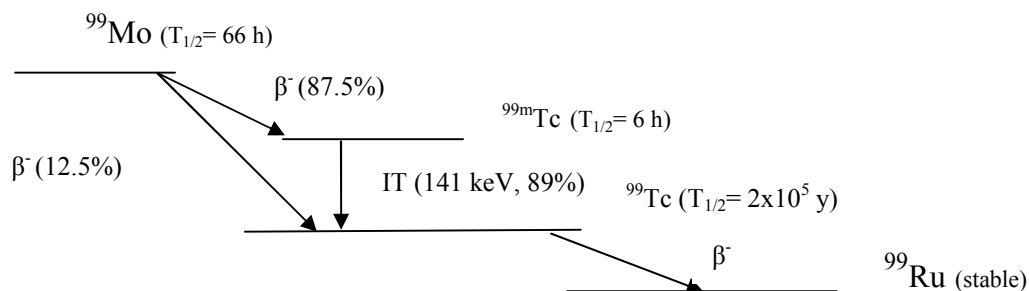


Fig. 1.2. Simplified ^{99}Mo decay scheme

The choice of $^{99\text{m}}\text{Tc}$ in designing radiopharmaceuticals stems from the various advantageous attributes of this radionuclide. It is a generator produced isotope which ensures its availability in areas which are far away from production site. Besides, this isotope exhibits excellent nuclear decay characteristics ($E_\gamma = 141 \text{ keV}$, $\sim 89\%$ abundance, $T_{1/2} = 6 \text{ h}$), ideally suited for diagnostic nuclear medicine (**Fig. 1.2**). Its half life of 6 hours, though sufficiently optimum for preparing the radiopharmaceutical, performing its quality control and injecting into the patient for imaging studies, is at the same time short enough to minimize the absorbed radiation dose. Rapid growth in this field in the last few decades is attributable, apart from its ideal radionuclidic characteristics, to the conception and development of $^{99}\text{Mo}/^{99\text{m}}\text{Tc}$ generators and lyophilized kits for ease of formulation of $^{99\text{m}}\text{Tc}$ compounds at hospital radiopharmacy. $^{99\text{m}}\text{Tc}$ has a rich and diverse redox chemistry and can be obtained from a ^{99}Mo - $^{99\text{m}}\text{Tc}$ generator in $^{99\text{m}}\text{TcO}_4^-$ form where $^{99\text{m}}\text{Tc}$ is in +7 oxidation state. Typically for radiolabeling of biomolecules with $^{99\text{m}}\text{Tc}$, $^{99\text{m}}\text{TcO}_4^-$ has to be reduced to lower oxidation states. In presence of reducing agent, $^{99\text{m}}\text{Tc}$ can exhibit

Chapter 1

multiple oxidation states, and the oxidation state in which a ^{99m}Tc -ligand complex will be formed depends upon the nature of the ligand, type of reducing agent and reaction conditions [13]. This approach of radiolabeling makes use of a large excess of ligand. Typical concentration of ^{99m}Tc in $^{99m}\text{TcO}_4^-$ eluate obtained from ^{99}Mo - ^{99m}Tc generator is $\sim 10^{-7}$ – 10^{-6} M, therefore excess ligand is required for stabilizing a particular oxidation state of ^{99m}Tc in presence of reducing agent [13]. However, this is not a desirable feature for a labeling a receptor imaging agent as excess uncomplexed ligand (referred to as cold ligand) will saturate the limited number of receptor sites available on the tumor cells and pose limitation on the binding of the radiolabeled molecules. This problem can be circumvented by using preformed radiosynthons referred to as ^{99m}Tc -cores. They constitute chemical motifs which control the molecular structure of the resulting radiopharmaceutical and ultimately, its biological properties [13]. Various such cores which have been used are ^{99m}Tc -monoxo core $[\text{}^{99m}\text{Tc}(\text{V})\text{O}]^{3+}$, ^{99m}Tc -dioxo core $[\text{}^{99m}\text{Tc}(\text{V})\text{O}_2]^+$, ^{99m}Tc -HYNIC (hydrazino nicotinic acid), ^{99m}Tc -nitrido $[\text{}^{99m}\text{Tc}(\text{V})\text{N}]^{2+}$ and ^{99m}Tc -tricarbonyl $[\text{}^{99m}\text{Tc}(\text{I})(\text{CO})_3]^+$. Two of these cores viz. $[\text{}^{99m}\text{Tc}(\text{V})\text{N}]^{2+}$ and $[\text{}^{99m}\text{Tc}(\text{CO})_3(\text{H}_2\text{O})_3]^+$ have been used in the present work for preparation of ^{99m}Tc -labeled radiolabeled agents.

1.6.1.1. $[\text{}^{99m}\text{TcN}]^{2+}$ core

This core is isoelectronic with $[\text{}^{99m}\text{TcO}]^{3+}$ core. The N^{3-} nitride species is a strong π -electron donor and has strong ability to stabilize the +5 oxidation state of Tc. $[\text{}^{99m}\text{TcN}]^{2+}$ core forms five coordinated complexes and can attain either a square pyramidal geometry or trigonal bipyramidal geometry. Square pyramidal complexes are

Chapter 1

formed with ligands having two π -donor atoms (S^- , S , O^- , NH_2) and two such ligands are utilized while forming such complexes. In square pyramidal geometry, four π -donor atoms occupy the basal plane and $Tc\equiv N$ moiety lies above the plane (**Fig. 1.3**). The trigonal bipyramidal geometry is acquired when two ligands, having a set of two π -donors and two π -acceptor atoms come together for complex formation [13,17].

1.6.1.2. [$^{99m}Tc(CO)_3(H_2O)_3$] $^+$ core

This is an organometallic core where ^{99m}Tc is in +1 oxidation state. In this core CO is a strong sigma donor and pi acceptor moiety and has the ability to stabilize the lower oxidation state of Tc. This core is now widely used for preparation of ^{99m}Tc -labeled radiolabeled agents as three labile water molecules can be easily replaced by donor atoms present in ligands (**Fig. 1.3**). This core can be prepared either by using commercially available potassium boranocarbonate kit [18] or by purging of CO gas at 1 atmosphere pressure in presence of sodium borohydride ($NaBH_4$) as reducing agent [13]. While both the methods yield > 98% of the [$^{99m}Tc(CO)_3(H_2O)_3$] $^+$ complex, the former method is preferred as in this case the use of toxic CO gas is avoided. In the work carried out in this thesis, the $^{99m}Tc(CO)_3$ -core has been prepared by using CO gas prior to the radiolabeling step. The labile water molecules in the [$^{99m}Tc(CO)_3(H_2O)_3$] $^+$ core can be easily replaced either by using three monodentate ligands, a set of one monodentate and one bi-dentate ligand or a tridentate ligand, thus opening up different possibilities leading to the formation of a variety of complexes [19]. Radiolabeling using this core can be achieved at low ligand concentration, however, heating is required for obtaining sufficient

Chapter 1

radiolabeling yields. The complexes obtained exhibit high thermodynamic stability and are kinetically inert which provides long term stability in serum or in vivo [13].

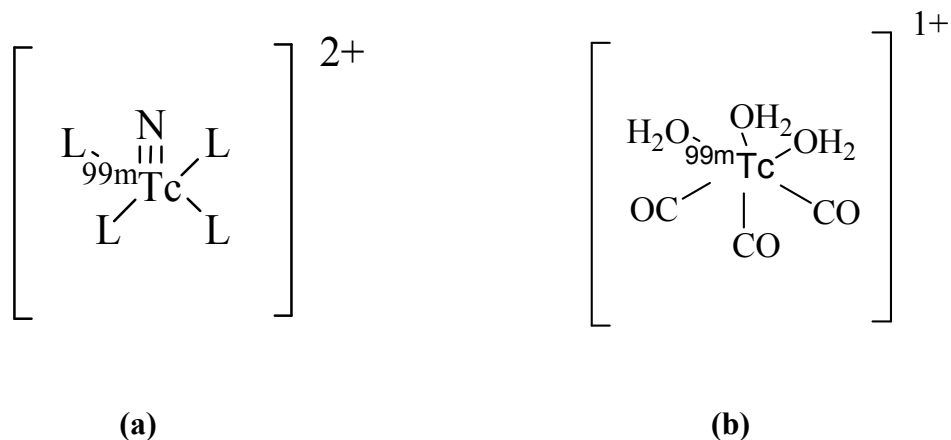


Fig. 1.3. Typical structures of (a) $[^{99m}\text{TcN}]^{2+}$ and (b) $[^{99m}\text{Tc}(\text{CO})_3(\text{H}_2\text{O})_3]^{1+}$ precursor complexes

1.6.2. Gallium-68

Gallium belongs to group IIIA of periodic table ($Z = 31$, $[\text{Ar}]3d^{10}4s^25p^1$). Gallium-68 is a potential PET isotope ($T_{1/2} = 68$ min) and offers distinctive advantages over that of the more widely used ^{18}F for diagnostic purposes. The major advantage of ^{68}Ga is the possibility of sourcing it from a ^{68}Ge - ^{68}Ga generator unlike that of other PET isotopes which require an on-site cyclotron for production [20-23]. Additionally, the long shelf-life of ^{68}Ge - ^{68}Ga generator (~ 1 -2 years), along with the possibility of more than one elutions per day ($\sim 50\%$ of the accumulated ^{68}Ga activity can be eluted after every consecutive hour), are the desirable features in envisaging ^{68}Ga -based radiopharmaceuticals for use in nuclear medicine [20-23]. A simplified decay scheme of ^{68}Ga is shown in **Fig.1.4**. Since ^{68}Ga availability is not dependent on the cyclotron, usage

Chapter 1

and distribution of ^{68}Ga -labeled radiopharmaceuticals is logistically favourable. Another advantage of Gallium-68 is that it is a n.c.a. (no carrier added) isotope as it is obtained from a chemically different parent i.e. ^{68}Ge , thereby is considered to be suitable for preparation of radiopharmaceuticals with high specific activity (specific activity of n.c.a. $^{68}\text{Ga} \sim 10^7$ Ci/g). Gallium exhibits a coordination number of 4, 5 and 6. In aqueous solutions, free hydrated Ga(III) is stable only under acidic conditions and as $p\text{H}$ is increased, insoluble $\text{Ga}(\text{OH})_3$ species starts forming rapidly and at $p\text{H} > 9.5$ soluble gallate ion $[\text{Ga}(\text{OH})_4]^-$ is the primary species [22,24,25]. Gallium-68 cannot be introduced directly in the structure of the biomolecule to form a, ‘true label’ contrary to the case of ^{18}F . Therefore, ^{68}Ga complexation requires the introduction of a suitable BFCA into the biomolecule (BM) [22]. The coordination number 6 is common for ^{68}Ga -labeled radiopharmaceuticals. ^{68}Ga forms thermodynamically stable and kinetically inert complexes with macrocyclic ligands with high values of stability constants (Log K). Log K or stability constant is equilibrium constant for the formation of a complex in solution. It is a measure of the strength of the interaction between the reagents that come together to form the complex. The typically used BFCAs are 1,4,7-triazacyclononane-1,4,7-triacetic acid (NOTA) (Log K \sim 31) and 1,4,7,10-tetraazacyclododecane-1,4,7,10-tetraacetic acid (DOTA) (Log K \sim 21.3) [22]. Various ^{68}Ga -labeled radiopharmaceuticals have been developed recently by conjugating the biomolecules with a BFCA and then radiolabeling the BM-BFCA conjugate with ^{68}Ga resulting into high radiolabeling yields [20-25] viz. ^{68}Ga -DOTA-Tyr3-octreotide (DOTA-TOC), ^{68}Ga -DOTA-1-Nal-octreotide (DOTA-NOC), ^{68}Ga -DOTA-bombesin, ^{68}Ga -NOTA-RGD etc. Acyclic BFCAs’ such as

Chapter 1

ethylene diaminetetraacetic acid (EDTA), DTPA (diethylene triamine pentaacetic acid) and their derivatives have also been used for radiolabeling biomolecules with ^{68}Ga , however most of these complexes have exhibited low *in vivo* and *in vitro* stabilities [20-25].

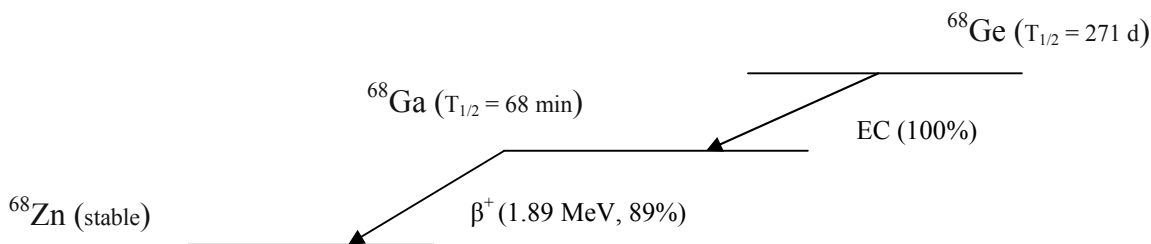


Fig. 1.4. Simplified decay scheme of ^{68}Ge

1.6.3. Yttrium-90

Yttrium-90 ($Z = 39$, $[\text{Kr}] 4d^1 5s^2$) is obtained from ^{90}Sr - ^{90}Y generator where ^{90}Sr ($T_{1/2}=28.8$ y) is in secular equilibrium with its short-lived daughter radionuclide i.e. ^{90}Y ($T_{1/2}=64.1$ h) (**Fig. 1.5**). Yttrium-90 thus obtained from ^{90}Sr - ^{90}Y generator is n.c.a. grade and has high specific activity ($> 10^5$ Ci/g). The suitable nuclear decay characteristics of ^{90}Y ($T_{1/2}=64.1$ h, $E_{\beta^-} = 2.28$ MeV (β^- max) and no γ emission) make it a good candidate for delivering therapeutic radiation doses to the tumor lesions. High energy β^- emission renders it suitable for treating tumors having large volumes. However absence of γ emission makes it difficult to follow the treatment while using ^{90}Y based radiopharmaceuticals. This is taken care of by carrying out imaging by preparing the ^{111}In complex of the same molecular carrier as surrogate [26]. Like Yttrium, Indium also exhibits +3 oxidation state, however there are some minor differences in solution and

Chapter 1

coordination chemistries between these elements. The parent radioisotope, ^{90}Sr is a long-lived isotope with a hard beta emission (0.546 MeV, 100% abundance) and has been found to accumulate in skeleton being a bone-seeker. Therefore the ^{90}Y used in radiolabeling should have permissible extent of ^{90}Sr resulting from breakthrough from the ^{90}Sr - ^{90}Y generator system. The maximum permissible level of ^{90}Sr in ^{90}Y , for use in radiopharmaceutical preparation is ($\sim\text{nCi}$ for per Ci of ^{90}Y). In the present work, ^{90}Y is sourced from a generator system where ^{90}Y is separated from ^{90}Sr by electrochemical means [27]. Yttrium is a 'pseudo lanthanide' and forms stable complexes in +3 oxidation state like most of the other lanthanides. The coordination number of Y(III) ion is typically between 7 and 10 while coordination numbers of 8 and 9 are more common. Similar to that of strontium (Sr) and other lanthanides, Yttrium is also a bone seeker which makes it crucial to ensure adequate in vivo stability of the ^{90}Y -BM complex, so as to prevent undue radiation dose to non target organs resulting out of dissociation. Yttrium-90 forms thermodynamically stable complexes with macrocyclic ligands such as DOTA (1,4,7,10-tetraazacyclododecane-1,4,7,10-tetraacetic acid) and DOTMP (1,4,7,10-tetraazacyclododecane-1,4,7,10-tetramethylene-phosphonic acid). Although multidentate acyclic ligands like DTPA, EDTA also form stable complexes with ^{90}Y , they are less inert kinetically as compared to those formed by macrocyclic ones [28].

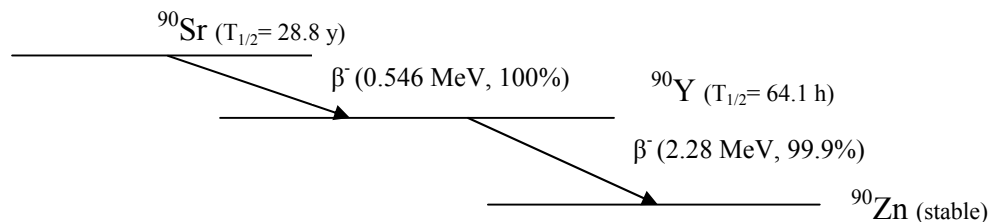


Fig. 1.5. Simplified decay scheme of ^{90}Sr

1.6.4. Lutetium-177

Lutetium-177 ($Z = 71$, $[\text{Xe}] 6s^2 4f^{14} 5d^1$) is an attractive radionuclide for the development of targeted radiotherapeutic agents owing to its suitable nuclear decay characteristics and cost-effective production feasibility using moderate flux reactors [29]. ^{177}Lu decays by the emission of β^- particles with E_{max} of 497 keV (12.2%) to stable ^{177}Hf . It also emits gamma photons in low abundances (208 keV, 11% and 113 keV, 6.4%), which are ideally suited for carrying out simultaneous scintigraphy and pharmacokinetic studies [29]. Moreover, the comparatively longer half-life (6.73 d) provides logistic advantages for distribution. A simplified decay scheme of ^{177}Lu is given below (**Fig. 1.5**).

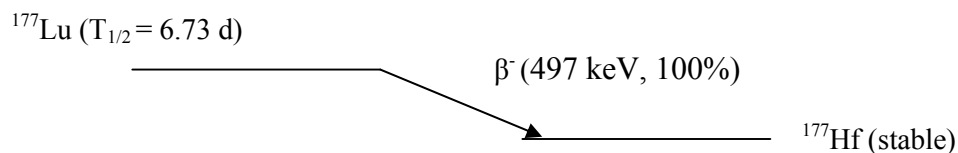


Fig. 1.6. Simplified decay scheme of ^{177}Lu

The feasibility of its large-scale production in adequately high specific activity and excellent radionuclidic purity using moderate flux reactors make ^{177}Lu an attractive choice for developing agents for targeted radiotherapy. Lutetium-177 obtained from

Chapter 1

reactors by (n, γ) reaction is in carrier added form as only a very small fraction of ^{176}Lu present in target gets converted into ^{177}Lu and after irradiation it contains large amounts of ^{176}Lu or carrier. The carrier-free ^{177}Lu can be obtained by another route which involves the neutron irradiation of ^{89}Yb yielding ^{90}Yb which undergoes beta emission to give ^{177}Lu . However the limitations of this method include difficulty in separation of chemically similar ^{177}Lu from ^{177}Yb in quantitative yields. Like yttrium, ^{177}Lu favors +3 oxidation state and exhibits coordination number 8 and 9 in its complexes. It forms very stable metal chelates with macrocyclic ligands such as DOTA (Log K=25.4) [30,31].

1.7. Biomolecules used in the present work

As discussed earlier (**Section 1.3**), a biomolecule used in a radiopharmaceutical preparation decides the target directing property and imparts the target-specificity to it. It is therefore often termed as the ‘biological vector’. A host of vectors are used in designing radiopharmaceuticals of which the most typical ones are peptides, antibodies, peptidomimetics, small receptor-specific organic molecules etc. While preparing radiopharmaceutical, it is important to bear in mind that the modification in the structure of biomolecule should cause minimal damage to its biospecificity or uptake. Radiopharmaceutical design envisages different targeting mechanisms for selective and specific localization of the radiolabeled agent in the site of interest. For aiming at specific targeting mechanism, the biological vector also need to be of a specific type and more often with better features than the naturally occurring candidate. An example of this is the choice of the peptide (Tyrosine-3-octreotate) which is an analog of somatostatin

Chapter 1

(naturally occurring 14 amino acid peptide with a short biological half-life) to target the overexpression of somatostatin receptors on neuroendocrine cancer. The work carried out and outlined in the thesis describes the use of four different types of carrier molecules viz. porphyrins, peptides, monoclonal antibodies (mAb) and nitroimidazoles for targeting three different types of cancer. In all the four cases, different BFCAs are used. The rationale w.r.t. the choice of BFCAs emerges from the complexation characteristics of the radiometal ions in the respective oxidation states. While using the four different carrier molecules, the uptake of the resultant radiolabeled species in tumor is decided by independent and unique mechanisms which are detailed individually in the respective chapters.

1.8. BFCA (bi-functional chelating agent)

Bi-functional chelating agent is an important constituent of a radiopharmaceutical design. Generally, direct incorporation of metallic radionuclides into the structure of the biomolecule as is found in case of true labels like ^{18}F Fluorodeoxyglucose though desirable is difficult and more often yields unstable metal complexes. Formation of a stable metal complex is essential to ensure the long term *in vivo* stability of the prepared radiopharmaceuticals. Thereby, metal-ligand complexes should be kinetically inert as well as thermodynamically stable. Thermodynamic stability is a measure of free energy of the complexation reaction and accounts for the stability of final product. Kinetic stability is a measure of the free energy of activation of a reaction. Out of thermodynamic and kinetic stability, latter is important w.r.t. use of radiolabeled biomolecules as there are multiple challenging ligands present *in vivo* whereby there is a possibility of occurrence

Chapter 1

of ligand exchange leading to dissociation of the metal complex and liberation of the free radiometal. The free metal thus released, in turn, accumulates in undesirable sites. When radiolabeling is not possible by direct route (e.g. isotope exchange observed mostly with radiohalogens) the radiopharmaceutical design envisages the use of a bi-functional chelating agent, (BFCA) [30-31]. As the name indicates, BFCAs are the chelating molecules which bind covalently with the biomolecule by effecting a chemical bond formation at one end via a pendant substituent (usually a $-NH_2$ or $-COOH$). The BFCAs at the other end possess a chelating moiety with suitable donor atoms such as N, O, S P etc. which form stable complexes with the radionuclide [13,30]. The common BFCAs used in the present work include macrocyclic ligands namely, *p*- NH_2 -benzyl-DOTA, *p*-NCS-benzyl-DOTA (**Fig. 1.7**).

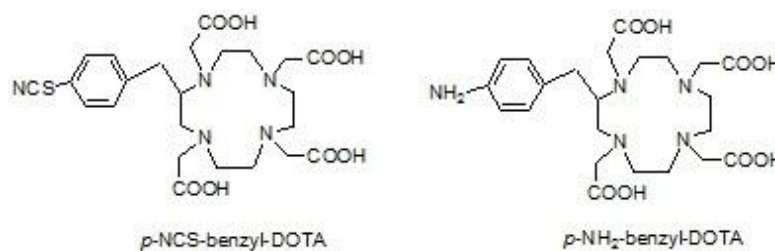


Fig. 1.7. Structures of *p*- NH_2 -benzyl-DOTA and *p*-NCS-benzyl-DOTA

1.9. Quality control of radiotracers

Since the radiopharmaceuticals are intended for administration in human patients, it is of prime importance to carry out strict quality control measures after preparation. Quality control procedures involve several specific tests and measurements that ensure the purity, potency, product identity, biologic safety and efficacy of the

Chapter 1

radiopharmaceuticals [32]. In addition to all quality control procedures common for non-radiolabeled pharmaceuticals, radiopharmaceuticals need to undergo some additional quality control measures for radionuclidic purity and radiochemical purity. The quality control tests can be categorized in two categories viz. physicochemical tests and biological tests.

1.9.1. Physicochemical tests

A number of *in vitro* physicochemical tests are performed to determine the purity and integrity of the radiopharmaceuticals. The most important among them are the determination of chemical-, radionuclidic- and radiochemical purities of the radiopharmaceutical preparations [32]. Along with these, several other parameters, such as, pH, ionic strength, osmolality, particle size (in case of radiocolloids or radiolabeled particulates), specific activity and radioactive concentration are also regularly checked [33]. Many of these tests are unique for radiopharmaceuticals because they contain radionuclides and are not applicable to conventional drugs.

1.9.1.1. Chemical purity

Chemical purity of a radiopharmaceutical is the fraction of the material in the desired chemical form, whether or not all of it is in the labeled form. Chemical impurities may come in a radiopharmaceutical preparation as some undesired species present in the ligand or radioactivity used for labeling or due to decomposition of materials before and after labeling. However, acid, alkali, buffer and stabilizing agents used in

Chapter 1

radiopharmaceutical preparations are not considered as impurities. The presence of chemical impurities may result in undesired labeled molecules and may also cause toxic effect. Purification of ligands are carried out using various techniques among which the present work involves use of column chromatography, semi-preparative and preparative TLC for purpose of purification.

1.9.1.1.1. Spectral techniques used for characterization of unlabeled precursors

Ultraviolet-visible (UV-Vis) spectra were recorded using JASCO V-530 UV/Vis spectrophotometer (Japan). Fourier transform-infra red (FT-IR) spectra were recorded in a JASCO FT/IR-420 spectrophotometer (Japan). Proton nuclear magnetic resonance (^1H -NMR) spectra were recorded in a 300 MHz Varian VXR 300s spectrometer (USA). Mass spectra were recorded using 410 Prostar binary LC mass spectrometer (Varian, USA) using electron spray ionization (ESI) technique.

1.9.1.2. Radionuclidic purity

Radionuclidic purity is defined as the fraction of the total radioactivity in the form of the desired radionuclide present in the radiopharmaceutical. Radionuclidic impurities mainly arise from extraneous nuclear reactions due to isotopic impurities in the target materials. The presence of these extraneous radionuclides as impurities increases undue radiation exposure to the patient and may also obscure scintigraphic images. Accurate determination of the level of radionuclidic impurity is very important and it is mostly done by γ ray spectrometry using a HPGe detector.

1.9.1.3. Radiochemical purity

Chapter 1

Radiochemical purity is defined as the fraction of total radioactivity in desired chemical form present in the radiopharmaceutical. Radiochemical impurities may arise during the preparation of the radiopharmaceutical or as result of its decomposition on storage due to the action of solvent, change of temperature and pH, presence of oxidizing or reducing agents and radiolysis. The presence of radiochemical impurities affects the biological efficacy of a radiopharmaceutical since the impurities may accumulate in different organs/tissue other than the target organ. This, in turn, results in unnecessary radiation dose burden to the patients and also poor quality images. A number of analytical techniques are used to detect and determine the radiochemical impurities in a given radiopharmaceutical. These include chromatography techniques such as, paper chromatography, thin layer chromatography, high performance liquid chromatography (HPLC), ion exchange chromatography, gel permeation chromatography, and also solvent extraction, paper and gel electrophoresis, precipitation etc. In present thesis, some of these techniques viz. paper and thin layer chromatography, HPLC coupled with a well-type NaI(Tl) detector (Jasco, Japan) were used to determine the extent of radiochemical impurities present in various radiochemical preparations.

1.9.1.3.1. Determination of radiochemical purity of $[^{99m}\text{Tc}(\text{CO})_3]^+$, $[^{99m}\text{TcN}]^{2+}$ and various ^{177}Lu , ^{90}Y , ^{68}Ga and $[^{99m}\text{Tc}(\text{CO})_3]^+$, $[^{99m}\text{TcN}]^{2+}$, ^{177}Lu , ^{90}Y and ^{68}Ga complexes

The radiochemical purity of $[^{99m}\text{Tc}(\text{CO})_3]^+$ core and $[^{99m}\text{Tc}(\text{CO})_3]^+$, $[^{99m}\text{TcN}]^{2+}$, ^{177}Lu , ^{90}Y and ^{68}Ga complexes was determined by high performance liquid chromatography (HPLC) using JASCO PU 2080 Plus dual pump HPLC system, Japan,

Chapter 1

with a JASCO 2075 Plus tunable absorption detector and a Gina Star radiometric detector system, using a C18 reversed phase HiQ Sil column (5 μ m, 4 x 250 mm). The gradient elution system consisted of H₂O + 0.1% trifluoroacetic acid (A) and acetonitrile + 0.1% trifluoroacetic acid (B) as mobile phase for characterization of [^{99m}TcN]²⁺, ¹⁷⁷Lu, ⁹⁰Y and ⁶⁸Ga complexes whereas aqueous 0.05M triethylammonium phosphate (TEAP) buffer (A) and methanol (B) were used as mobile phase for [^{99m}Tc(CO)₃]⁺ core and [^{99m}Tc(CO)₃]⁺ labeled complexes. Radiochemical purity of [^{99m}TcN]²⁺, ¹⁷⁷Lu, ⁹⁰Y and ⁶⁸Ga was determined using paper chromatography (PC). The radiochemical purity of free ¹⁷⁷Lu, ⁹⁰Y and ⁶⁸Ga was determined using saline as mobile phase. While radiochemical purity of [^{99m}TcN]²⁺ was determined by carrying out the PC using two different solvent systems as mobile phase viz. ethanol:CHCl₃:toluene:0.5M NH₄OAc (6:3:3:0.5 v/v) and saline.

1.9.2. Biological Quality Control Tests

Biological quality control tests of radiopharmaceuticals are essentially identical with non-radioactive pharmaceuticals and these include determination of sterility, toxicity and apyrogenicity of the radiolabeled preparations [32-35].

The present work involved the *in vitro* evaluation of the radiolabeled agents in serum and in cancer cell lines. *In vivo* evaluation of the agents was carried out in normal animals or animals bearing specific tumors.

9.2.1. Serum stability and binding studies

The *in-vitro* serum binding studies were carried out by incubating radiolabeled agents (50 μ L) with human serum (450 μ L) at 37°C up to 3 h. For determining the serum

Chapter 1

binding, serum proteins were precipitated by adding equal volume of acetonitrile to it. The mixture was subsequently centrifuged at 8000 rpm for 4 min and the supernatants as well as pellet were counted separately in a NaI(Tl) counter. Percentage serum binding was calculated from the counts observed in the both fractions. Whereas, stability of the radiolabeled preparations was studied by incubating the preparation (100 μ L) with human serum (400 μ L) at 37 °C up to 6 h. For determining the serum stability, aliquots (100 μ L) were withdrawn at regular intervals and the serum proteins were precipitated by adding equal volume of acetonitrile to it. The mixtures were subsequently centrifuged and the supernatants were analyzed by HPLC.

1.9.2.2. Biological evaluation in animal models

In the present work, animal experimentation has been carried out in Swiss mice and C57BL/6 mice. The animals were bred and reared in the laboratory animal facility of Radiation Biology and Health Sciences Division, BARC under standard management practice. Solid tumors were developed in Swiss mice by implantation of $\sim 1 \times 10^6$ HSDM1C1 murine fibrosarcoma cells whereas melanoma tumors were developed by injecting same number of viable cells in C57BL/6 mice subcutaneously on the dorsum of each animal. For carrying out imaging studies tumor cells were injected in the right thigh of each animal. The tumors were allowed to grow till they were approximately 10 mm in diameter after which the animals were used for the experiment. For the biodistribution studies, the radioactive preparation (~ 3.7 MBq per animal in 100 μ L volume) was administered intravenously through the lateral tail vein. Individual sets of animals were utilized for studying the bio-distribution at different time points. At the end of the

Chapter 1

respective time periods, the animals were sacrificed and the relevant organs were excised for measurement of retained activity. The organs were weighed and the activity associated with them was measured in a flat-bed type NaI(Tl) counter with suitable energy windows for ^{99m}Tc , ^{68}Ga , ^{177}Lu and ^{90}Y . The activity retained in each organ/tissue was expressed as percentage injected dose per gram (%ID/g). All procedures performed were in strict compliance with the national laws governing the conduct of animal experiments.

1.10. Determination of partition coefficient ($\text{LogP}_{\text{o/w}}$) of radiolabeled complexes

The partition coefficients of the radiolabeled complexes were determined in octanol-water system following a reported procedure [36]. An aliquot of the radiolabeled porphyrin derivative (100 μL) was thoroughly mixed with saline (900 μL) and octanol (1 mL) using a vortex mixer and subsequently centrifuged at 3000 rpm for 4 min so as to get a clear separation of the two layers. The octanol layer (800 μL) was withdrawn and equal volume of fresh saline was added to it. The resulting solution was centrifuged again in the same manner mentioned above. Equal aliquots from the two layers (500 μL) were withdrawn and radioactivity associated with each layer was determined using NaI (Tl) scintillation detector. Partition coefficient ($\text{LogP}_{\text{o/w}}$) of the radiolabeled porphyrin derivative was calculated from these data.

1.11. Radioactive counting

All radioactive countings were performed using a well-type NaI(Tl) scintillation counter, obtained from Electronic Corporation of India Limited (India), unless mentioned otherwise. The high performance liquid chromatography (HPLC) analyses were

Chapter 1

performed on a JASCO PU 2080 Plus dual pump HPLC system, Japan, with a JASCO 2075 Plus tunable absorption detector and a Gina Star radiometric detector system, using a C18 reversed phase HiQ Sil column (5 μ m, 4 x 250 mm). All the solvents used for HPLC were degassed and filtered prior to use and were of HPLC grade. Radioactive counting associated with the animal studies were carried out using a flat-type NaI(Tl) scintillation counter, procured from Electronics Corporation of India Limited (India).

1.12. Work carried out in the present thesis

Chapter 1 of the thesis is the Introduction which intends to provide an overview of the area of research and the work carried out. The various tumor-targeting approaches and their utilization in designing and preparation of diagnostic and therapeutic radiotracers are discussed in this chapter. The general protocols and procedures adopted for carrying out quality control studies of the radiolabeled preparations and the biological evaluations in animal models have also been described. Four different strategies for targeting the radiotracer to the tumor site, which are determined by the choice of the different types of carrier molecules, have been demonstrated in the three subsequent chapters (Chapters 2-4).

CHAPTER 2

PREPARATION OF RADIOLABELED (^{68}Ga , ^{177}Lu AND ^{90}Y)

PORPHYRIN DERIVATIVES FOR TARGETING TUMOR

Chapter 2

2.1. Introduction

This Chapter is based on the use of porphyrins as the molecular carrier in designing agents for use in targeting tumors. The rationale for their selection, possible mechanism of tumor localization has been discussed. Preparation of three different porphyrin-based radiolabeled agents and their biological evaluations in order to assess their tumor targeting potential has been discussed in **Section 2.2, 2.3 and 2.4** of this Chapter. Porphyrins are tetrapyrrolic macrocyclic aromatic compounds having 18 π -electrons and a planar, cyclic structure. Porphine is the example of simplest porphyrin molecule (**Fig. 2.1**). Porphyrins are not foreign to the human body and are found in hemoglobin, myoglobin, vitamin B12 etc. Porphyrins having a delocalized electron cloud of 18 π -electrons give rise to strong absorption in visible region (one Soret band at 400-450 nm followed by four low intensity Q bands in the range of 500-750 nm) [37,38]. The molar extinction coefficient exhibited by porphyrins is very high ($\sim 10^5 \text{ mol}^{-1} \text{ dm}^3 \text{ cm}^{-1}$) which makes them suitable candidates as photo sensitizers [38]. The tumor localizing potential of porphyrin molecules (hematoporphyrin) was first revealed by Policard in 1924 [39]. A combination of excellent photosensitizing properties and tumor localizing ability makes them good candidates for photodynamic therapy (PDT). In PDT, a photo sensitizer (PS) localized at disease site upon irradiation with a light of suitable wavelength goes from ground state to the higher singlet energy state (^1PS) and subsequently undergoes intersystem crossing to yield an excited triplet state (^3PS). Now the energy of PS in triplet excited state (^3PS) can be relieved via two pathways viz. type I and type II. In type I energy transfer takes place directly from ^3PS to cellular species via electron transfer or

Chapter 2

hydrogen atom abstraction whereas type II pathway involves direct transfer of energy between ^3PS and molecular oxygen which subsequently gets excited from ground triplet state to excited singlet state. Singlet state oxygen is highly reactive and causes oxidation of various cellular molecules and induces cell death *via* multiple pathways of apoptosis, necrosis and/or autophagy. Singlet oxygen has a very short lifespan (<40 ns in biological systems) and a limited radius of action (<20 nm). Therefore, the primary site of photodynamic damage is highly proximal to the area of its production and is dependent upon the subcellular localization of the PS [40]. PDT is more commonly used for treating cancers of head and neck [40], bladder [41], prostate [38,41]. Photofrin[®] is a porphyrin derivative which has been approved by FDA (food drug and administration) in 2003 for treatment of various kinds of cancers. Porphine is the simplest form of porphyrin (**Fig.2.1**) and can be substituted for preparation of different derivatives. Apart from these, there can be extended porphyrins, such as pthalocyanins, dihydroporphyrin (chlorin), tetrahydroporphyrin(bacteriochlorins) etc. [37-38,41,42]

Chapter 2

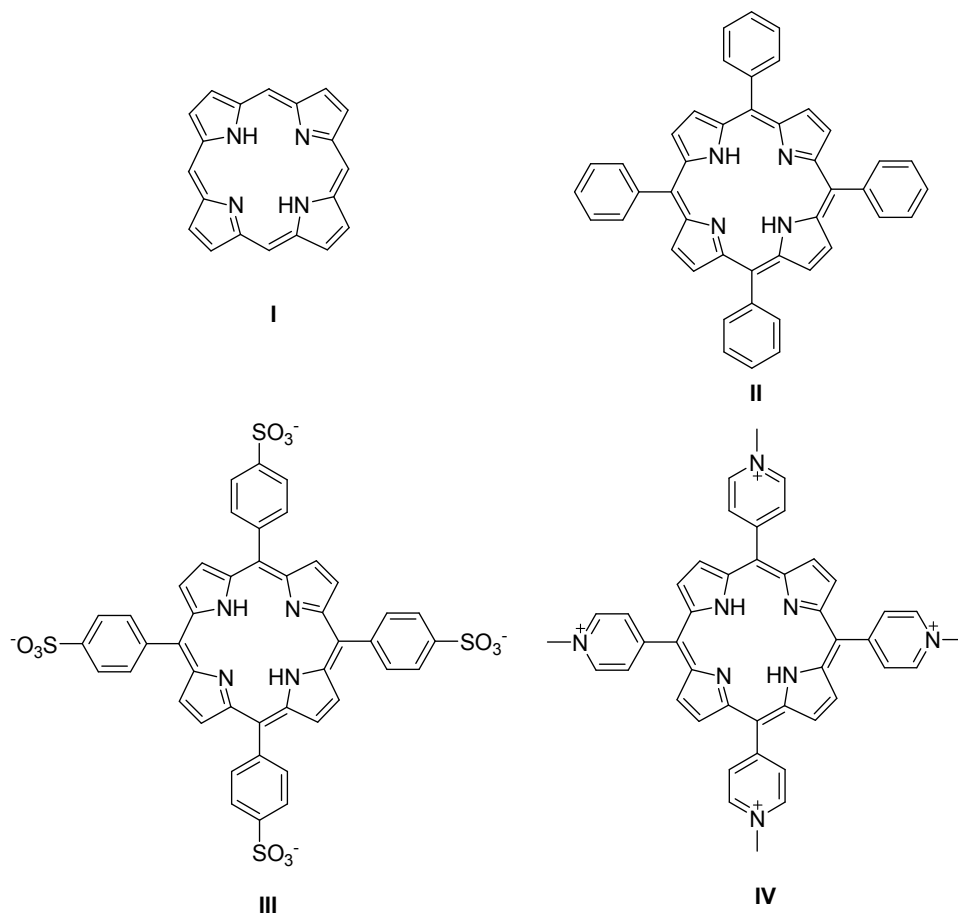


Fig. 2.1. Structures for simplest porphyrin molecule (I), lipophilic porphyrin (II) negatively charged porphyrin (III) and positively charged porphyrin (IV)

A large number of porphyrin derivatives have been prepared and tested for their ability to target tumor cells [23,43-46]. The tumor targeting ability of porphyrin derivatives have made them attractive candidates for preparation of radiolabeled porphyrins and evaluating them in different tumor models [23,43-46] has become a relevant study. However, the lipophilicity of porphyrin cores has always been a concern as it leads to uptake in non-target organs and limits their use as radiolabeled tracers for targeted tumor imaging and

Chapter 2

therapy. This problem can be circumvented by introducing hydrophilic substituents at the peripheral positions in the porphyrin molecule. The lipophilicity issue can also be addressed by preparation of charged porphyrins, both cationic as well as anionic. In case of charged porphyrins, charge is introduced either by using quarternized amines or sulphonic acid containing substituents [47]. The hydrophilicity of synthesized porphyrin derivatives is an important feature for their use as radiopharmaceuticals in order to make their administration feasible in human body as well as to reduce uptake in non-target organs. As far as targeting tumor lesions is concerned, different mechanisms have been proposed in the literature for lipophilic porphyrins and charged ones [48,49]. For lipophilic porphyrin derivatives, one among the various targeting pathways is the passive diffusion which takes the advantage of physiological and morphological differences in normal and tumor cells viz. defective cellular lining of neovasculature and poorly developed lymphatic drainage [40]. Additionally the relatively acidic intracellular microenvironment in solid tumor cells increases the hydrophobicity of macromolecules (porphyrins) with $-\text{COOH}$ group thereby enhancing their retention in the tumor cells [40]. In case of charged porphyrins (cationic) the mechanisms of tumor cell penetration involve either receptor-mediated cell internalization and/or electrostatic interactions between positive charges present on peripheral substituents in porphyrin derivatives and negative charges present on cell membrane. The most important feature of cationic porphyrins is their ability to bind with cell DNA (deoxyribonucleic acid) which makes them suitable candidates for targeting tumor cells [40,47,49].

Chapter 2

In this chapter three types of porphyrins are chosen for carrying out radiolabeling with three radioisotopes viz., ^{68}Ga , ^{177}Lu and ^{90}Y . The studies are detailed under **Sections 2.2, 2.3 and 2.4.**

2.2. Preparation and preliminary bio-evaluation of $^{177}\text{Lu}/^{90}\text{Y}$ -labeled-*p*-NCS-benzyl-DOTA coupled 5-(*p*-aminopropyleneoxyphenyl)-10,15,20-tris-(*p*-carboxymethyleneoxyphenyl)porphyrin

Radiotherapy of tumors employing open sources of radiotherapeutic agents which are systemically administered in the body is a fast emerging area in the field of nuclear medicine [50-54]. The success of therapy via systemic administration largely depends on the choice of appropriate carrier moiety having good target to non-target ratio and suitable pharmacokinetic properties that could result in good *in-vivo* tumor localization and fast clearance from non-target tissue/organs [55-56]. In this direction, a variety of structurally different substrates both synthetically obtained as well as naturally occurring ones which exhibit tumor-specificity have been used as molecular vectors for tagging with a wide variety of radioisotopes. In this respect, porphyrin and its derivatives have received considerable attention as carrier moieties as they are known to exhibit inherent affinity for localization in tumors [57-60]. Therefore, considerable effort has been devoted for developing suitable porphyrin derivatives and standardizing labeling protocol with therapeutic radionuclides in order to obtain potential agents for targeted tumor therapy [29,43,44,61-64].

The macrocyclic tetrapyrrolic ring of the porphyrin moiety is lipophilic which leads to their non-selective accumulation. Therefore, careful selection of the peripheral

Chapter 2

substituents could improve the selective tumor targeting ability of the porphyrins. It is noteworthy to mention that an optimum balance of lipophilicity, which governs the uptake and retention in the tumor with hydrophilicity that controls the clearance of the activity from the non-target organs are essential in order to have an ideal porphyrin based tumor targeting agent [29,43,44]. The substituents at the peripheral position of the porphyrin ring dramatically change its physical, chemical and biological properties [65-71]. In this respect, the use of unsymmetrical porphyrins where one peripheral substituent can be utilized to couple with the desired BFCA while the remaining three are left free to manoeuvre the balance between lipophilicity and hydrophilicity is expected to provide the better target-specificity. Working in this direction, an unsymmetrical porphyrin derivative, namely 5-(*p*-aminopropyleneoxyphenyl)-10,15,20-tri(*p*-carboxymethyleneoxyphenyl)porphyrin was synthesized as a carrier moiety for developing an agent for targeted tumor therapy. The presence of three 4-(carboxymethyleneoxy)phenyl substituents at peripheral positions are expected to enhance the hydrophilicity while the availability of a suitable substituent (amino group) at fourth position will facilitate its coupling with the BFCA to render the moiety suitable for radiolabeling. The amino group can be coupled with a variety of BFCAs. In the present case *p*-NCS-benzyl-DOTA (*p*-isothiocyanatobenzyl-1,4,7,10-tetraazacyclododecane-1,4,7,10-tetraacetic acid) was the BFCA of choice owing to its ability to form complexes with radio lanthanides having high thermodynamic stability and superior kinetic inertness [30,51]. Lutetium-177 and ⁹⁰Y were the radiolanthanides of choice as nuclear decay characteristics of both provide distinct advantages in terms of radiotherapy of tumor

Chapter 2

lesions (nuclear decay characteristics of ^{90}Y and ^{177}Lu are discussed in **Sections 1.6.3** and **1.6.4** of Chapter 1 respectively). The soft beta emission by ^{177}Lu ($E_{\beta\text{max}} = 0.497 \text{ keV}$) is suitable for treating metastatic and small sized lesions. In case of ^{90}Y the hard beta emission ($E_{\beta\text{max}} = 2.28 \text{ MeV}$) helps in the treatment of large volume of tumors where beta cross-fire effect (beta cross fire effect is due to long path length of beta particle that crosses multiple individual cells) helps to target even those tumor cells in tumor lesion where radiolabeled agent has not been able to localize [52,72-74].

2.2.1. Experimental

2.2.1.1. Materials and methods

4-hydroxybenzaldehyde, ethylbromoacetate, di-*t*-butyldicarbonate, trifluoroacetic acid, bromopropylamine and pyrrole used for the synthesis of the porphyrin derivative were purchased from Aldrich Chemical Company, USA. Propionic acid, triethylamine and nitrobenzene were obtained from S.D. Fine Chemicals, India. *p*-NCS-benzyl-DOTA was procured from Macrocyclics, USA. Pyrrole and triethylamine were freshly distilled before use. All other chemicals and solvents used for the present study were of AR grade and were purchased from reputed local manufacturers. Column chromatography and analytical thin-layer chromatography (TLC) were performed using silica gel (60-120 mesh size) and silica gel plates (silica gel 60 F₂₅₄), respectively, both of which were purchased from Merck (India). Other techniques and methods used in present chapter have been discussed in **Section 1.9.1** of Chapter 1.

2.2.1.2. Production of ^{177}Lu

Chapter 2

^{177}Lu was produced by irradiating enriched Lu_2O_3 (82% in ^{176}Lu) target at a thermal neutron flux of $1 \times 10^{14} \text{ n.cm}^{-2}.\text{s}^{-1}$ for a period of 21 d at the ‘DHRUVA’ reactor of BARC (Bhabha Atomic Research Centre). In a typical batch, 200 μg of Lu_2O_3 was irradiated in the form of a thin film coated in a quartz boat. Following irradiation, the target was cooled for 24 h to eliminate the possibility of the presence of $^{176\text{m}}\text{Lu}$ ($T_{1/2} = 3.7$ h) in processed $^{177}\text{LuCl}_3$ as radionuclidic impurity. The target was subsequently dissolved in 1 M HCl by gentle warming inside a lead-shielded plant. The resultant solution was evaporated to near-dryness and reconstituted in double distilled water. The last step involving the evaporation and reconstitution is repeated twice. Radioactivity assay as well as the radionuclidic purity of the processed ^{177}Lu was determined following the reported procedure [73].

2.2.1.3. Source of ^{90}Y

Yttrium-90 used for the present study was obtained from an electrochemical ^{90}Sr - ^{90}Y generator, developed in-house [27]. In brief, a 2M HNO_3 solution containing ^{90}Sr in equilibrium with ^{90}Y is used as an electrolyte and ^{90}Y with high radiochemical purity was obtained by a two-step electrolysis process. The first electrolysis was performed for 90 min in $^{90}\text{Sr}(\text{NO}_3)_2$ feed solution at pH 2-3 at a potential of -2.5 V with 100-200 mA current using platinum electrodes. The platinum cathode on which ^{90}Y was deposited during the first cycle of electrolysis was removed and used as an anode in the second step along with a fresh circular platinum electrode as cathode. The second electrolysis step was performed for 45 min in 3 mM HNO_3 at a potential of -2.5 V with 100 mA current. The ^{90}Y deposited on the circular cathode after the second electrolysis was dissolved in

Chapter 2

hydrochloric acid to obtain $^{90}\text{YCl}_3$, which was subsequently used for all the studies. Yttrium-90 obtained by this method had high radionuclidic purity ($(817 \pm 411 \text{ nCi})$ of ^{90}Sr per Ci of ^{90}Y) which was ascertained by extraction paper chromatography (EC). EC is a kind of paper chromatography where an extractant or chelate (2-ethyl hexyl-2-ethyl hexyl phosphonic acid in this case) is impregnated at the point of spot. ^{90}Sr remains at the point of spot while ^{90}Y forms a complex with chelate and moves with the solvent front. Yttrium-90 obtained with this level of radionuclidic purity is suitable for therapeutic applications in nuclear medicine.

2.2.1.4. Synthesis

Synthesis of 5-(*p*-aminopropyleneoxyphenyl)-10,15,20-tris-(*p*-carboxymethyleneoxyphenyl)porphyrin (2e)

Synthesis of the porphyrin derivative, namely 5-(*p*-aminopropyleneoxyphenyl)-10,15,20-tris-(*p*-carboxymethyleneoxyphenyl)porphyrin was achieved by a multi-step procedure described below:

4-carboethoxymethyleneoxybenzaldehyde (2a)

4-carboethoxymethyleneoxybenzaldehyde (**2a**) was synthesized by the addition of ethylbromoacetate (8 g, 48 mmol) in a drop-wise manner to a refluxing solution of 4-hydroxybenzaldehyde (4.8 g, 40 mmol) and anhydrous K_2CO_3 (6.9 g, 50 mmol) in dry acetone (20 mL). The reaction was continued for 8 h and the progress of the reaction was monitored by TLC using chloroform as the developing solvent. After completion of the reaction, solvent was evaporated and the residue was taken in chloroform, which was subsequently washed with brine, dried with anhydrous Na_2SO_4 and evaporated to give the

Chapter 2

crude product. The crude product was purified by silica gel column chromatography using chloroform as eluting solvent whereby pure 4-carboethoxymethyleneoxybenzaldehyde was obtained as a colorless viscous liquid (5.7 g, yield 70%).

FT-IR (ν .cm⁻¹): 1740 (>C=O)

¹H-NMR (CHCl₃, δ ppm): 1.24 (t, 3H, J = 7.8 Hz, -COOCH₂CH₃), 4.20 (q, 2H, -COOCH₂CH₃), 4.75 (s, 2H, -OCH₂), 6.97 (d, 2H, J = 7.2 Hz, ArH), 7.85 (d, 2H, J = 7.1 Hz, ArH), 9.90 (s, 1H, >CHO).

ESI-MS (m/z): (calc.) C₁₁H₁₂O₄ 208.21; (obs.) (M+1) 209.15

5,10,15-tri(p-carboethoxymethyleneoxyphenyl)-20-(p-hydroxyphenyl)porphyrin (2b)

To the refluxing mixture of 4-carboethoxymethyleneoxybenzaldehyde (**I**) (3 g, 14.4 mmol), 4-hydroxybenzaldehyde (0.59 g, 4.8 mmol), propionic acid (25 mL) and nitrobenzene (8 mL), pyrrole (1.30 g, 19.2 mmol) was added in a drop-wise manner [75]. The refluxing was continued for an additional hour and the resultant reaction mixture was allowed to cool overnight at 4°C. Subsequently nitrobenzene and propionic acid were removed from the reaction mixture by distillation under reduced pressure which gave the crude product. The crude product was purified by silica gel column chromatography using 0.2% ethyl acetate in benzene as eluting solvent whereby 182 mg of pure 5,10,15-tri(p-carboethoxymethyleneoxyphenyl)-20-(p-hydroxyphenyl)porphyrin was obtained (yield 4%).

FT-IR (KBr, ν cm⁻¹): 3210-3080 (-OH), 1740 (>C=O)

Chapter 2

$^1\text{H-NMR}$ (CDCl_3 , δ ppm): -2.89 (s, 2H, $>\text{NH}$), 1.28 (t, 9H, $J = 7.4$ Hz, $-\text{COOCH}_2\text{CH}_3$), 4.26 (q, 6H, $-\text{COOCH}_2\text{CH}_3$), 4.78 (s, 6H, $-\text{OCH}_2-$), 7.12-7.25 (m, 8H, ArH), 8.12-8.19 (m, 8H, ArH), 8.95 (8H, s, pyrrole)

ESI-MS (m/z): (calc.) $\text{C}_{56}\text{H}_{48}\text{O}_{10}\text{N}_4$ 936.34; (obs.) ($M+1$) 937.25

5-(p-aminopropyleneoxyphenyl)-10,15,20-tris-(p-carboethoxymethyleneoxyphenyl)porphyrin (2d)

The synthesis of compound (**2d**) from compound (**2b**) was carried out via the intermediate compound (**2c**). To a solution of 5,10,15-tri(*p*-carboethoxymethyleneoxyphenyl)-20-(*p*-hydroxyphenyl)porphyrin (**2b**) (131 mg, 0.14 mmol), was added *N*-Boc-3-bromopropylamine (33 mg, 0.14 mmol) [76] under refluxing condition for 8 h in presence of anhydrous K_2CO_3 (39 mg, 0.28 mmol) using dry acetone as solvent. The progress of the reaction was monitored by TLC using 0.1% of methanol in chloroform as eluting solvent. After completion of the reaction, solvent was evaporated and the residue was dissolved in chloroform. The chloroform layer was washed with brine, dried over anhydrous Na_2SO_4 , filtered and subsequently evaporated in a rotary evaporator. The crude product (**2c**) thus obtained was purified by silica gel column chromatography using 0.05% methanol in chloroform as eluting solvent. The Boc-deprotection of the intermediate (**2c**), thus obtained, was carried out by stirring a mixture of (**2c**) with trifluoroacetic acid (1 mL) in dry dichloromethane (5 mL) for a period of 3 h at room temperature. The reaction was subsequently quenched by the addition of saturated aqueous NaHCO_3 (10 mL) solution. The organic layer was separated, dried and

Chapter 2

concentrated under vacuum whereby 90 mg of the intermediate porphyrin (**2d**) (overall yield 65 %) was obtained

FT-IR (KBr, ν .cm⁻¹): 3310 (-NH₂), 1740 (>C=O), 1650(-NH bending)

¹H-NMR (CDCl₃, δ ppm): -2.89 (s, 2H, >NH), 1.28 (t, 9H, J = 7.4 Hz, -COOCH₂CH₃), 2.10 (m, 2H, -OCH₂CH₂CH₂-), 2.85 (t, 2H, J = 7.8 Hz, -OCH₂CH₂CH₂-), 3.95 (t, 2H, J = 7.4 Hz, -OCH₂CH₂CH₂-), 4.28 (q, 6H, -COOCH₂CH₃), 4.80 (s, 6H, -OCH₂-), 7.18-7.30 (m, 8H, ArH), 8.02-8.10(m, 8H, ArH), 8.90 (m, 8H, pyrrole)

ESI-MS (m/z): (calc.) C₅₉H₅₅O₁₀N₅ 994.10; (obs.) (M+Na) 1017.25

5-(p-aminopropyleneoxyphenyl)-10,15,20-tri(p-carboxymethyleneoxyphenyl) porphyrin (2e)

To the solution of porphyrin (**2e**) (90 mg, 0.09 mmol) in tetrahydrofuran (20 mL), 10 mL of 2N KOH solution was added and the solution was stirred at room temperature for 96 h. After completion of the reaction, solvent was evaporated whereby the crude product obtained was subsequently purified by column chromatography using 5% methanol in dichloromethane as the eluting solvent. This resulted in ~53 mg of pure 5-(p-aminopropyleneoxyphenyl)-10,15,20-tri(p-carboxymethyleneoxyphenyl)porphyrin (**2e**) (yield 65%).

FT-IR (KBr, ν cm⁻¹): 3250-3085 (-OH, NH₂), 1730 (>C=O), 1650 (-NH bending)

¹H-NMR (CDCl₃, δ ppm): -2.89 (s, 2H, >NH), 2.15 (m, 2H, -OCH₂CH₂CH₂-), 2.98 (t, 2H, J = 7.7 Hz, -OCH₂CH₂CH₂-), 4.10 (t, 2H, J = 7.4 Hz, -OCH₂CH₂CH₂-), 4.79 (s, 6H, -OCH₂COOH), 7.09-7.20 (m, 8H, ArH), 8.08-8.15 (m, 8H, ArH), 8.95 (s, 8H, pyrrole)

ESI-MS (m/z): (calc.) C₅₆H₄₈O₁₀N₄ 909.30, (obs.) (M+K) 948.65

Chapter 2

Synthesis of porphyrin-*p*-NCS-benzyl-DOTA conjugate (**2f**)

To the solution of porphyrin (**2e**) (11 mg, 12 μ mol) in acetonitrile (5 mL) an aqueous solution of *p*-NCS-benzyl-DOTA (8 mg, 12 μ mol) was added and the reaction mixture was stirred at room temperature for 48 h after adjusting the *pH* to 9 using 2 N KOH solution. The *pH* was maintained at 9 throughout the reaction. The progress of the reaction was monitored by TLC using 5% ammonium hydroxide in methanol as mobile phase. The crude product thus obtained was purified by preparative TLC using 3% ammonium hydroxide in methanol as mobile phase whereby 14 mg of pure porphyrin-*p*-NCS-benzyl-DOTA (**2f**) conjugate was obtained (yield ~80%).

The conjugate was characterized by FT-IR and ^1H -NMR spectroscopy and these data are presented below:

FT-IR (KBr, $\nu\text{ cm}^{-1}$): 3210-3080 (-OH, NH_2), 1725 ($>\text{C}=\text{O}$), 1650 (-NH bending)

^1H -NMR (D_2O , $\delta\text{ ppm}$): -2.80 (s, 2H, $>\text{NH}$), 2.20 (m, 2H, $-\text{OCH}_2\text{CH}_2\text{CH}_2-$), 2.72-2.74 (brs, 15H, $\text{NCH}_2\text{CH}_2\text{N}$), 2.96 (d, 2H, $J = 6.7\text{ Hz}$, $\text{NCHCH}_2-\text{C}_6\text{H}_4-$), 3.50 (s, 8H, $-\text{NCH}_2\text{COOH}$), 3.69 (t, 2H, $J = 7.5\text{ Hz}$, $-\text{OCH}_2\text{CH}_2\text{CH}_2-$), 4.25 (t, 2H, $J = 7.6\text{ Hz}$, $-\text{OCH}_2\text{CH}_2\text{CH}_2-$), 4.80 (s, 6H, $-\text{OCH}_2\text{COOH}$), 7.10-7.35 (m, 12H, ArH), 8.10-8.15 (m, 8H, ArH), 8.90 (s, 8H, pyrrole)

ESI-MS (m/z): (calc.) $\text{C}_{77}\text{H}_{76}\text{O}_{18}\text{N}_{10}\text{S}$ 1460.51; (obs.) (M+K) 1499.45

2.2.1.5. Radiolabeling of compound **2f** with ^{177}Lu and ^{90}Y

A stock solution of porphyrin-*p*-NCS-benzyl-DOTA conjugate (**2f**) was prepared by dissolving the conjugate in 0.1 M ammonium acetate buffer (*pH*=5) with a concentration of 5 mg/mL. Lutetium-177 labeling of the conjugate was achieved by

Chapter 2

incubating a mixture of 20 μL of the stock solution (containing 100 μg conjugate) with 20 μL of $^{177}\text{Lu}/^{90}\text{Y}$ activity in presence of 210 μL of 0.1 M ammonium acetate buffer ($\text{pH}=5$). Reaction was carried out for a period of 1 h at 60-70°C. Various reaction parameters, such as, amount of conjugate, incubation period and temperature was varied in order to achieve maximum complexation yields.

2.2.1.6. Quality control studies

$^{177}\text{Lu}/^{90}\text{Y}$ -labeled porphyrin-*p*-NCS-benzyl-DOTA conjugate was characterized by employing PC (paper chromatography) as well as HPLC. PC was performed using acetonitrile:water (1:1, v/v) as the eluting solvent. For HPLC studies, 20 μL of the radiolabeled conjugate was injected into the reversed phase HPLC column and the elution profile was monitored by tracking the radioactive peak in the chromatogram. The gradient system consisting of eluting solvents water (solvent A) and acetonitrile (solvent B) with 0.1% trifluoroacetic acid was used (0-4 min 5% B, 4-6 min 5% B to 20% B, 6-9 min 20% B to 60% B, 9-12 min 60% B, 12-18 min 60% B to 95% B, 18-20 min 95% B to 5% B) and the flow rate was maintained at 1 mL/min.

2.2.1.7. Stability studies

The stability of the $^{177}\text{Lu}/^{90}\text{Y}$ -labeled porphyrin-*p*-NCS-benzyl-DOTA was ascertained by storing the radiolabeled conjugate at room temperature and estimating the radiochemical purity over a period of time following the standard quality control procedures mentioned above.

2.2.1.8. Biodistribution studies

Chapter 2

Tumor targeting affinity of ^{177}Lu and ^{90}Y -labeled porphyrin-*p*-NCS-benzyl-DOTA conjugates was evaluated in fibrosarcoma tumor bearing Swiss mice. Biodistribution experiments were executed by following the procedural details mentioned in **Section 1.9.2.2** of Chapter 1. Different study points were chosen for carrying out biodistribution studies for ^{177}Lu and ^{90}Y -labeled complexes. For ^{177}Lu -labeled complex (**2g**) the post injection (p.i.) time points chosen were 30 min, 1 d and 2d while for ^{90}Y -labeled complex (**2i**) 30 min, 3 h, 1 d, 2 d and 4 d were the time points at which biodistribution studies were carried out. 5 animals were utilized at each time point.

2.2.1.9. Scintigraphy studies

Lutetium-177 has low energy and low abundance gamma emission (208 keV(13%) and 113 keV(11%)) suitable for detection by gamma camera. This imparts theranostic potential to ^{177}Lu whereby diagnosis and therapy using the same radionuclide can be carried out. The concept of theranostics unifies diagnosis and therapy providing a basis for individualized patient treatment [77]. Since ^{90}Y is pure beta emitter, imaging was not possible with ^{90}Y -labeled porphyrin-*p*-NCS-benzyl-DOTA conjugate. The accumulation and retention pattern of ^{177}Lu -labeled porphyrin-*p*-NCS-benzyl-DOTA conjugate in tumor were studied by recording serial scintigraphic images in Swiss mice (age 6-8 weeks, body weight 20-25 g) bearing fibrosarcoma tumors. The animals were injected with ~200 μL of the radiolabeled preparation (200 μCi , 7.4 MBq) through the tail vein and serial scintigraphic images were recorded at 16 h, 48 h and 72 h p.i. using a LEHR collimator. Prior to the acquisition of images, the animals were anesthetized by

Chapter 2

administering a combination of xylazine hydrochloride and ketamine hydrochloride. All the images were recorded by acquiring 500 K counts using 256×256 matrix size.

2.2.2. Results and discussion

2.2.2.1. Production of ^{177}Lu

148-185 GBq (4-5 Ci) of ^{177}Lu was produced corresponding to specific activity of 840-1051 MBq/ μg (22.7-28.4 mCi/ μg) in each batch by irradiation of 200 μg of enriched Lu_2O_3 (82% enriched in ^{176}Lu) target at a thermal neutron flux of $1 \times 10^{14} \text{ n.cm}^{-2}.\text{s}^{-1}$ for 21 d. Radionuclidic purity of ^{177}Lu produced was found to be 7.4 kBq (0.20 μCi) of $^{177\text{m}}\text{Lu}$ per 37 MBq (1 mCi) of ^{177}Lu at the end-of-bombardment. This corresponds to 0.02% of the total activity produced, thereby indicating the radionuclidic purity of ^{177}Lu to be 99.98%. No other radio-metallic impurities were observed.

2.2.2.2. Production of ^{90}Y

Yttrium-90 was obtained from an electrochemical ^{90}Sr - ^{90}Y generator, developed in-house. Y-90 was separated from ^{90}Sr once in a week and in every batch $\sim 100 \text{ mCi}$ (3.7 GBq) of ^{90}Y was produced [27]. The ‘no carrier added’ grade ^{90}Y was obtained in high radiochemical yield (>90%) and with good radionuclidic purity as presence of only $30.23 \pm 15.21 \text{ kBq}$ ($817 \pm 411 \text{ nCi}$) of ^{90}Sr per 1 Ci (37 GBq) of ^{90}Y is detected in the eluted ^{90}Y [45].

2.2.2.3. Synthesis of 5-(*p*-aminopropyleneoxyphenyl)-10,15,20-tri(*p*-carboxymethyleneoxyphenyl)porphyrin and porphyrin-*p*-NCS-benzyl-DOTA conjugate

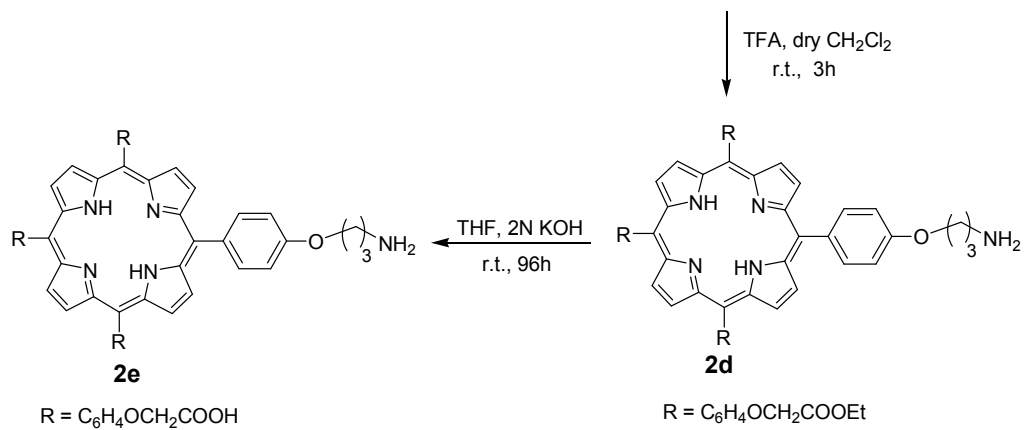
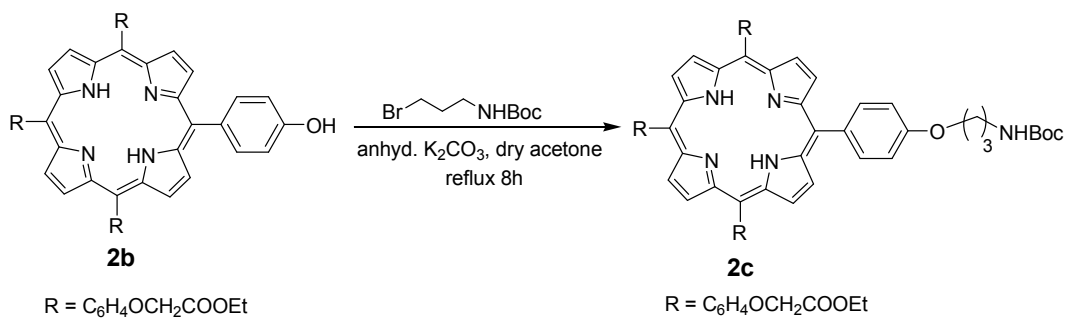
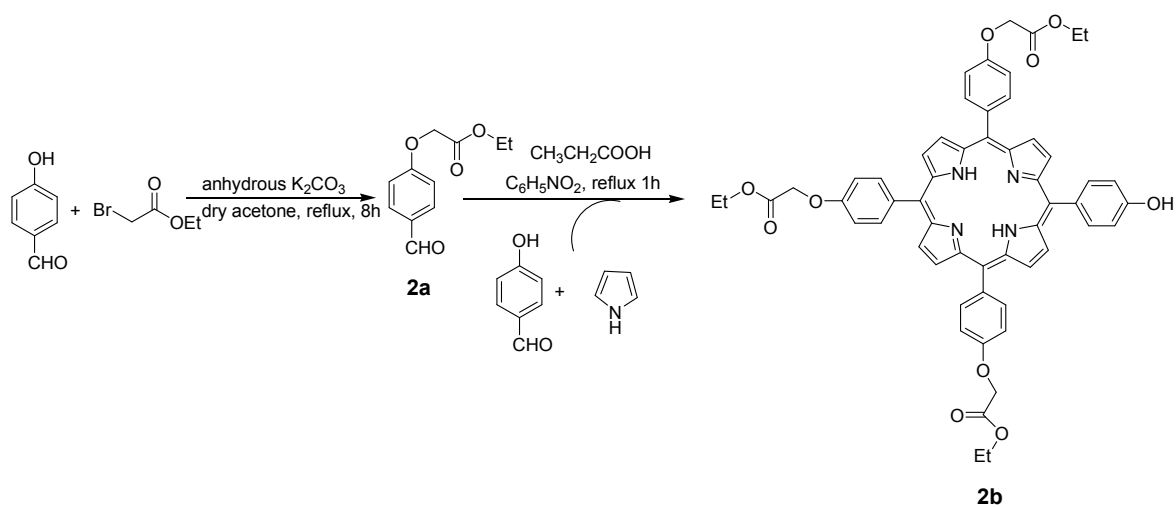
Chapter 2

5-(*p*-aminopropoxyphenyl)-10,15,20-tri(*p*-carboxymethyleneoxyphenyl) porphyrin (**2e**) was synthesized by a multi-step process (**Fig. 2.2**). In the first step, 4-hydroxybenzaldehyde was reacted with ethylbromoacetate in dry acetone using anhydrous potassium carbonate as base to yield 4-carboethoxymethyleneoxybenzaldehyde (**2a**). Synthesis of 5-(4-hydroxyphenyl)-10,15,20-tri(carboethoxymethyleneoxyphenyl)porphyrin (**2b**) was carried out by reacting 4-carboethoxymethyleneoxybenzaldehyde (**2a**), 4-hydroxybenzaldehyde and pyrrole in presence of nitrobenzene and propionic acid (**Fig. 2.2**). The synthetic procedure in the above step involved rigorous optimization of the stoichiometric ratio of the reactants to arrive at the maximum yield of the desired product. Completion of the reaction was monitored using TLC (2% ethyl acetate in benzene) and the reaction mixture was purified using column chromatography in a repetitive manner. The formation of porphyrin ring was confirmed by UV-Vis spectrum which shows the presence of four weak bands in the region of 500-650 nm (Q bands) and a high intensity band at 410 nm (Soret band), both being characteristics of the formation of the porphyrin moiety. Moreover, ¹H-NMR spectrum shows a two proton singlet at high field ($\delta = -2.89$ ppm), which provides confirmatory evidence in favor of the formation of porphyrin ring. The porphyrin derivative (**2a**) thus obtained was further modified by reaction with N-Boc-3-bromopropylamine, which, in turn, was prepared by the reaction of 3-bromopropylaminehydrobromide with di-*t*-butyldicarbonate (**Fig. 2.2**). Subsequently, the de-protection of Boc-protected porphyrin derivative (**2c**) was carried out using trifluoroacetic acid in dry dichloromethane to yield the porphyrin having –NH₂ functional

Chapter 2

group for coupling with *p*-NCS-benzyl-DOTA. The alkaline hydrolysis of three ester groups present in porphyrin derivative (**2d**) was achieved in a near-quantitative yield using 2N potassium hydroxide in tetrahydrofuran as solvent (**Fig. 2.2**). The hydrolysis of the ester group was confirmed by the IR band at 1670 cm^{-1} ($>\text{C}=\text{O}$ stretching) in place of 1735 cm^{-1} , present in the ester precursor, along with a broad peak at 3000 cm^{-1} (O-H stretching) in FT-IR spectrum. The coupling between the porphyrin derivative (**2e**) and *p*-NCS-benzyl-DOTA was achieved through a reaction in presence of 2N potassium hydroxide in acetonitrile (**Fig. 2.2**). All the intermediates formed during the synthesis of the porphyrin derivative and the final product were characterized by employing standard spectroscopic techniques such as, FT-IR and ^1H -NMR spectroscopy.

Chapter 2



Chapter 2

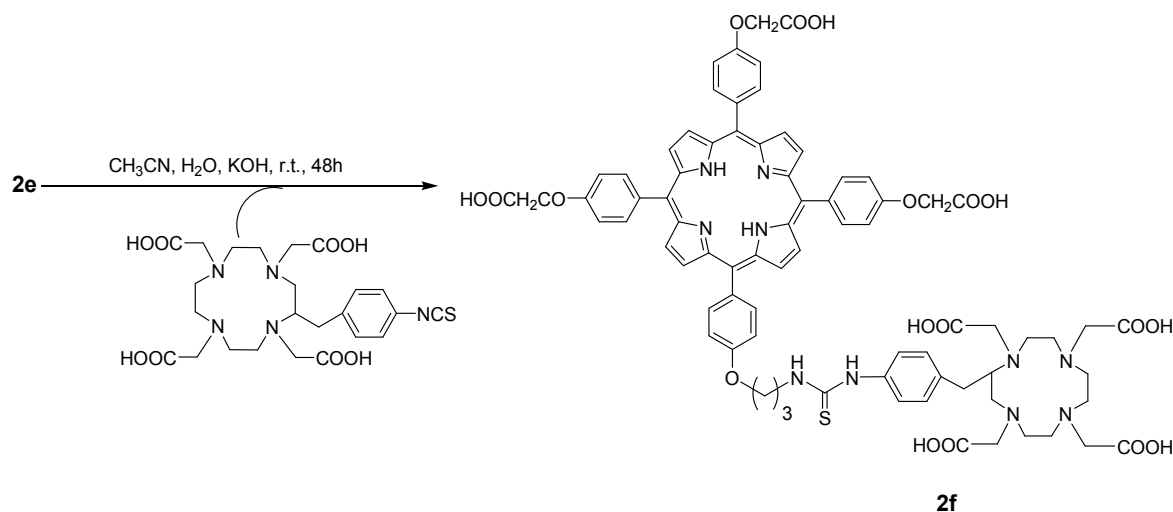


Fig. 2.2. Scheme for synthesis of porphyrin-*p*-NCS-benzyl-DOTA conjugate

2.2.2.4. Radiolabeling of porphyrin-*p*-NCS-benzyl-DOTA conjugate with ^{177}Lu

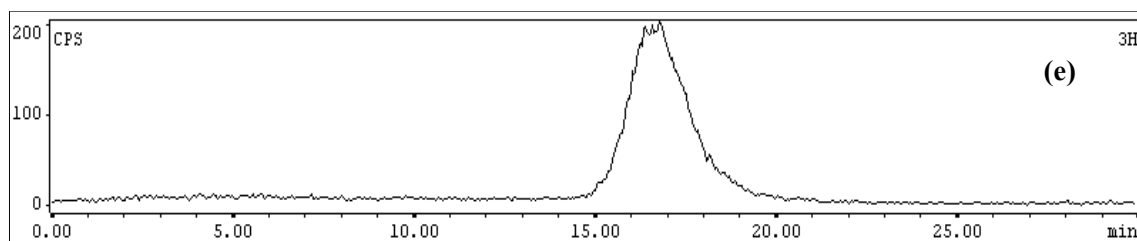
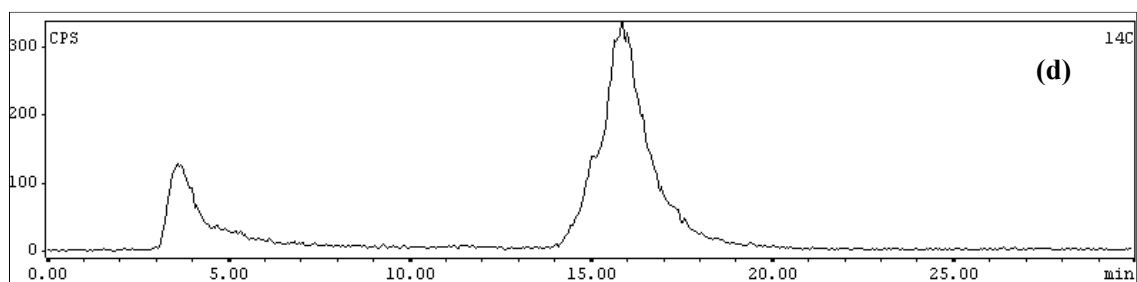
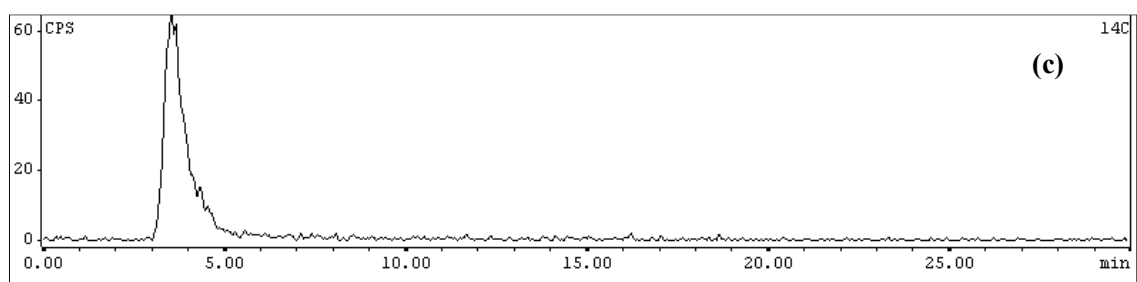
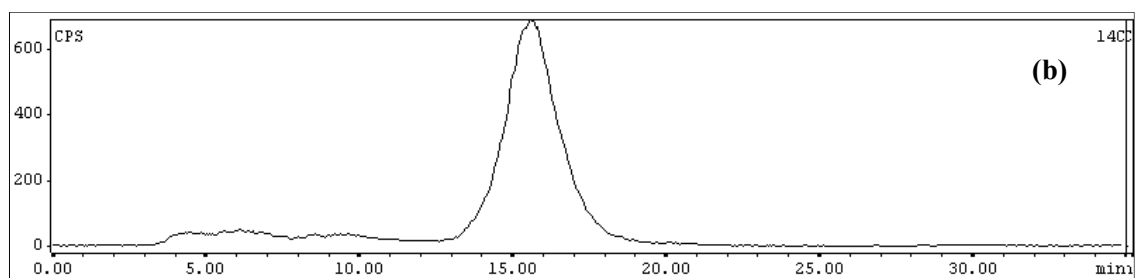
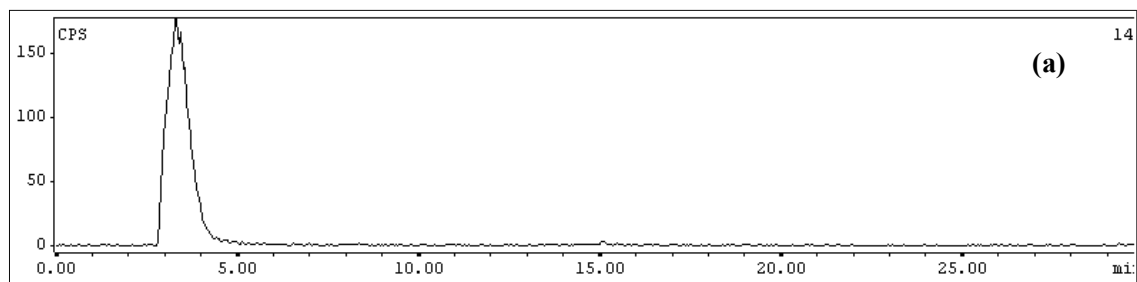
Different reaction parameters such as, amount of conjugate, incubation time and temperature were varied in order to obtain maximum yield of ^{177}Lu -labeled porphyrin-*p*-NCS-benzyl-DOTA conjugate. It was observed that >95% complexation yield could be achieved when 100 μg of the conjugate (**2f**) was incubated with ^{177}Lu at $\text{pH} \sim 5$ for a period of 1 h at 60-70°C whereas ~85% complexation yield was obtained corresponding to ^{90}Y -labeled porphyrin-*p*-NCS-benzyl-DOTA conjugate when radiolabeled under identical conditions. The ^{90}Y -labeled porphyrin-BFCA conjugate was further purified by using C-18 Sep-pak[®] cartridge. Radiochemical purity of the purified complex was determined by HPLC studies and found to be ~ 99% (**Fig. 2.3**).

Characterization of the $^{177}\text{Lu}/^{90}\text{Y}$ -labeled porphyrin-*p*-NCS-benzyl-DOTA conjugate and determination of their radiochemical purity was carried out by PC and HPLC studies. In PC carried out using acetonitrile:water (1:1, v/v) as the eluting solvent,

Chapter 2

it was observed that radiolabeled conjugates move towards the solvent front ($R_f = 0.8-0.9$) while uncomplexed $^{177}\text{Lu}/^{90}\text{Y}$ remained at the point of spotting ($R_f = 0.0$) under identical conditions. In HPLC, the radiolabeled conjugates eluted as single species with a retention time of 16 ± 0.1 min while the uncomplexed $^{177}\text{Lu}/^{90}\text{Y}$ eluted out within 3 ± 0.1 min. Typical HPLC patterns of $^{177}\text{Lu}/^{90}\text{Y}$ -labeled porphyrin-*p*-NCS-benzyl-DOTA conjugates as well as those of free ^{177}Lu and ^{90}Y are shown in **Fig. 2.3**.

Chapter 2



Chapter 2

Fig.2.3. Typical HPLC profiles of (a) $^{177}\text{LuCl}_3$ (b) ^{177}Lu -labeled porphyrin-*p*-NCS-benzyl-DOTA complex (c) $^{90}\text{YCl}_3$ (d) ^{90}Y -labeled porphyrin-*p*-NCS-benzyl-DOTA complex without purification (e) ^{90}Y -labeled porphyrin-*p*-NCS-benzyl-DOTA complex after purification

2.2.2.5. *In-vitro* stability studies

In-vitro stability of the $^{177}\text{Lu}/^{90}\text{Y}$ -labeled porphyrin-*p*-NCS-benzyl-DOTA complexes was studied by incubating them at room temperature and analyzing their radiochemical purities using the quality control method described above for different time intervals. The complex was found to retain its radiochemical purity to >90% till 3 d post-preparation, upto which the study was continued.

2.2.2.6. Biodistribution studies

Bio-evaluation of ^{177}Lu -labeled *p*-NCS-benzyl-DOTA-porphyrin conjugate was carried out in Swiss mice bearing fibrosarcoma tumors. The results of the biodistribution studies (**Table 2.1**) revealed significant tumor uptake within 30 min p.i. (5.33 ± 1.11 %IA/g). It was observed that the radiolabeled agent showed gradual clearance from all the non-target organs except kidneys and skeleton with the progress of time. Tumor uptake was also observed to decrease gradually with time. An increase in the skeletal uptake of the tracer was observed with time. It is noteworthy to mention that tumor to blood ratio was observed to increase from (0.60 ± 0.21) at 30 min p.i. to (13.56 ± 0.22) at 48 h p.i. while muscle uptake remained almost constant, however, the tumor to muscle ratio decreased from (5.67 ± 0.44) to (2.22 ± 0.12) respectively, between the same time points.

Chapter 2

The radiolabeled conjugate exhibited predominant urinary excretion, as ~70% of the injected activity was observed to be cleared via renal pathway within 24 h p.i.

The uptake of ^{90}Y -labeled porphyrin-BFCA conjugate in the tumor and different organs/tissue of Swiss mice bearing fibrosarcoma tumors at different post-injection times is shown in **Table 2.2**. The results of the biodistribution studies revealed significant tumor uptake within 30 minutes p.i. (3.46 ± 0.41 %IA/g). Accumulation of activity is also observed in various organs/tissue, such as blood (3.70 ± 0.37 %IA/g), liver (3.89 ± 1.01 %IA/g), GIT (2.71 ± 0.86 %IA/g), kidneys (6.87 ± 1.95 %IA/g), and lungs (3.68 ± 1.17 %IA/g) at this time point. However, the uptake in the non-target organs was observed to reduce considerably with the progress of time. Tumor uptake was also observed to reduce with time and found to be 0.14 ± 0.12 %IA/g at 4 days p.i. However, due to the clearance of activity from muscle and blood, tumor/blood and tumor/muscle ratios increased considerably with time. The non-accumulated activity exhibited major clearance through renal pathway owing to the hydrophilicity of the radiolabeled complex.

Chapter 2

Table 2.1. Biodistribution pattern of ^{177}Lu -labeled porphyrin-*p*-NCS-benzyl-DOTA conjugate in Swiss mice (n=5) bearing fibrosarcoma tumors

Organ/Tissue	% Injected activity in per g of organ (% IA/g)		
	30 min	24 h	48 h
Blood	8.90±0.27	0.31±0.02	0.18±0.02
Liver	6.61±0.15	3.44±0.03	4.18±0.03
Intestine	2.77±0.28	1.11±0.43	0.58±0.09
Kidneys	6.24±0.65	7.41±0.27	7.58±0.58
Stomach	2.65±0.03	0.32±0.08	0.61±0.03
Heart	4.05±0.05	0.34±0.01	0.27±0.58
Lungs	7.82±0.39	0.35±0.03	1.05±0.03
Bone	3.78±0.47	9.53±0.11	8.59±0.03
Muscle	0.94±0.10	0.40±0.03	1.10±0.61
Spleen	3.26±0.12	1.95±0.09	1.63±0.08
Tumor	5.33±1.11	4.48±0.02	2.44±0.02
Excretion ^a	47.59±0.61	69.41±0.44	71.72±0.82

% Excretion has been indirectly calculated by subtracting the activity accounted for in all the organs from total injected activity

Chapter 2

Table 2.2. Biodistribution pattern of ^{90}Y -labeled porphyrin-*p*-NCS-benzyl-DOTA complex in Swiss mice (n=5) bearing fibrosarcoma tumor

Organ / Tissue	% Injected activity per gram (% IA/g) of organ / tissue				
	30 min	3 h	1 d	2 d	4 d
Blood	3.70 ±0.37	0.21±0.10	0.17±0.12	0.12±0.05	0.00±0.00
Liver	3.89 ±1.01	2.46±0.24	0.97±0.39	0.51±0.31	0.34±0.15
GIT	2.71±0.86	1.10±0.16	0.60±0.11	0.36 ±0.20	0.05±0.02
Kidney	6.87±1.95	5.02±0.75	2.80±1.01	1.75±0.89	0.94±0.61
Stomach	1.60±0.25	0.52±0.16	0.34±0.05	0.22±0.10	0.15±0.02
Heart	1.58±0.25	0.46±0.26	0.25±0.01	0.10±0.01	0.00±0.00
Lungs	3.68±1.17	1.95±0.76	1.02±0.32	0.95±0.11	0.00±0.00
Skeleton	0.89±0.03	0.75 ±0.03	0.67±0.04	0.45±0.07	0.00±0.00
Muscle	0.29±0.11	0.09±0.10	0.01±0.08	0.01±0.05	0.00±0.00
Spleen	1.82 ±0.33	1.80±0.43	0.80±0.40	0.55±0.19	0.27±0.11
Tumor	3.46 ±0.41	1.63±0.21	1.50±0.04	1.02±0.10	0.14±0.12
Excretion [#]	69.51±1.66	83.98±0.75	90.73±1.02	93.87±1.25	97.78±0.83
Tumor/Muscle	10.85±0.87	17.10±1.02	150±0.75	102±0.95	Very high
Tumor/Blood	0.90±0.54	7.46±0.43	8.80±0.76	8.48±0.10	Very high

[#]%Excretion has been indirectly calculated by subtracting the activity accounted for all the organs from total injected activity.

2.2.2.7. Scintigraphy studies

The whole-body scintigraphic images of the Swiss mice bearing fibrosarcoma tumors recorded at 16 h, 48 h and 72 h post-administration of ^{177}Lu labeled *p*-NCS-benzyl-DOTA-porphyrin conjugate are shown in **Fig. 2.4**. The images provide

Chapter 2

documentary evidence of accumulation of the radiolabeled conjugate in tumors of the animals.

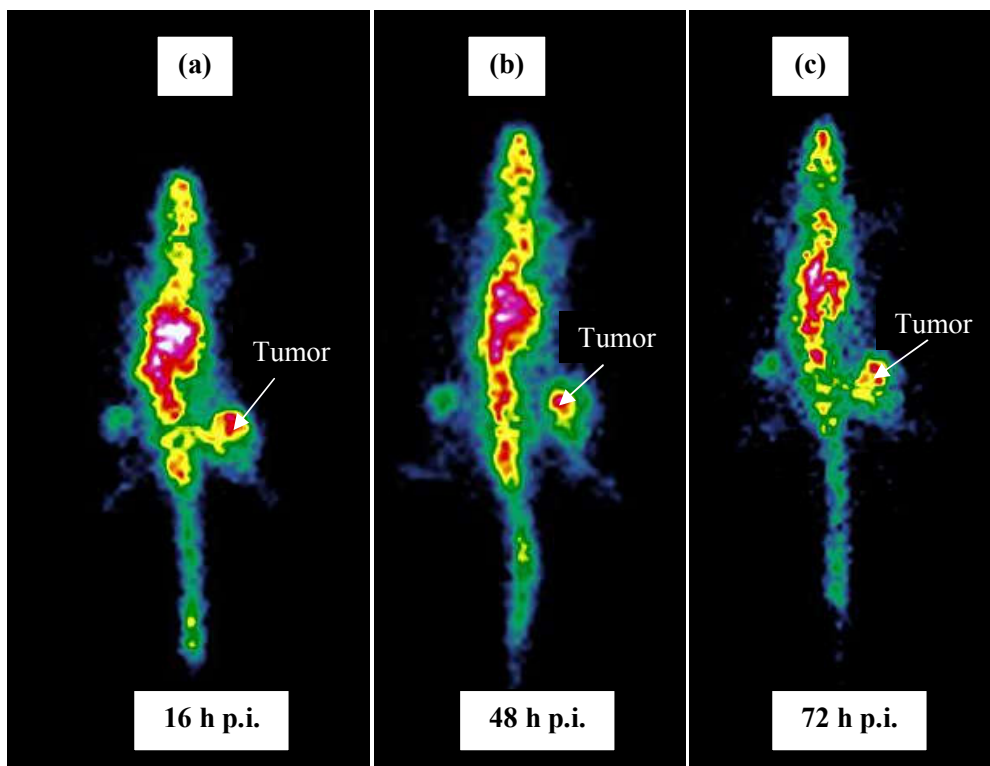


Fig. 2.4. Whole-body scintigraphic images of the Swiss mice bearing fibrosarcoma tumors (in right thigh) injected with 7.4 MBq (200 μ Ci) of ^{177}Lu -labeled porphyrin-*p*-NCS-benzyl-DOTA conjugate, recorded at (a) 16 h (b) 48 h and (c) 72 h post-administration.

2.2.3. Conclusions

The present work describes the synthesis of a water soluble unsymmetrical porphyrin conjugate with a macrocyclic bi-functional chelating agent namely *p*-NCS-benzyl-DOTA and its radiolabeling with ^{177}Lu and ^{90}Y . The porphyrin-DOTA conjugate was radiolabeled with $^{177}\text{Lu}/^{90}\text{Y}$ with high radiochemical purity. Biodistribution studies of

Chapter 2

the radiolabeled conjugates were carried out in Swiss mice bearing fibrosarcoma tumor where radiolabeled conjugate exhibited good uptake in tumor and retention therein with significant tumor to muscle ratio. The non-accumulated activity showed clearance through renal pathway. Scintigraphic studies carried out with ^{177}Lu labeled *p*-NCS-benzyl-DOTA-porphyrin complex also provided evidence in favor of significant accumulation and retention in the tumor. The observed uptake in skeleton could be attributed to presence of ~5% free ^{177}Lu in the radiolabeled preparation which was used for carrying out the biodistribution studies while no or minimal skeletal accumulation was observed in case of ^{90}Y -labeled *p*-NCS-benzyl-DOTA-porphyrin complex as radiochemical purity of radiolabeled preparation used for carrying out biodistribution studies was ~99%.

2.3. Radiosynthesis and bioevaluation of ^{68}Ga -labeled 5,10,15,20-tetra(4-methylpyridyl)porphyrin for possible application as a PET radiotracer for tumor imaging

Cationic porphyrins have the favorable features of being less lipophilic and readily soluble in water [79-82]. Additionally certain cationic porphyrins are known to be DNA intercalators [49 and 83-86]. Radiolabeling of such cationic porphyrins with suitable diagnostic or therapeutic radioisotopes could therefore result in agents with possible potential in tumor diagnosis as well as in targeted radiotherapy. Earlier efforts in this direction have demonstrated high uptake of the radiolabeled porphyrins in the tumor, albeit, with uptake in non-target organs [29,43,44,45]. In order to circumvent this

Chapter 2

problem, as well as to ensure delivery of the radiation specifically to the tumor DNA, a cationic porphyrin viz. 5,10,15,20-tetra(4-methylpyridyl)porphyrin was synthesized. It has been shown that 5,10,15,20-tetra(4-methylpyridyl)porphyrin binds to DNA with high affinity (10^6 - 10^7 M⁻¹) [86]. This porphyrin is water soluble as well as less lipophilic in nature and its intercalative property within double-stranded DNA has been well established [49]. The ability of metallated cationic porphyrins to bind with DNA base-pairs was envisaged as a strategy for designing the radiotracer for targeting the DNA of tumor lesions.

The tumor localization takes place via an initial receptor-mediated cell internalization followed by binding to DNA [85]. Moreover, Aveizer et al [49] have reported the specificity of 5,10,15,20-tetra(4-methylpyridyl)porphyrin towards binding with fibroblast growth factor and vascular endothelial growth factor receptors. All these factors provided the necessary impetus for the present study wherein this water soluble cationic porphyrin has been radiolabeled with a positron emitting radioisotope viz, ⁶⁸Ga. Gallium-68 is a PET isotope (T_{1/2}= 68 min) and offers distinctive advantages over that of the more widely used ¹⁸F, for diagnostic purposes. The major advantage of ⁶⁸Ga is the possibility of sourcing it in carrier-free form from a ⁶⁸Ge-⁶⁸Ga generator which can be procured in hospital radiopharmacy units unlike that of other PET isotopes which require an on-site cyclotron for production [53-56]. Additionally, the long shelf-life of ⁶⁸Ge-⁶⁸Ga generator, along with the possibility of more than one elutions per day, are the desirable features in envisaging ⁶⁸Ga-based radiopharmaceuticals for use in nuclear medicine [20-23].

Chapter 2

The work presented here involves the synthesis of the symmetrical meso-substituted tetracationic porphyrin namely, 5,10,15,20-tetra(4-methylpyridyl)porphyrin by following a standard two-step procedure. The porphyrin thus synthesized was radiolabeled with ^{68}Ga and its efficacy as a PET radiotracer was evaluated in biodistribution studies in Swiss mice bearing fibrosarcoma tumors.

2.3.1. Experimental

2.3.1.1. Materials and methods

4-pyridinecarboxyaldehyde and pyrrole used for the synthesis of the porphyrin derivative were purchased from Aldrich Chemical Company, USA. Propionic acid, iodomethane and nitrobenzene were obtained from S.D. Fine Chemicals, India. Pyrrole was freshly distilled before use. All other chemicals and solvents used for the present study were of AR grade and were purchased from reputed local manufacturers. Column chromatography and analytical thin-layer chromatography (TLC) were performed using silica gel (60-120 mesh size) and silica gel plates (silica gel 60 F₂₅₄), respectively, both of which were purchased from Merck (India). Other techniques and methods used in present chapter have been discussed in **Section 1.9.1.4** of Chapter 1.

Gallium-68 used in the present study was eluted from a 1.11 GBq (30 mCi) ^{68}Ge - ^{68}Ga radionuclide generator obtained from Eckert & Ziegler (Germany). Purification of the $^{68}\text{GaCl}_3$ was performed using Strata™ X-C cation exchange column procured from Phenomenex (India). All radioactive counting associated with the radiochemical studies was carried out by using well-type NaI(Tl) scintillation counter, obtained from Electronic

Chapter 2

Corporation of India Limited (India), after adjusting the baseline at 450 keV and keeping a window of 100 keV, thereby utilizing the 511 keV annihilation photo-peak of ^{68}Ga .

2.3.1.2. Synthesis

Synthesis and characterization of 5,10,15,20-tetra(4-methylpyridyl)porphyrin (2j)

Synthesis of 5,10,15,20-tetra(4-methylpyridyl)porphyrin was accomplished following a two-step procedure mentioned below:

Synthesis of 5,10,15,20-tetra(pyridyl)porphyrin (2i)

5,10,15,20-tetra(pyridyl)porphyrin was synthesized by refluxing pyridine-4-carboxyaldehyde (4.28 g, 40 mmol) and pyrrole (2.67 g, 40 mmol) in presence of nitrobenzene (10 mL) using propionic acid (50 mL) as solvent for a period of 2 h. The reaction mixture was allowed to attain room temperature and residual solvents were removed by vacuum distillation. The solid residue, thus obtained, was washed with hot water and subsequently purified by silica gel chromatography using 0.5% methanol in chloroform as the eluting solvent. This yielded 0.6 g of 5,10,15,20-tetra(pyridyl)porphyrin (yield 2.4%), which was characterized by standard spectroscopic techniques viz. UV-Vis, ^1H -NMR spectroscopy as well as by mass spectrometry.

UV-Vis, CHCl_3 ; (λ_{max} , nm): 415, 512, 544, 587, 642

^1H -NMR (CDCl_3 , δ ppm): -2.92 (s, 2H, -NH), 8.87 (s, 8H, pyrrole), 8.18 (d, 8H, $J = 5.7$ Hz, m -ArH), 9.06 (d, 8H, $J = 4.5$ Hz, o -ArH) [Fig. 2.5]

ESI-MS (m/z): (calc.) $\text{C}_{40}\text{H}_{26}\text{N}_8$ 618.7; (obs.) $(\text{M}+\text{H})^+$ 619.8

Chapter 2

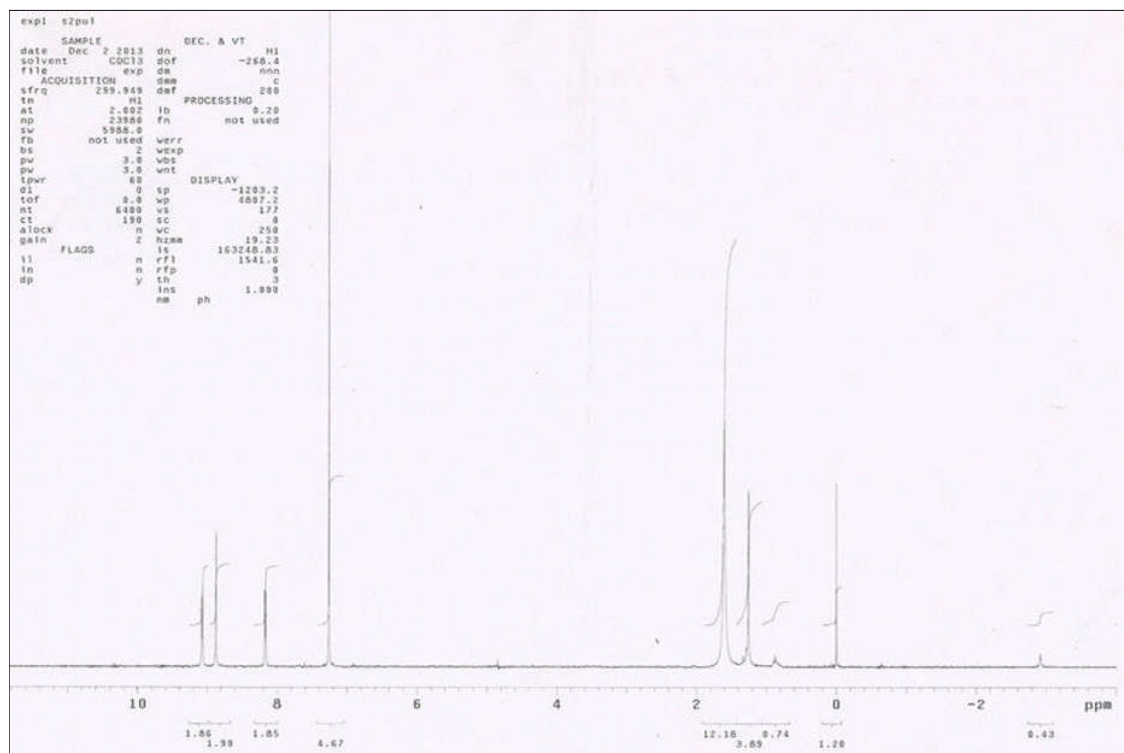


Fig. 2.5. ^1H -NMR spectrum of 5,10,15,20-tetra(pyridyl)porphyrin (**2i**)

Synthesis of 5,10,15,20-tetra(4-methylpyridyl)porphyrin (2j)

5,10,15,20-tetra(4-methylpyridyl)porphyrin was synthesized by stirring of 5,10,15,20-tetra(pyridyl)porphyrin (0.05 g, 0.08 mmol) with excess CH_3I (6.81 g, 48 mmol) in dry DMF (30 mL) at room temperature for 24 h. The reaction mixture was filtered and the precipitate, thus obtained, was thoroughly washed with dichloromethane whereby 0.05 g of 5,10,15,20-tetra(4-methylpyridyl)porphyrin (yield 60%) was obtained. The final product was characterized by standard spectroscopic techniques viz. UV-Vis, ^1H -NMR spectroscopy as well as by mass spectrometry.

UV-Vis, H_2O ; (λ_{max} , nm): 419, 515, 551, 590, 642

Chapter 2

$^1\text{H-NMR}$, DMSO, δ ppm: -3.10 (s, 2H, -NH), 4.72 (s, 12H, $^+\text{N-CH}_3$), 9.20 (s, 8H, pyrrole), 9.00 (d, 8H, $J = 6.6$ Hz, *m*-ArH), 9.47 (8H, d, $J = 6.6$ Hz, *o*-ArH) [Fig. 2.6]

ESI-MS (m/z): (calc.) $\text{C}_{44}\text{H}_{38}\text{N}_8\text{I}_4$ 1186.4; (obs.) $(\text{M-I})^+$ 1059.4

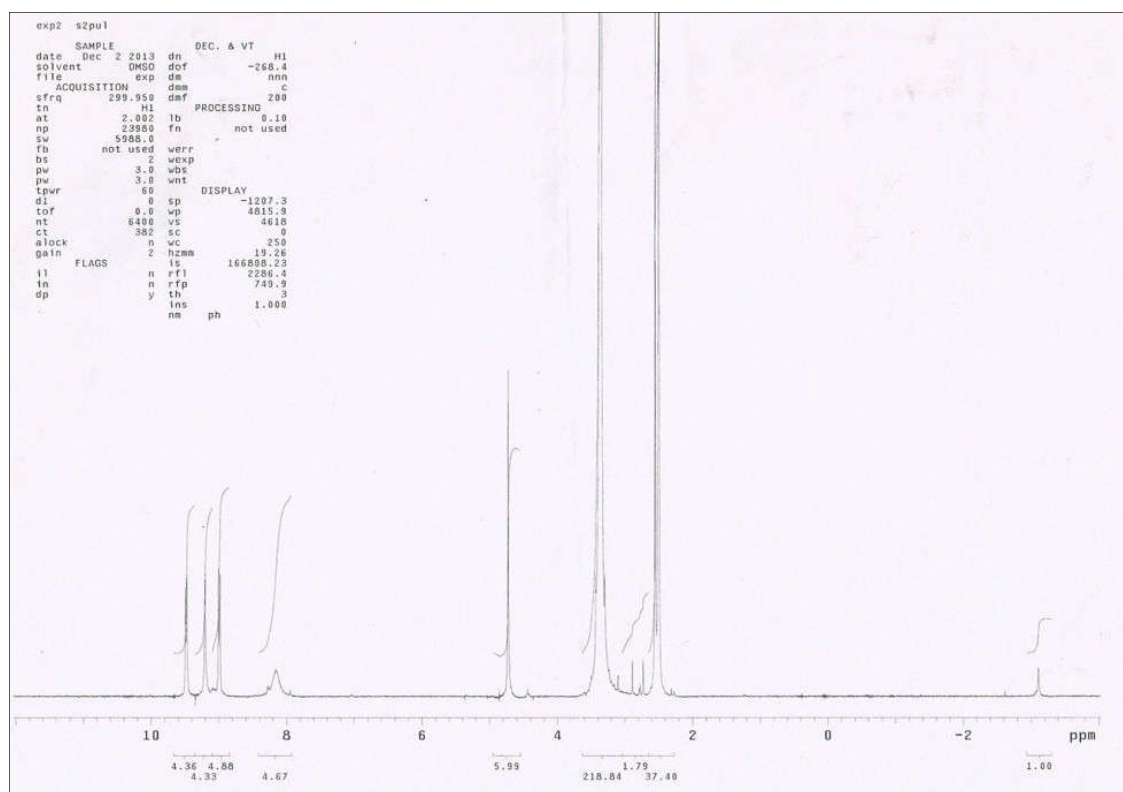


Fig. 2.6. $^1\text{H-NMR}$ spectrum of 5,10,15,20-tetra(4-methylpyridyl)porphyrin (**2j**)

2.3.1.3. Elution and purification of ^{68}Ga

Gallium-68, used for the present study, was eluted from a 1.11 GBq (30 mCi) ^{68}Ge - ^{68}Ga radionuclide generator system. The generator was eluted with 5 mL of 0.1 N HCl. $^{68}\text{GaCl}_3$, thus obtained, was further purified by using a StrataTM X-C cation exchange column prior to radiolabeling, following the procedure mentioned below. The column was pre-conditioned by passing 0.5 mL methanol followed by 0.5 mL of 0.1 N HCl prior to the loading of eluted $^{68}\text{GaCl}_3$ on the column. The column was subsequently washed

Chapter 2

with 20% 0.1 N HCl in acetone and ^{68}Ga was eluted using 0.2% 0.05 N HCl in acetone. Finally, acetone was removed by gentle warming and ^{68}Ga was reconstituted in supra-pure water, which was used for subsequent radiochemical studies.

2.3.1.4. Preparation of ^{68}Ga -labeled 5,10,15,20-tetra(4-methylpyridyl)porphyrin

Gallium-68-labeled 5,10,15,20-tetra(4-methylpyridyl)porphyrin was prepared by incubating 0.5 mg of 5,10,15,20-tetra(4-methylpyridyl)porphyrin with $^{68}\text{GaCl}_3$ (200 μL , 2 mCi, 74 MBq) in presence of sodium acetate buffer (300 μL , pH=4) in a boiling water bath for a period of 45 min. The radiolabeled porphyrin, thus obtained, was characterized by reversed phase HPLC employing gradient elution technique mentioned below.

For further purification, ^{68}Ga -labeled 5,10,15,20-tetra(4-methylpyridyl)porphyrin was loaded on a C-18 reversed phase Sep-Pak[®] cartridge. The cartridge was pre-conditioned by passing 4 mL of ethanol followed by 2 mL of double distilled water prior to the loading of radiolabeled preparation. Free GaCl_3 was eluted using 600 μL of double distilled water and subsequently radiolabeled porphyrin was eluted out from the column using 1 mL of ethanol. Ethanol present in this purified preparation was removed by gentle warming and the preparation was reconstituted with normal saline before using for biological studies.

2.3.1.5. Characterization of ^{68}Ga -labeled 5,10,15,20-tetra(4-methylpyridyl)porphyrin

Radiochemical purity of ^{68}Ga -labeled 5,10,15,20-tetra(4-methylpyridyl)porphyrin was determined by HPLC using acetonitrile (A) and water (B) mixed with 0.1% trifluoroacetic acid as the mobile phase employing gradient elution technique (0-28 min

Chapter 2

90% A, 28-30 min 10% A, 30-32 min 90% A). A flow rate of 1 mL/min was maintained. Elution profile was monitored by NaI(Tl) detector as well as UV-visible spectrophotometer.

2.3.1.6. Preparation of Ga-labeled 5,10,15,20-tetra(4-methylpyridyl)porphyrin (2k)

In order to ensure the radiometallation of the porphyrin core with ^{68}Ga , corresponding inactive gallium ($^{69/71}\text{Ga}$) labeled 5,10,15,20-tetra(4-methylpyridyl)porphyrin was prepared and characterized. Gallium complex of 5,10,15,20-tetra(4-methylpyridyl)porphyrin was prepared by heating a mixture of the porphyrin derivative (10 mg, 0.0084 mmol) and GaCl_3 (14.7 mg, 0.08 mmol) in 0.2 M sodium acetate buffer ($\text{pH}=4$) at 50 °C for 12 h. The product, thus obtained, was purified by using C-18 Sep-Pak[®] cartridges for removal of unreacted gallium following the protocol similar to the one mentioned above used for the purification of the corresponding radiolabeled analogue. The purified gallium complex of the porphyrin derivative was characterized by employing UV-Vis and ^1H -NMR spectroscopy.

UV-Vis, H_2O ; (λ_{max} , nm): 424, 518, 557

^1H -NMR, D_2O , δ ppm: 4.97 (s, 12H, $^+\text{N-CH}_3$), 9.07 (s, 8H, pyrrole), 8.93-8.99 (m, 8H, *m*-ArH), 9.23-9.32 (m, 8H, *o*-ArH)

ESI-MS (m/z): (calc.) $\text{C}_{44}\text{H}_{36}\text{N}_8\text{I}_4\text{Ga.H}_2\text{O.Cl}$ 1307.2; (obs.) $(\text{M}+\text{Na})^+$ 1330.4

2.3.1.7. Determination of partition coefficient ($\text{LogP}_{\text{o/w}}$) of ^{68}Ga -labeled 5,10,15,20-tetra(4-methylpyridyl)porphyrin

Chapter 2

The partition coefficient of the ^{68}Ga -labeled 5,10,15,20-tetra(4-methylpyridyl)porphyrin complex was determined following the protocol mentioned in **Section 1.10** of Chapter 1.

2.3.1.8. Stability of ^{68}Ga -labeled 5,10,15,20-tetra(4-methylpyridyl)porphyrin

The stability of ^{68}Ga -labeled 5,10,15,20-tetra(4-methylpyridyl)porphyrin was studied by incubating the preparation at room temperature and determining the radiochemical purity by the quality control method mentioned above at various time intervals. The serum stability of the radiolabeled preparation was also studied by following the protocol mentioned in **Section 1.9.2.1** of Chapter 1.

2.3.1.9. Biodistribution studies

The pharmacokinetics and biological distribution of ^{68}Ga -labeled porphyrin derivative were studied by carrying out biodistribution studies in Swiss mice bearing fibrosarcoma tumors following the procedure mentioned in **Section 1.9.2.2** of Chapter 1. Each animal, weighing 20-25 g, was intravenously injected with $\sim 100\ \mu\text{L}$ of the radiolabeled preparation ($\sim 50\ \mu\text{Ci}$, 1.85 MBq) through the tail vein. Biological distribution of the radiotracer was studied for three different post-injection time points viz. 30 min, 1 h and 2 h and for each time point, three animals were used.

2.3.2. Results and discussion

2.3.2.1. Synthesis and characterization of 5,10,15,20-tetra(4-methylpyridyl)porphyrin (2j)

Chapter 2

The porphyrin derivative, 5,10,15,20-tetra(4-methylpyridyl)porphyrin (**2j**) was synthesized following a two-step procedure (**Fig. 2.7**). The first step involved the formation of 5,10,15,20-tetra(pyridyl)porphyrin (**2i**) by refluxing an equimolar mixture of pyrrole and 4-pyridine carboxyaldehyde in propionic acid in presence of nitrobenzene. This resulted in the formation of the crude porphyrin derivative which was subsequently purified by column chromatography. The purified product was characterized by standard spectroscopic techniques

In the second step purified 5,10,15,20-tetra(4-methylpyridyl)porphyrin (**2i**) was allowed to react with excess of methyl iodide in dimethylformamide to yield 5,10,15,20-tetra(4-methylpyridyl)porphyrin (**2j**). The product, after purification, was characterized by standard spectroscopic techniques.

The presence of one intense Soret band at ~ 400 nm and four Q-bands in the higher wavelength region observed in the UV-Vis spectra of both compound (**2i**) and (**2j**) indicated the formation of the porphyrin moiety. This was further confirmed by the presence of proton signals corresponding to two protons in the highly up-field region ($\delta = -2.92$ and -3.10 ppm respectively) in the ^1H -NMR spectra of both compound (**2i**) and (**2j**). The observance of the ^1H -NMR signals at the expected positions as well as peak integrals provided confirmatory evidence in favour of the formation of desired porphyrin derivatives. It was further confirmed by the observance of the molecular ion peaks in the expected m/z values in the mass spectrometric analysis of the product.

Chapter 2

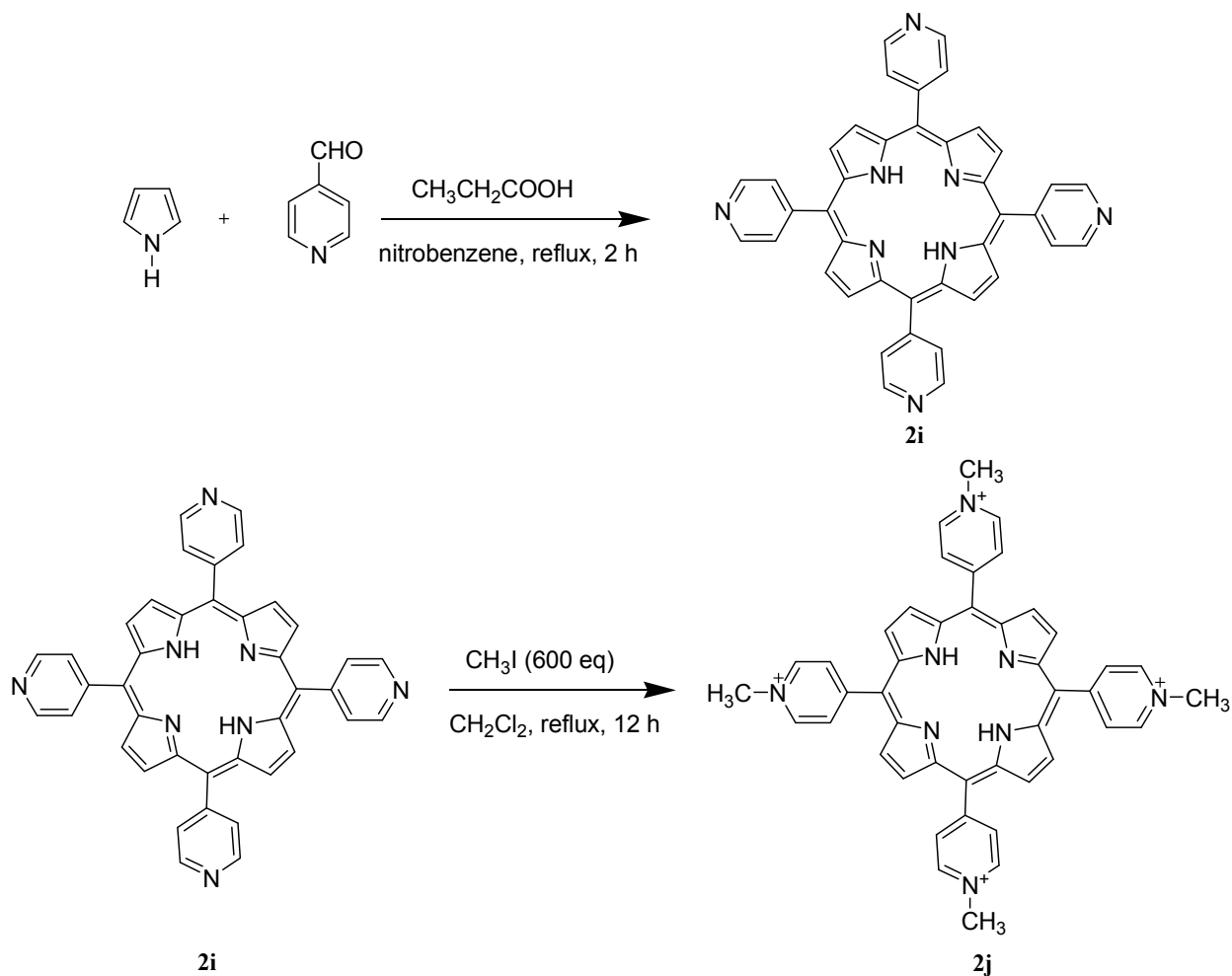


Fig. 2.7. Scheme for synthesis of 5,10,15,20-tetra(4-methylpyridyl)porphyrin

2.3.2.2. Preparation and characterization of ^{68}Ga -labeled 5,10,15,20-tetra(4-methylpyridyl)porphyrin

Several reaction parameters such as amount of ligand, incubation temperature and incubation period were varied in order to arrive at the optimized radiolabeling protocol. It was observed that a maximum complexation yield of ~90% could be obtained when 0.5 mg of the porphyrin derivative was incubated with $^{68}\text{GaCl}_3$ at 100 °C for a period of 45

Chapter 2

min. The extent of complexation was determined by HPLC studies where ^{68}Ga -labeled porphyrin derivative exhibited a retention time of 6 min whereas the free ^{68}Ga was eluted out from the column at 3.5 min under identical conditions. Typical HPLC chromatogram of free $^{68}\text{GaCl}_3$ and ^{68}Ga -labeled 5,10,15,20-tetra(4-methylpyridyl)porphyrin are shown in **Fig. 2.8. (a) and 2.7. (b)**, respectively.

The radiolabeled complex was further purified by using Sep-Pak[®] cartridges, which enabled the removal of uncomplexed $^{68}\text{GaCl}_3$ from the complex. After purification, ^{68}Ga -labeled 5,10,15,20-tetra(4-methylpyridyl)porphyrin complex could be obtained with >99% radiochemical purity. The HPLC profile of the radiolabeled complex recorded after purification is shown in **Fig. 2.8. (c)**.

Chapter 2

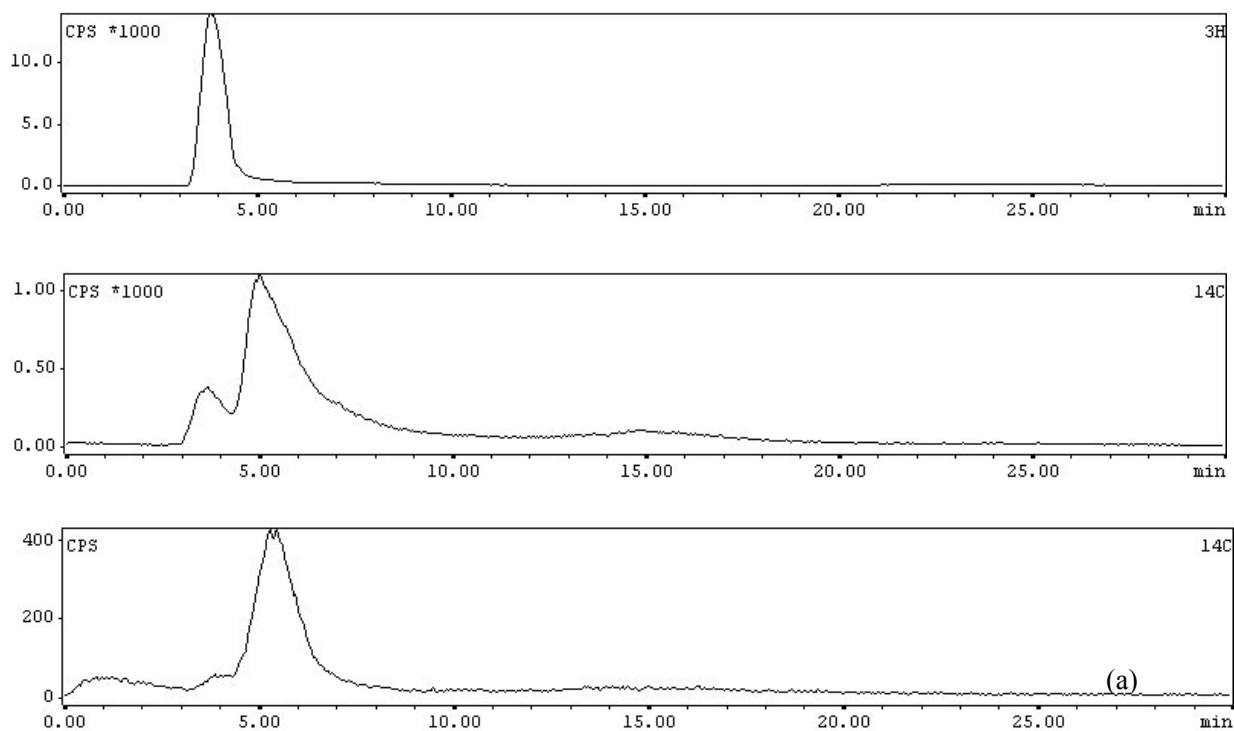


Fig.2.8. HPLC elution profiles of (a) $^{68}\text{GaCl}_3$ (b) ^{68}Ga -labeled 5,10,15,20-tetra(4-methylpyridyl)porphyrin, before purification and (c) after purification (b)

2.3.2.3. Preparation and characterization of Ga-labeled 5,10,15,20-tetra(4-methylpyridyl)porphyrin (2k)

An attempt was made to synthesize the corresponding inactive porphyrin complex with Ga in order to ensure the incorporation of Ga-68 in the core of the porphyrin moiety in the radiolabeled complex. The inactive gallium-porphyrin complex was characterized by normal spectroscopic techniques viz. UV-Visible, ^1H -NMR.

Chapter 2

The absence of two Q-bands in higher wavelength region in the UV-Vis spectrum indicated the metallation of the porphyrin core. Typical UV-Vis spectra of 5,10,15,20-tetra(pyridyl)porphyrin (**2i**), 5,10,15,20-tetra(4-methylpyridyl)porphyrin (**2j**) and Ga-labeled 5,10,15,20-tetra(4-methylpyridyl)porphyrin (**2k**) are shown in **Fig. 2.9**. Confirmatory evidence in favor of the presence of gallium in the core of the porphyrin moiety was also obtained from the ^1H -NMR spectroscopy where the signal corresponding to the two highly up-field protons was observed to disappear.

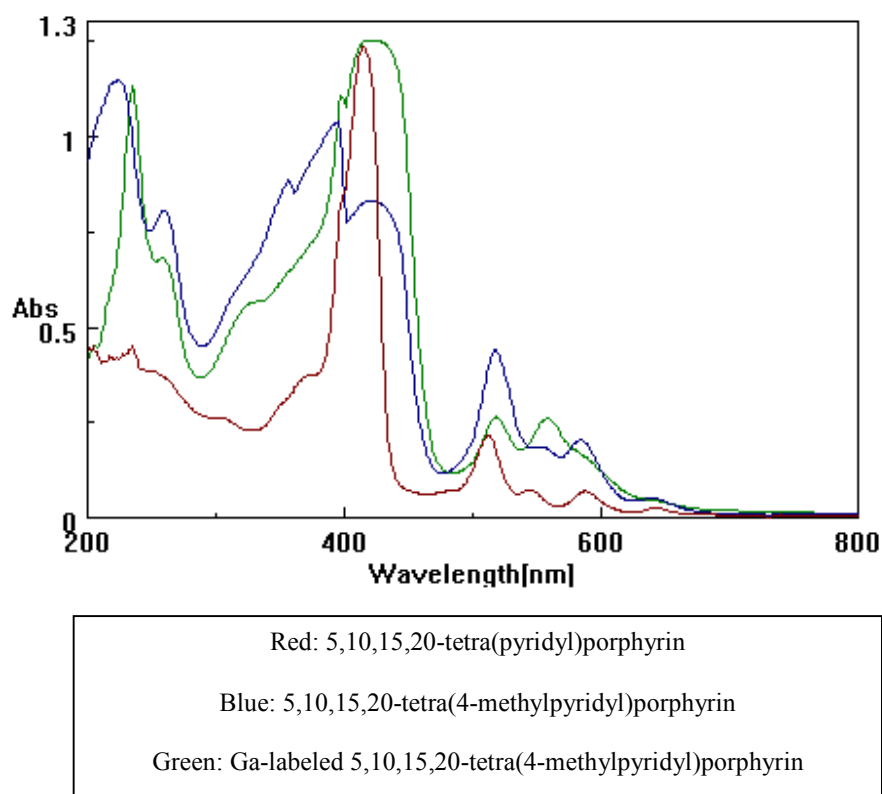


Fig. 2.9. Overlaid UV-Visible profiles of 5,10,15,20-tetra(pyridyl)porphyrin, 5,10,15,20-tetra(4-methylpyridyl)porphyrin and Ga-labeled 5,10,15,20-tetra(4-methylpyridyl)porphyrin

Chapter 2

2.3.2.4. Stability of ^{68}Ga -labeled 5,10,15,20-tetra(4-methylpyridyl)porphyrin

The purified ^{68}Ga -labeled 5,10,15,20-tetra(4-methylpyridyl)porphyrin complex was observed to retain its radiochemical purity to >98% at room temperature till 3 h post-preparation, up to which the stability study was continued. On the other hand, the complex retained its radiochemical purity to 98% up to 2 h post-preparation, when stored in human serum.

2.3.2.5. Determination of partition coefficient ($\text{Log } P_{o/w}$) of ^{68}Ga -labeled 5,10,15,20-tetra(4-methylpyridyl)porphyrin

The partition coefficient ($\text{Log } P_{o/w}$) of ^{68}Ga -labeled 5,10,15,20-tetra(4-methylpyridyl)porphyrin complex was found to be -4.3, which indicates the highly hydrophilic nature of the complex.

2.3.2.6. Biological studies

The results of the biodistribution studies carried out in Swiss mice bearing fibrosarcoma tumors are tabulated in **Table 2.3**. The complex exhibited significantly high tumor uptake of $(6.47 \pm 0.87) \% \text{IA/g}$ within 30 min post-administration. Significant accumulation of activity ($\% \text{IA/g}$) was also observed in several organs/tissue such as, blood (6.42 ± 0.44) lungs (4.86 ± 0.00) intestine (2.25 ± 0.42) , liver (4.80 ± 0.18) , spleen (2.06 ± 0.18) and muscles (1.46 ± 0.09) at this time point. However, initially accumulated activity, from all the organs/tissue was observed to diminish with the progress of time. Although the activity retained in the tumor also decreased with time $(6.07 \pm 0.03 \% \text{IA/g}$ and $4.48 \pm 1.11 \% \text{IA/g}$ at 1 h and 2 h post-injection, respectively), tumor to blood ratio was

Chapter 2

found to gradually increase with the passage of post-administration time (0.89 ± 0.04 , 1.80 ± 0.14 and 2.87 ± 0.47 at 30 min, 1 h and 2 h, respectively). Similarly, tumor to muscle ratio was also found to slowly improve with the progress of time (4.41 ± 0.62 , 6.34 ± 1.10 and 6.99 ± 1.63 at 30 min, 1 h and 2 h, respectively). The high uptake in the kidneys observed throughout the period of study is probably due to the excretion of the non-accumulated activity via the renal pathway. This may be due to the highly hydrophilic nature of the radiolabeled porphyrin derivative, which is evident from its significantly high $\text{Log } P_{o/w}$ value of -4.3.

Chapter 2

Table 2.3. Biodistribution pattern of ^{68}Ga -labeled 5,10,15,20-tetra(4-methylpyridyl)porphyrin complex in Swiss mice (n=5) bearing fibrosarcoma tumors

Organ/ Tissue	% Injected activity/g of organ/tissue		
	(%IA/g)		
	30 min	1 h	2 h
Blood	6.42±0.44	3.53±0.37	1.42±0.24
Lungs	4.86±0.01	3.68±0.28	1.59±0.19
Heart	2.01±0.48	1.71±0.64	0.74±0.16
Stomach	1.76±0.73	0.74±0.11	0.37±0.12
Intestine	2.25±0.42	1.48±0.20	0.90±0.09
Liver	4.80±0.18	3.47±0.51	2.40±0.47
Spleen	2.06±0.18	1.60±0.12	1.01±0.21
Kidney	16.20±0.78	15.31±0.56	12.40±1.55
Muscle	1.46±0.09	0.61±0.15	0.65±0.06
Tumor	6.47±0.87	6.07±0.03	4.48±1.11
Excretion [#]	31.76±1.60	53.86±1.05	54.08±1.75
Tumor/Blood	0.89±0.04	1.80±0.14	2.87±0.47
Tumor/Muscle	4.41±0.62	6.34±1.10	6.99±1.63

[#]% Excretion has been indirectly calculated by subtracting the activity accounted for all the organs from total injected activity

Chapter 2

2.3.3. Conclusions

A cationic water-soluble porphyrin derivative, which is a known DNA intercalator, has been synthesized in-house and radiolabeled with ^{68}Ga , obtained from a commercial ^{68}Ge - ^{68}Ga generator, with high radiochemical purity. The radiolabeled porphyrin derivative, thus obtained, was found to be quite hydrophilic and exhibited adequate stability *in-vitro* as well as in human serum. Preliminary biological evaluation carried out in Swiss mice bearing fibrosarcoma tumor revealed significant uptake and retention of the radiotracer in the tumor. The non-target uptake observed in the initial time points gradually decreased with time which was reflected in the improved tumor to blood and tumor to muscle ratios achieved at the later time points. This studies indicate the potential of ^{68}Ga -labeled 5,10,15,20-tetra(4-methylpyridyl)porphyrin as a PET radiotracer for tumor imaging. However, further detailed studies are warranted to unravel the actual potential of the developed radiotracer.

2.4. Synthesis and bio-evaluation of a ^{177}Lu -labeled unsymmetrical cationic porphyrin derivative as a tumor targeting agent

Cationic porphyrins have remarkable ability to target the DNA of the tumor cells [46,49,79-86]. After preparation of a ^{68}Ga -labeled cationic porphyrin derivative namely, 5,10,15,20-tetra(*p*-N-methylpyridyl)porphyrin (**2j**) as a PET (Positron Emission Tomography) radiotracer for targeting tumor-lesions, ^{177}Lu -labeling of this cationic porphyrin derivative was envisaged with a view to preparing a radiolabeled porphyrin using a therapeutic radioisotope [23,87]. While the ionic size of Ga^{+3} (62 pm) allows

Chapter 2

direct complexation of the porphyrin moiety in the core, $^{177}\text{Lu}^{+3}$ (86 pm) labeling could only be envisaged in the peripheral residues by using a chelating molecule [20,30]. Towards this, a suitable bi-functional chelating agent (BFCA) namely, *p*-NH₂-benzyl-DOTA was chosen as the BFCA, since it is documented that this BFCA forms thermodynamically stable (Log K= 25.4) and kinetically inert complexes with ^{177}Lu [30,31]. Coupling of *p*-NH₂-benzyl-DOTA with cationic porphyrin derivative (TMP) required structural modification which was accomplished by synthesizing an unsymmetrical cationic porphyrin derivative with a side chain containing terminal carboxylic acid group. Unsymmetrical porphyrin derivative was coupled with *p*-NH₂-benzyl-DOTA via an amide bond. The potential of ^{177}Lu as a therapeutic radionuclide has already been well documented in the literature [73]. The nuclear decay characteristics of ^{177}Lu [$E_{\beta(\text{max})}(\text{keV}) = 497$, $T_{1/2} = 6.73$ d, $E_{\gamma}(\text{keV}) = 113(11\%), 208(13\%)$] are suitable for targeted therapy of small or medium sized tumors. The radionuclide can be produced with high radionuclidic purity and adequate specific activity for targeted therapy in medium flux research reactors. Moreover, the longer half-life of the radionuclide provides logistic advantages towards its distribution.

The present work involves the synthesis of an unsymmetrical cationic porphyrin derivative viz., 5-carboxymethyleneoxyphenyl-10,15,20-tri(*p*-N-methylpyridyl)porphyrin (UPTMPyA), its conjugation with *p*-NH₂-benzyl-DOTA and subsequent radiolabeling of the conjugate with ^{177}Lu . The preliminary biological evaluation of the radiolabeled conjugate was also performed in Swiss mice bearing fibrosarcoma tumors.

2.4.1. Experimental

Chapter 2

2.4.1.1. Materials and methods

4-pyridinecarboxyaldehyde, bromoethyl acetate, 4-hydroxybenzaldehyde and pyrrole used for the synthesis of the porphyrin derivative were purchased from Aldrich Chemical Company, USA. Propionic acid, iodomethane and nitrobenzene were obtained from S.D. Fine Chemicals, India. *p*-NH₂-benzyl-DOTA was procured from Macrocyclics, USA. Pyrrole was freshly distilled before use. All other chemicals and solvents used for the present study were of AR grade and were purchased from reputed local manufacturers. Column chromatography and analytical thin-layer chromatography (TLC) were performed using silica gel (60-120 mesh size) and silica gel plates (silica gel 60 F₂₅₄), respectively, both of which were purchased from Merck (India). Other techniques and methods used in present chapter have been discussed in **Section 9.1.3.1** of Chapter 1. Production and processing of ¹⁷⁷Lu used in radiolabeling experiments was carried out following procedures mentioned in **Section 2.2.1.2** of this chapter.

2.4.1.2. Synthesis

Synthesis of 5-carboxymethyleneoxyphenyl-10,15,20-tri(*p*-N-methylpyridyl) porphyrin was carried out by following a three-step synthetic procedure described below (**Fig. 2.10**).

All the intermediates and final product were characterized by employing standard spectroscopic techniques such as, FT-IR and ¹H-NMR spectroscopy as well as by ESI-MS

Synthesis of 4-carboethoxymethyleneoxybenzaldehyde (2l):

Chapter 2

4-carboethoxymethyleneoxybenzaldehyde (**2l**) was synthesized by adding ethylbromoacetate (8 g, 48 mmol) in a drop-wise manner to a refluxing solution of 4-hydroxybenzaldehyde (4.8 g, 40 mmol) and anhydrous potassium carbonate (6.9 g, 50 mmol) in dry acetone (20 mL). The reaction was continued for 8 h and the progress of the reaction was monitored by TLC using chloroform as the eluent. On completion of reaction, solvent was evaporated and the residue was taken in chloroform, washed with brine, dried under anhydrous sodium sulphate and evaporated to obtain the crude product. The crude product was purified by silica gel column chromatography using chloroform as eluting solvent whereby pure 4-carboethoxymethyleneoxybenzaldehyde was obtained as a colorless viscous liquid (5.7 g, yield 70%).

FT-IR (ν cm^{-1}): 1740 ($>\text{C}=\text{O}$)

^1H -NMR (CDCl_3 , δ ppm): 1.24 (t, 3H, $J = 7.8$ Hz, $-\text{COOCH}_2\text{CH}_3$), 4.20 (q, 2H, $-\text{COOCH}_2\text{CH}_3$), 4.75 (s, 2H, $-\text{OCH}_2$), 6.97 (d, 2H, $J = 7.2$ Hz, ArH), 7.85 (d, 2H, $J = 7.1$ Hz, ArH), 9.90 (s, 1H, $>\text{CHO}$)

ESI-MS (m/z): (calc.) $\text{C}_{11}\text{H}_{12}\text{O}_4$ 208.21; (obs.) (M+H) 209.15

Synthesis of 5-carboethoxymethyleneoxyphenyl-10,15,20-tripyridylporphyrin (2m):

5-carboethoxymethyleneoxyphenyl-10,15,20-tripyridylporphyrin (**2m**) was synthesized by refluxing a mixture of pyrrole (7.3 g, 0.09 mmol), 4-pyridenecarboxaldehyde (4.53 g, 0.07 mmol), 4-carboethoxymethyleneoxybenzaldehyde (**2l**) (5 g, 0.02 mmol), nitrobenzene (5 mL) and propionic acid (100 mL) for 2 h. The crude reaction mixture was allowed to attain room temperature after which the residual solvents were removed by distillation. The crude product thus obtained was extracted

Chapter 2

with chloroform and was further purified by silica gel chromatography using 1% methanol in chloroform as the eluting solvent, which resulted in pure 5-carboethoxymethyleneoxyphenyl-10,15,20-tripyritylporphyrin (**2m**) (0.3 mg, yield ~1.7%).

FT-IR (ν cm^{-1}): 1740 ($>\text{C}=\text{O}$)

^1H -NMR (CDCl_3 , δ ppm): -2.85 (s, 2H, -NH), 1.41 (t, 3H, $-\text{COOCH}_2\text{CH}_3$), 4.43 (q, 2H, $J = 7.2$ Hz, $-\text{COOCH}_2\text{CH}_3$), 7.44 (m, 2H, -ArH), 8.20 (d, 2H, $J = 5.4$ Hz, pyrrole), 9.06 (d, 2H, $J = 6$ Hz, pyridine)

ESI-MS (m/z): (calc.) $\text{C}_{45}\text{H}_{33}\text{N}_7\text{O}_3$ 719.7; (obs.) (M) 720.3

Synthesis of 5-carboethoxymethyleneoxyphenyl-10,15,20-tri(p-N-methylpyridyl)porphyrin (2n):

5-carboethoxymethyleneoxyphenyl-10,15,20-tris(p-N-methylpyridyl)porphyrin (**2n**) was synthesized by allowing compound 2m (0.2 g, 0.27 mmol) to react with excess of CH_3I at room temperature for 48 h. The yield of the reaction was found to be 90% (0.19 g).

FT-IR (ν cm^{-1}): 1740 ($>\text{C}=\text{O}$)

^1H -NMR (CDCl_3 , δ ppm): -2.10 (s, 2H, -NH), 1.40 (t, 3H, $J = 7.2$ Hz, $-\text{COOCH}_2\text{CH}_3$), 3.67 (s, 2H, $-\text{OCH}_2$), 4.45 (m, 2H, $-\text{COOCH}_2\text{CH}_3$), 4.53 (s, 9H, N- CH_3), 7.42 (d, 2H, $J = 9$ Hz, -ArH), 8.17 (m, 2H, -ArH), 8.43 (d, 2H, $J = 6.3$ Hz, pyrrole), 8.98 (d, 2H, $J = 6.3$ Hz, pyrrole), 9.12 (d, 6H, $J = 6.6$ Hz, pyridine), 9.39 (d, 6H, $J = 6.6$ Hz, pyridine).

ESI-MS (m/z): (calc.) $\text{C}_{48}\text{H}_{42}\text{N}_7\text{O}_3$ 764.9; (obs.) (M) 765.8, (M- CH_3) 749.5, (M-2 CH_3) 734.6

Chapter 2

Synthesis of p -NH₂-benzyl-DOTA conjugated 5-carboxymethyleneoxyphenyl-10,15,20-tri(p -N-methylpyridyl)porphyrin (2o)

The porphyrin derivative (**2n**) was conjugated with the BFCA using a two-step procedure, carried out *in-situ*, involving the hydrolysis of compound (**2n**) followed by coupling with p -NH₂-benzyl-DOTA. 5-carboxymethyleneoxyphenyl-10,15,20-tris(p -N-methylpyridyl)porphyrin (**2n**) (0.2 g, 0.27 mmol) was hydrolyzed by stirring with 2 N NaOH (5 mL) at room temperature for 48 h. A fraction of the hydrolysed compound (**2n**) was used as such for the coupling reaction with p -NH₂-benzyl-DOTA and was carried out by stirring an aqueous solution of p -NH₂-benzyl-DOTA (0.01 g, 0.02 mmol) with an aqueous solution of the hydrolysed porphyrin derivative (0.03 g, 0.04 mmol) at room temperature for a period of 48 h. The crude product thus obtained was purified by preparative TLC using 30% saturated potassium chloride solution in methanol as mobile phase whereby 0.02 g (yield ~45%) of pure porphyrin- p -NH₂-benzyl-DOTA (**2o**) conjugate was obtained. The conjugated product was characterized by FT-IR spectroscopy and ESI-MS.

FT-IR (ν cm⁻¹): 1639 (>C=O)

ESI-MS (m/z): (calc.) C₆₉H₇₀I₃N₁₂O₁₀ 1608.3; (obs.) (M+Na) 1631.6

2.4.1.3. Radiolabeling of UPTMPyA- p -NH₂-benzyl-DOTA with ¹⁷⁷LuCl₃

A stock solution of UPTMPyA- p -NH₂-benzyl-DOTA conjugate (**2o**) was prepared by dissolving the conjugate in 0.1 M ammonium acetate buffer (pH=5) with a concentration of 5 mg/mL. Lutetium-177 labeling of the conjugate was achieved by incubating a mixture of 20 μ L of the stock solution (100 μ g conjugate) with 20 μ L of

Chapter 2

$^{177}\text{LuCl}_3$ (0.4 μg , 296 MBq) in presence of 210 μL of 0.1 M ammonium acetate buffer ($\text{pH}=5$) at 80 $^\circ\text{C}$ for a period of 1 h.

2.4.1.4. Characterization of ^{177}Lu -labeled UPTMPyA-*p*-NH₂-benzyl-DOTA complex

^{177}Lu -labeled UPTMPyA-*p*-NH₂-benzyl-DOTA conjugate was characterized by HPLC. The radiolabeled conjugate (15 μL) was injected into the reverse phase HPLC column and the elution profile was monitored by tracking the radioactive peak in the chromatogram. The gradient system consisting of eluting solvents water (solvent A) and acetonitrile (solvent B) with 0.1% trifluoroacetic acid was used (0-4 min 5% B, 4-6 min 5% B to 20% B, 6-9 min 20% B to 60% B, 9-12 min 60% B, 12-18 min 60% B to 95% B, 18-20 min 95% B to 5% B) and the flow rate was maintained at 1 mL/min.

2.4.1.5. Preparation of Lu complex of UPTMPyA-*p*-NH₂-benzyl-DOTA

Preparation of inactive Lutetium complex of UPTMPyA-*p*-NH₂-benzyl-DOTA conjugate (**2o**) was attempted in order to characterize the corresponding radioactive complex. The inactive complex was prepared by refluxing UPTMPyA-*p*-NH₂-benzyl-DOTA conjugate (**2o**) (0.01 g, 0.01 mmol) with LuCl_3 (0.008 g, 0.05 mmol) in 200 μL of 0.1 M ammonium acetate buffer ($\text{pH}=5$) for a period of 2 h. The complex was characterized by HPLC by monitoring the retention time of absorption signal of Lu complex of porphyrin-*p*-NH₂-benzyl-DOTA as well as by comparing the UV-Visible profiles of UPTMPyA-*p*-NH₂-benzyl-DOTA conjugate and Lu complex of UPTMPyA-*p*-NH₂-benzyl-DOTA obtained from a UV-Visible spectrophotometer.

2.4.1.6. Determination of partition coefficient ($\text{LogP}_{\text{o/w}}$)

Chapter 2

The partition coefficient of ^{177}Lu -labeled porphyrin derivative was determined by following the protocol mentioned in **Section 1.10** of Chapter 1.

2.4.1.7. *In-vitro* serum binding and stability studies

The *in-vitro* serum binding studies were carried out by following the standard procedure described in **Section 1.9.2.1** of Chapter 1.

2.4.1.8. Biodistribution studies

The pharmacokinetics and biological distribution of ^{177}Lu -labeled porphyrin derivative were studied by carrying out biodistribution studies in Swiss mice bearing fibrosarcoma tumors. By following the procedure mentioned in **Section 1.9.2.2** of Chapter 1 biological distribution of the radiotracer was studied for four different post-administration time points viz. 30 min, 3 h, 24 h and 48 h. Five animals were used for the study for each time point.

2.4.2. Results and discussion

2.4.2.1. Production of ^{177}Lu

Production, processing and quality control studies of ^{177}Lu were carried out as per procedure mentioned in **Section 2.1.2.2** of this chapter.

2.4.2.2. Synthesis and characterization of 5-carboxymethyleneoxyphenyl-10,15,20-tri(*p*-N-methylpyridyl)porphyrin

Chapter 2

The envisaged porphyrin derivative, 5-carboxymethyleneoxyphenyl-10,15,20-tri(*p*-N-methylpyridyl)porphyrin, was synthesized following a three-step procedure using 4-hydroxybenzaldehyde as the starting material. In the first step, 4-hydroxybenzaldehyde was converted to 4-carboethoxymethyleneoxybenzaldehyde using bromoethylester under refluxing conditions. The second step of this synthetic sequence involved the formation of 5-carboethoxymethyleneoxyphenyl-10,15,20-tripyritylporphyrin (**2m**). This constitutes a crucial step as it required the careful estimation of the stoichiometric ratio of the three reactants viz. pyrrole, 4-pyridinecarboxaldehyde and 4-carboethoxymethyleneoxybenzaldehyde. The optimized stoichiometric ratio was found to be 4:3:1, respectively. However, the yield of this reaction was poor owing to the formation of various side-products [88]. The desired porphyrin derivative was purified by silica gel column chromatography and its formation was confirmed by spectroscopic techniques viz. ¹H-NMR, FT-IR and ESI-MS. The signal obtained in the highly shielded region (δ -2.85) of the ¹H-NMR corresponding to the two NH protons in the porphyrin core, indicated the formation of the porphyrin moiety, which was further confirmed by ESI-MS. In the third step, the porphyrin derivative (**2m**) was reacted with excess of CH₃I to yield the quarternized porphyrin derivative (**2n**). The downfield shift in the signal of pyridyl protons after methylation reaction in the ¹H-NMR spectrum indicated the quarternization of the pyridyl nitrogens. This was further confirmed by ESI-MS. The fourth and final step involved the *in-situ* reactions involving the hydrolysis of compound **2n** and its subsequent conjugation with *p*-NH₂-benzyl-DOTA (**Fig. 2.10**). The UPTMPyA-*p*-NH₂-benzyl-DOTA conjugate was characterized by ESI-MS.

Chapter 2

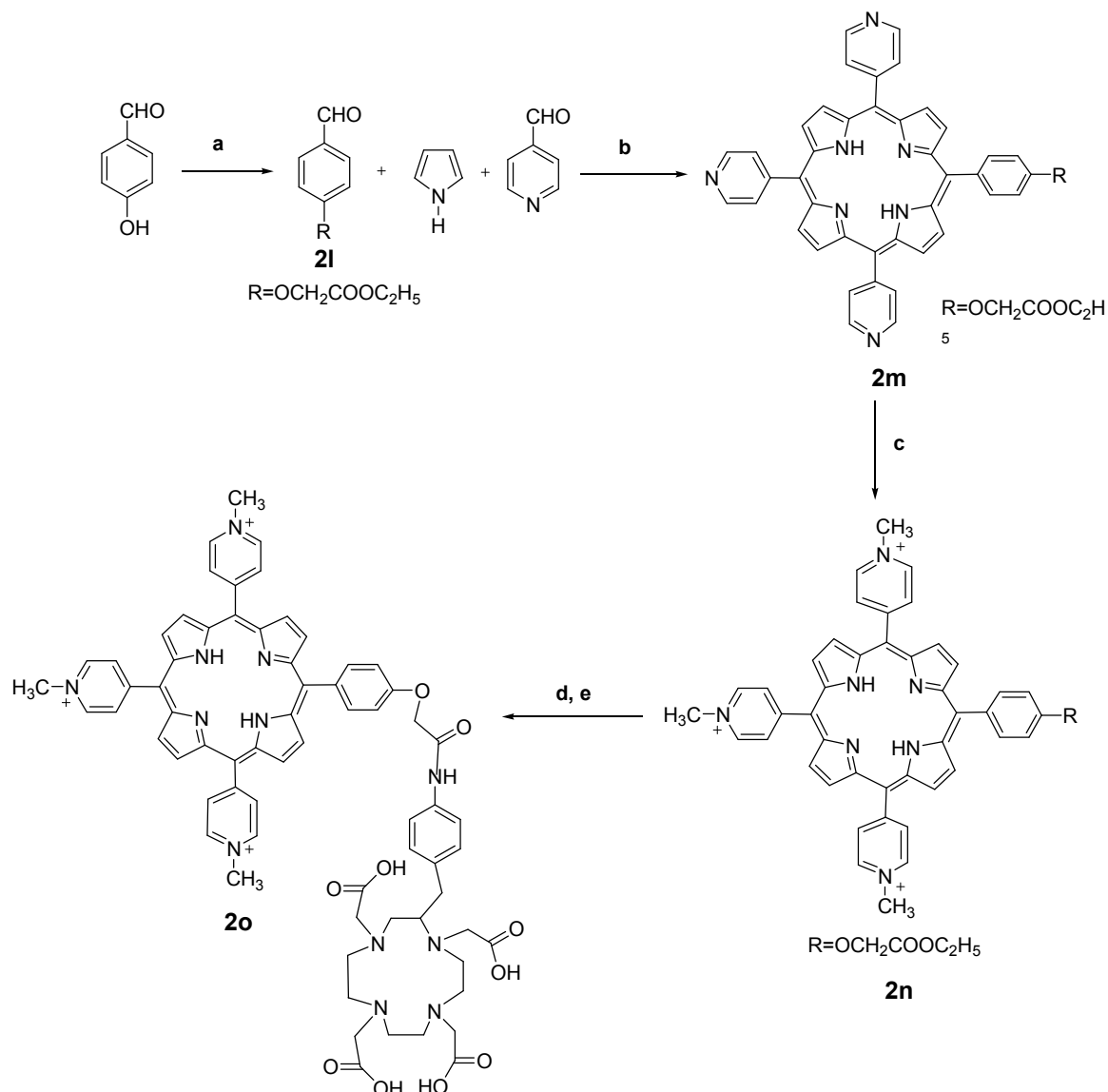


Fig.2.10. Synthesis of *p*-NH₂-benzyl-DOTA conjugated 5-carboxymethyleneoxyphenyl-10,15,20-tris(*p*-N-methylpyridyl)porphyrin (a) ethylbromoacetate, dry acetone, K₂CO₃, reflux 8 h (b) nitrobenzene, propionic acid, reflux, 2 h (c) CH₃I, R.T. stirring, 48 h (d) 2 N NaOH, R.T. stirring, 48 h (e) *p*-NH₂-benzyl-DOTA, 2 N NaOH, R.T. stirring 24 h

Chapter 2

2.4.2.3. Radiolabeling of porphyrin-*p*-NH₂-benzyl-DOTA with ¹⁷⁷LuCl₃

Radiochemical purity of the ¹⁷⁷Lu-labeled UPTMPyA-*p*-NH₂-benzyl-DOTA conjugate was determined by HPLC. In HPLC, the radiolabeled complex exhibited a retention time of 14 min while free ¹⁷⁷LuCl₃ showed a retention time of 3.5 min under identical conditions. A typical HPLC chromatogram of the radiolabeled conjugate is shown in **Fig. 2.11**. It was observed that ¹⁷⁷Lu-labeled UPTMPyA-*p*-NH₂-benzyl-DOTA conjugate could be prepared with a radiochemical purity >95% under optimized reaction conditions.

Chapter 2

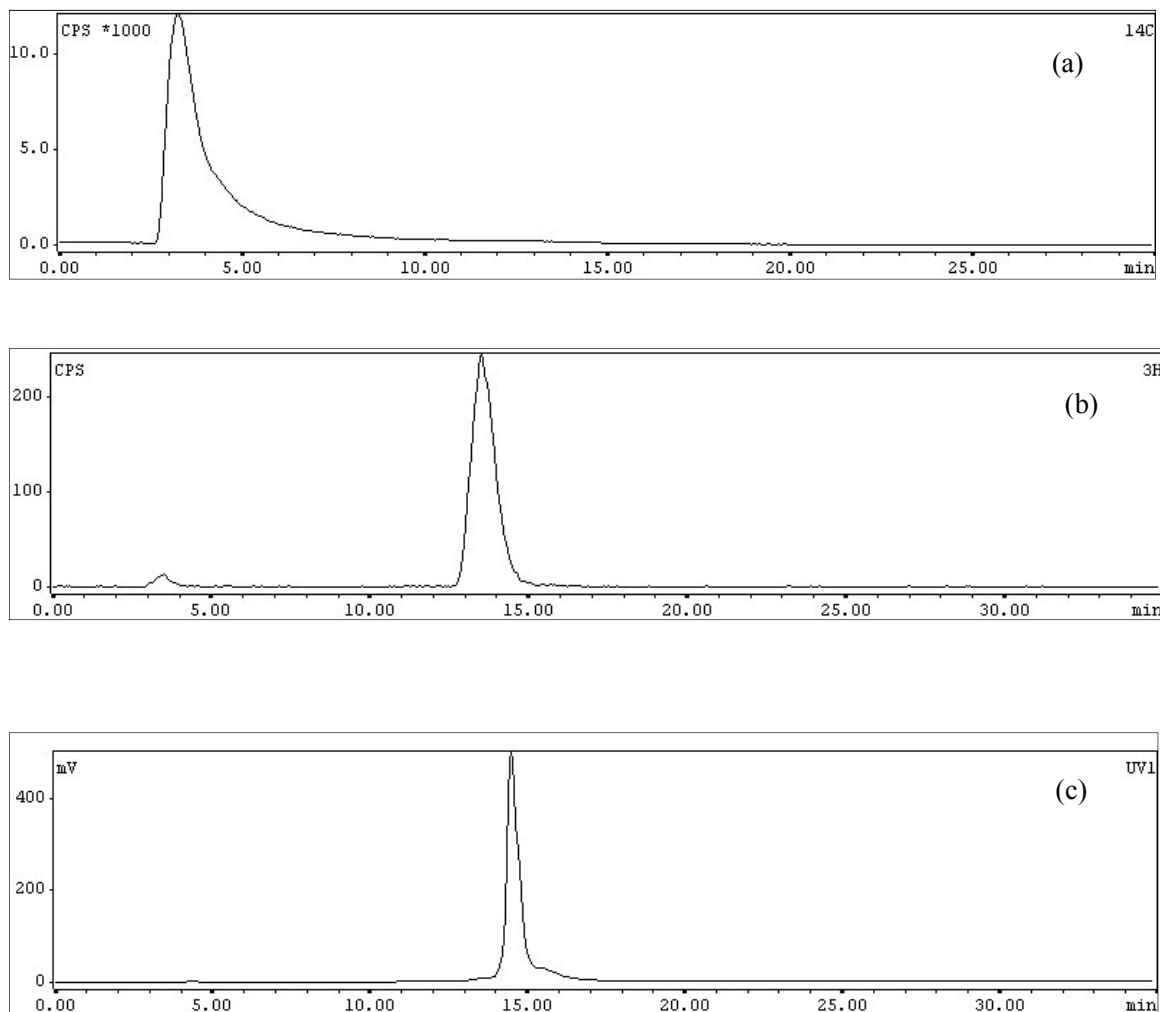


Fig. 2.11. HPLC profiles of (a) $^{177}\text{LuCl}_3$ (b) ^{177}Lu -labeled-UPTMPyA-*p*-NH₂-benzyl-DOTA complex (c) Lu-labeled-UPTMPyA-*p*-NH₂-benzyl-DOTA

2.4.2.4. Preparation of Lu complex of UPTMPyA-*p*-NH₂-benzyl-DOTA

Preparation of corresponding inactive Lu complex was attempted to draw a comparison of the HPLC chromatograms of the radiolabeled complex with that of the inactive Lu-complex. The retention time observed in the HPLC chromatogram of cold

Chapter 2

Lu-labeled porphyrin-*p*-NH₂-benzyl-DOTA was in close agreement with that of ¹⁷⁷Lu-labeled porphyrin-*p*-NH₂-benzyl-DOTA (Fig. 2.11) which indicated the structural similarity between the radiolabeled and corresponding inactive complex.

Also, UV-Vis spectra of the porphyrin-*p*-NH₂-benzyl-DOTA conjugate and Lu complex of the conjugate were recorded under identical conditions and compared with each other. It is evident from Fig. 2.12 that all the four Q bands observed in the higher wavelength region of the conjugate remained intact in the inactive Lu labeled conjugate. This provides indirect evidence towards the fact that porphyrin core remained uncomplexed in the radiolabeling while ¹⁷⁷Lu labeling took place in the peripheral DOTA core.

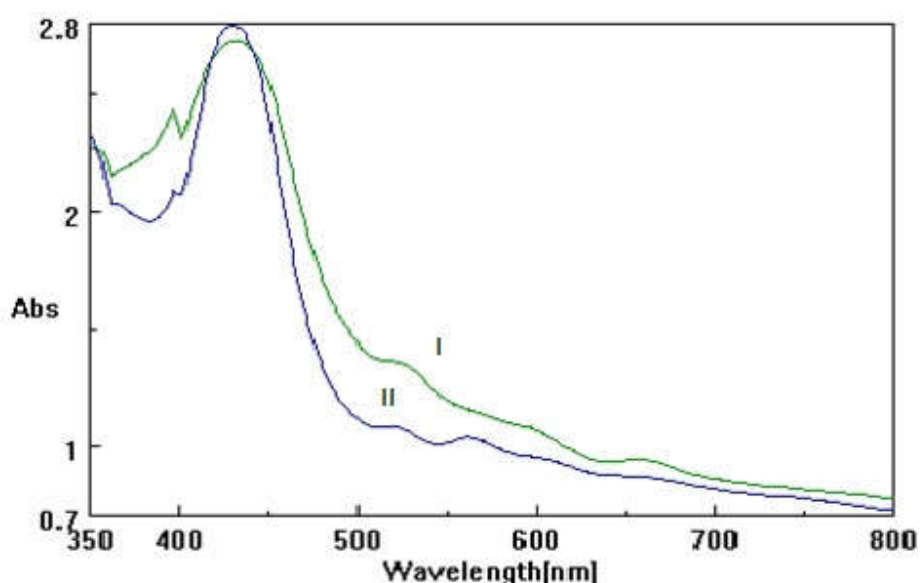


Fig. 2.12. Overlaid UV-Visible profile of (I) UPTMPyA-*p*-NH₂-benzyl-DOTA and (II) Lu-labeled-UPTMPyA-*p*-NH₂-benzyl-DOTA complex

Chapter 2

2.4.2.5. Determination of partition coefficient ($\text{Log} P_{o/w}$)

The partition coefficient ($\text{Log} P_{o/w}$) of ^{177}Lu -labeled porphyrin-*p*-NH₂-benzyl-DOTA in the octanol-water system was found to be -3.87. This indicates that the complex is highly hydrophilic in nature.

2.4.2.6. Determination of *in-vitro* serum binding and stability studies

A percentage protein binding of ~44% was shown by ^{177}Lu -labeled porphyrin-*p*-NH₂-benzyl-DOTA when incubated in serum at 37 °C for 3 h. Also, the radiolabeled porphyrin derivative was found to be stable in the serum for 6 h up to which study was carried out.

2.4.2.7. Biodistribution studies

Preliminary biological evaluation of the ^{177}Lu -labeled porphyrin-*p*-NH₂-benzyl-DOTA was carried out by biodistribution studies in Swiss mice bearing fibrosarcoma tumors. The results of the biodistribution studies in Swiss mice are tabulated in **Table 2.4**. Bio-distribution studies revealed early accumulation of the radiolabeled agent in the tumor (2.14 ± 0.48 %IA/g at 30 min p.i.) with uptake in blood (2.70 ± 0.05 %IA/g), liver (1.22 ± 0.30 %IA/g), GIT (1.24 ± 0.04 %IA/g) and kidneys (3.40 ± 1.50 %IA/g). Non-accumulated activity exhibited major clearance through renal pathway (80.46 ± 3.40). At 3 h post-injection, activity was observed to be almost cleared from blood as well as most of the organs except GIT (2.04 ± 0.90 % IA). The tumor uptake was also found to be reduced considerably at this time point (0.13 ± 0.01 %IA/g). However, tumor to blood (1.15 ± 0.01 at 30 min p.i. to 4.08 ± 0.43 at 3 h p.i.) and tumor to muscle (4.44 ± 0.23 at 30 min p.i. to

Chapter 2

very high at 3 h p.i.) ratios were found to be improved at this time point. The initially accumulated activity in the non-target organs was observed to completely clear away at 24 h post-administration. However, the tumor uptake was also observed to be substantially reduced at this time point (0.05 ± 0.00 %IA/g at 24 h p.i.). This behaviour could be attributed to the highly hydrophilic nature of the complex as is evident from $\text{LogP}_{\text{o/w}}$ value of the radiolabelled complex.

Table 2.4. Bio distribution table for ^{177}Lu -labeled-UPTMPyA-*p*-NH₂-benzyl-DOTA complex in Swiss mice (n=5) at different time points.

Organ/Tissue	%Injected activity per g of organ/tissue			
	30 min	3 h	24 h	48 h
Blood	2.70±0.05	0.03±0.00	0.00±0.00	0.00±0.00
Lungs	0.83±0.13	0.03±0.01	0.18±0.00	0.00±0.00
Heart	0.52±0.17	0.03±0.00	0.18±0.01	0.00±0.00
Stomach	0.66±0.05	0.11±0.03	0.01±0.03	0.00±0.00
GIT	1.24±0.04	2.04±0.90	0.04±0.00	0.02±0.00
Liver	1.22±0.30	0.20±0.06	0.04±0.00	0.03±0.00
Spleen	0.67±0.11	0.04±0.00	0.13±0.01	0.02±0.00
Kidney	3.40±1.50	0.63±0.20	0.37±0.03	0.20±0.00
Muscle	0.67±0.17	0.00±0.00	0.00±0.00	0.00±0.00
Bone	1.64±0.11	0.00±0.00	0.00±0.00	0.00±0.00
Tumor	2.14±0.48	0.13±0.01	0.05±0.00	0.03±0.00
Excretion [#]	80.46±3.40	93.08±2.4	95.6±2.50	99.45±0.30

Chapter 2

2.4.3. Conclusions

An unsymmetrical cationic porphyrin derivative namely, 5-carboxymethyleneoxyphenyl-10,15,20-tri(*p*-N-methylpyridyl)porphyrin was synthesized and coupled with *p*-NH₂-benzyl-DOTA. The porphyrin-*p*-NH₂-benzyl-DOTA conjugate was radiolabeled with ¹⁷⁷LuCl₃ with a radiochemical purity > 95%. The preliminary bioevaluation studies carried out in fibrosarcoma bearing Swiss mice revealed the accumulation of the complex in tumor at time point as early as 30 min p.i. with fast clearance at later time points. The uptake at 30 min p.i. could be enhanced possibly by increasing the lipophilicity of the radiotracer.

Chapter 3

PREPARATION OF RADIOLABELED MONOCLONAL ANTIBODIES AND PEPTIDES AS RECEPTOR SPECIFIC TUMOR TARGETING AGENTS

Chapter 3

In this chapter, targeting receptor overexpression on specific tumor, using two different kinds of molecular vectors viz. monoclonal antibodies and RGD peptide is discussed under two sub-headings **3(a)** and **3(b)**.

3(a) PREPARATION OF ^{177}Lu -LABELED MONOCLONAL ANTIBODIES RITUXIMAB AND TRASTUZUMAB AND THEIR PRECLINICAL EVALUATION

3a.1. Antibodies

Antibodies (Ab), also known as an immunoglobulin (Ig), are proteins produced by B-cells and are used by the immune system to identify foreign objects called antigens [89-91]. Antigens are Y-shaped molecules and consist of two heavy chains (~50 kDa each) and two light chains (~25 kDa each). Both heavy and lighter chains are held together by disulfide linkages.

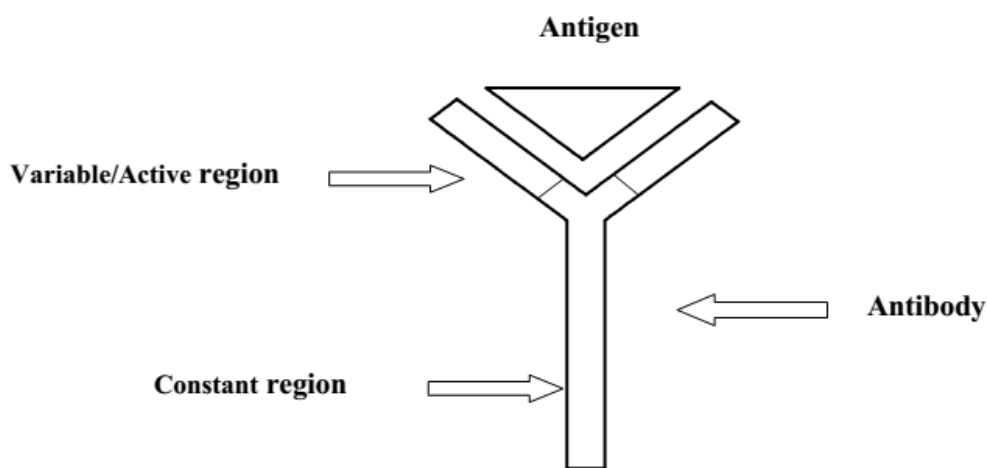


Fig. 3a.1. Schematic representation of antibody-antigen interaction

Chapter 3

Antibodies can be categorized into different classes and in placental mammals there are five types, designated as IgA, IgD, IgG, IgE and IgM, (Ig = immunoglobulin) of which IgG is the antibody most abundantly present in the blood plasma [1-3]. The antibodies have more or less similar general structure except for a portion of their tip which holds variability called as variable region whereas rest of the portion of antibody remains more or less same in different antibodies and thereby called as constant region. Another classification of antibodies is based on the extent of contributions of murine and human origin in variable region of their structure depending upon which they can be categorized as murine, chimeric, humanized and human. Antibodies are very specific with respect to their binding with antigens and interaction between antibody and antigen could be considered as a lock and key type of arrangement [89-91]. Antibodies can be monovalent (monoclonal) or polyvalent (polyclonal). Monoclonal antibodies (mAbs) are the antibodies prepared from same B-cell clone and are specific towards binding with same epitope (an epitope is the binding site on an antigen) whereas polyclonal antibodies are those which are synthesized from different B-cell clones and can target different epitopes [89-91].

3a.2. Immunotherapy and radioimmunotherapy

Paul Ehrlich's first conceived that tumors over expressing certain antigens can be targeted using specific antibodies [92]. However, the technique could not be adapted until Koehler and Milstein prepared monoclonal antibodies (mAbs) through the hybridoma technique [93]. Antibodies have been used for the treatment of various cancerous lesions and their therapeutic action is based upon two major mechanisms namely, ADCC

Chapter 3

(antibody dependent cell mediated cellular cytotoxicity) and CDC (complement dependent cytotoxicity). The treatment involving antibodies is termed as immunotherapy. Along with cold antibodies, radiolabeled antibodies have also been used for treatment of cancers. The therapy which involves the use of radiolabeled antibodies for specifically targeting tumor cells and delivering requisite radiation dose at the site of disease is known as radioimmunotherapy (RIT). Besides therapy antibodies labeled with suitable isotopes can also be used for imaging of cancerous lesions. The essence of radioimmunotherapy (RIT) involves use of monoclonal antibodies labeled with specific radionuclides, to serve as targeted molecular vehicles for the delivery of the radionuclides to the tumor sites [94,95]. The targeting potential is dependent on the interdependent factors such as the specificity and affinity of the antibody, the antigen concentration in the tumor and the radiotoxicity of the radionuclide. Initially used radiolabeled antibodies for therapy were of murine origin and have some problems such as short *in vivo* residence time, generation of human anti mouse antibody (HAMA) response [96]. Therefore, use of chimeric and humanized antibodies in place of murine antibodies for preparation of radiolabeled antibodies for treatment of cancers was proposed [96-98]. Radioimmunotherapy (RIT) offers some advantages over the use of unlabeled antibodies for the treatment of certain cancers for example lymphomas as lymphomas are very sensitive to radiation as well as cross-fire effect of the radionuclide helps to target the tumor cells within such tumor lesions which do not show the overexpression of the antigen receptors or where radiolabeled antibody has not formed the complex with antigen [98]. Additionally, owing to long half-life of antibody-antigen complex, antibody do not get internalized and remain

Chapter 3

at the cell surface for longer periods of time thereby efficiently delivering the requisite radiation dose at the tumor site. [97-99].

The selection of radionuclides for RIT also depends on factors such as half life of the radionuclide and energy of the particulate emissions with radionuclides having half lives of a few days being preferred for RIT to match with the biological uptake of antibodies. Yttrium-90 and ^{131}I are the more commonly used radionuclides for radioimmunotherapy since both have good therapeutic efficacy due to significant radiation dose which is delivered while undergoing beta decay. The longer ^{177}Lu half life (6.7 days) compared to the 2.7 day half-life for ^{90}Y offers an advantage in terms of logistics of distribution and subsequent planning of the treatment. Additional advantage in the use of ^{177}Lu is that the, low energy of the β^- particles of ^{177}Lu , lowers the bone marrow toxicity. The other advantage of the longer half life leads to reduction in the dose rate, while providing the same dose over a period of time with lower amount of activity, as well as help in eliminating the non-targeted antibody from circulation before it delivers bulk of the radiation dose to the non-targeted tissues. Also, by using ^{177}Lu , scintigraphy can be performed to quantify the localization of the radioimmunoconjugate due to presence of less abundant low energy gamma emission along with β^- emission in ^{177}Lu . The β^- particles of ^{177}Lu has maximum energy of 497 keV and an average energy of 133 keV which translates into the ability to deposit radiation dose to cells at approximately 12 cell diameters from a cell on which the immunoconjugate is targeted. The maximum cell-interaction potential is therefore expected to be approximately 50 cell diameters. The shorter range of ^{177}Lu compared to that of ^{90}Y may not as effective as in terms of dose

Chapter 3

delivery to larger tumors, but may be suitable for many small solid tumors. The shorter range β^- particles is expected to spare much of the non-diseased tissues and the lower renal toxicity of ^{177}Lu over that of ^{90}Y is an advantageous feature which has provided impetus to the development of ^{177}Lu -based mAbs [100].

These mAbs approved by the US Food and Drug Administration (FDA) for immunotherapy of a variety of cancer types include Rituximab[®] (for B-cell lymphomas), Trastuzumomab[®] (for breast cancer), Alemtuzumab[®] (for chronic lymphocytic leukemia), Cetuximab[®] (colorectal, head & neck cancers), and Bevacizumab[®] (for colorectal cancers). The two radiolabeled mAbs approved by FDA for radioimmunotherapy (RIT) are based on anti-CD20 antibodies, Zevalin[®] (labeled with ^{90}Y) and Bexxar[®] (labeled with ^{131}I) [100].

The monoclonal antibodies which have been labeled with ^{177}Lu and evaluated in biological systems are listed in **Table 3a.1**. In most of these studies DOTA has been used as the chelating moiety where the coupling group to the antibody was attached to either the N atom of the DOTA framework (e.g. DOTA-NHS ester) or to the C atom on the main carbocyclic backbone of the DOTA moiety (e.g. *p*-SCN-benzyl-DOTA). The studies in this field show that ligand structure and physical characteristics, such as thermodynamic stability, dissociation rates, and serum stability are factors which influence the *in vivo* dissociation of radiolabeled coordination complexes. Such studies were carried out with a series of different BFCAs with different backbone-substitution in DTPA ligands. The correlation of the *in vivo* stability of conjugated coordination

Chapter 3

complexes with that of the aforementioned physical parameters provide important clues towards screening of radiolabeled agents intended for use as radiopharmaceuticals.

These studies involve rigorous standardization of the protocols for conjugation, which include variation of the mAb concentration, antibody to BFCA ratio, pH, temperature (room temperature or 37°C) and reaction time. The chelate to antibody ratio is critical to retain the immunoreactivity of the monoclonal antibody post labeling. The methods reported for the determination of the average number of chelates per antibody molecule and the availability of these methods relevant to the development of ^{177}Lu -labeled mAbs to estimate the number of protein-bound chelating groups are few in number [101-103].

Table 3a.1. Examples of ^{177}Lu -labeled mAbs studied for radioimmunotherapy [100]

Antibody	Targeting antigen	Type of cancer targeted
Rituximab	CD 20	Non-Hodgkin's lymphoma
Anti-L-CAM	L1 cell adhesion protein	Neuroblastoma, renal and ovarian
Anti tenascin (Ch81C6)	Tenascin	Brain tumor
Anti-VEGF (VG76e)	Vascular endothelial growth factor	
CC-49	Tumor associated antigen (TAG-72)	Colon, Ovarian, adenocarcinoma etc.
CC-49 single chain Fv	Tumor associated	Several cancers such as colon,

Chapter 3

construct	antigen (TAG-72)	ovarian and adenocarcinoma.
CC-49 single chain Fv	Tumor associated	Colon, Ovarian, adenocarcinoma
construct (pre-targeting)	antigen (TAG-72)	etc.
Cetuximab	EGFR	Several targets
cG250	RCC	Renal cell carcinoma
7E11	PSMA	Prostate Cancer
Epratuzumab (hLL2)	CD 22	Non-Hodgkin's lymphoma
huA33	Antigen 33 (A 33)	Colorectal cancer
hu3S193	PSMA	Prostate cancer
J-591	Prostate specific membrane antigen	Prostate cancer
MOv18	α -isoform of folate receptor	Prostate cancer
Pertuzumab	HER-2, tyrosine kinase receptor	Breast cancer and others
RS-7	Epithelial glycoprotein	Small cell lung carcinoma
Trastuzumab (Herceptin [®])	HER 2	Breast cancer
U36	CD44v6	Head and neck squamous cell carcinoma

Chapter 3

In present study, two monoclonal antibodies namely, Rituximab and Trastuzumab were used for radiolabeling with ^{177}Lu . Over past few years, attempts have been made to radiolabel Rituximab and Trastuzumab with various therapeutic isotopes so as to evaluate their potential as radioimmunotherapeutic agents [103,104]. Present work involves the labelling of these two antibodies with ^{177}Lu . Potential of ^{177}Lu as a therapeutic isotope in the treatment of tumors is well known and had already been discussed in details in chapter one. Direct incorporation of ^{177}Lu in the antibody structure is not feasible owing to absence of suitable arrangement of functional groups which could complex directly with the radionuclide, however radiolabeling can be done by using a bi-functional chelating agent (BFCA). The macrocyclic ligand, *p*-NCS-benzyl-DOTA (*p*-isothiocyanatobenzyl-1,4,7,10-tetraazacyclododecane-1,4,7,10-tetraacetic acid) known to form thermodynamically stable and kinetically inert complexes with ^{177}Lu [30,31] was chosen as BFCA. Initial conjugation and radiolabeling procedures were optimized using the readily available antibody namely, IgG (Immunoglobulin G). The optimized parameters for conjugation and radiolabeling thus arrived at were then used to prepare the corresponding ^{177}Lu -labeled Rituximab and ^{177}Lu -labeled-Trastuzumab. Also, an attempt was made to evaluate the *in vivo* pharmacokinetic behaviour of ^{177}Lu -labeled Rituximab in normal Swiss mice.

3a.3. Experimental

3a.3.1. Material and methods

Anti-CD20 antibody Rituximab (BioSim; Reditux™) was obtained in solution (100 mg/mL) from Dr Reddy's Laboratories, Hyderabad, India. Anti-HER2 antibody

Chapter 3

Trastuzumab (CANMAb™) was obtained from Biocon, India. *p*-NCS-benzyl-DOTA was procured from Macrocyclics, USA. Ammonium acetate, sodium carbonate, sodium bicarbonate, acetic acid used were of AR grade and were procured from reputed chemical manufacturers. PD-10 (Sephadex G-25 M) columns used for antibody purification were obtained from GE-healthcare. HPLC analyses were performed using a TSK-Gel G3000SWXL size-exclusion column (7.8×300 mm), pre-equilibrated with 0.05 M phosphate buffer (pH 7.4), at a flow rate of 0.5 mL/min. The elution was monitored by detecting the radioactivity signal using a NaI(Tl) detector coupled with the HPLC system. All the solvents used for HPLC were of HPLC grade and were filtered prior to use.

3a.3.2. Preparation of ¹⁷⁷Lu-labeled-Rituximab and Trastuzumab

3a.3.2.1. Preparation and purification of *p*-NCS-benzyl-DOTA coupled IgG

The antibody-BFCA conjugate was prepared by incubation of IgG (5 mg, 33 nmol) with *p*-NCS-benzyl-DOTA (230 µg, 330 nmol) at 37°C for 17 h. The *p*-NCS-benzyl-DOTA-IgG conjugate obtained was subsequently purified to remove free *p*-NCS-benzyl-DOTA by pre-packed PD10 columns using NH₄OAc buffer (pH=5.5) as eluent. The PD-10 columns were conditioned with 25 mL of NH₄OAc buffer (pH=5.5) prior to loading of antibody-BFCA reaction mixture. After conditioning, *p*-NCS-benzyl-DOTA-IgG conjugate was loaded onto the preconditioned PD-10 column and purification was carried out by using NH₄OAc buffer (pH=5.5). The eluate was collected in 1 mL fractions and fractions containing majority of the antibody-BFCA conjugate were identified by injecting 10 µL of each fraction in HPLC and observing the corresponding UV-Vis ($\lambda_{280\text{ nm}}$) profiles. After identification of the eluted fraction containing majority of *p*-NCS-

Chapter 3

benzyl-DOTA-IgG conjugate, concentration of the conjugate was estimated in the same by using Bio Rad protein assay following the reported standard procedure [105].

3a.3.2.2. Preparation of *p*-NCS-benzyl-DOTA-Rituximab

Conjugation of Rituximab with *p*-NCS-benzyl-DOTA was carried out by following the same procedure as was standardized with IgG. However, an additional pre-concentration step was involved as commercially procured Rituximab was obtained in a concentration of 100 mg/10 mL and 500 μ L aliquot of Rituximab (5 mg) was used each time for conjugation reaction preceded by a pre concentration step leading to a volume reduction from 500 μ L to \sim 100 μ L using Amicon ultracentrifugal filtration units under a relative centrifugal force (RCF) of \sim 2100 g. After conjugation, purification of Rituximab-*p*-NCS-benzyl-DOTA was carried out by following the same procedure as was standardized with IgG.

3a.3.2.3. Preparation of *p*-NCS-benzyl-Trastuzumab

Preparation as well as purification of *p*-NCS-benzyl-DOTA-Trastuzumab was carried out by following the same procedure as mentioned in **3a.3.2.1**.

3a.3.2.4. Radiolabeling of *p*-NCS-benzyl-DOTA-IgG conjugate

A stock solution of *p*-NCS-benzyl-DOTA-IgG (4 mg / mL of NH₄OAc buffer (pH=5.5)) was prepared and radiolabeling with ¹⁷⁷Lu was carried out by incubating *p*-NCS-benzyl-DOTA-IgG (500 μ g, 125 μ L) with ¹⁷⁷Lu (50 μ L, 10 mCi) at 37°C for 1 h.

3a.3.2.5. Radiolabeling of *p*-NCS-benzyl-DOTA-Rituximab

Chapter 3

Radiolabeling of *p*-NCS-benzyl-DOTA-Rituximab was carried out following the procedure as mentioned in **3a.3.2.4**.

3a.3.2.6. Radiolabeling of *p*-NCS-benzyl-DOTA-Trastuzumab

Radiolabeling of *p*-NCS-benzyl-DOTA coupled Trastuzumab was carried out following the procedure as mentioned in **3a.3.2.4**.

3a.3.2.7. Determination of average number of BFCAs attached per antibody molecule

Average number of BFCAs attached per antibody molecule was calculated following a protocol mentioned in the literature [97]. General procedure involved the incubation of antibody-BFCA conjugate (500 μ g, 3.38 nmol) with excess amount of natural Lu (0.59 μ g, 33.8 nmol) containing tracer amount of ^{177}Lu (2 mCi) at 37 °C for 1 h. The reaction mixture thus obtained was incubated with DTPA (diethylene triamine pentaacetic acid) (13.3 μ g, 33.8 nmol) at room temperature for 10 min. An aliquot of reaction mixture (10 μ L) was injected in HPLC and peak area corresponding to $^{177}\text{Lu}/^{\text{nat}}\text{Lu}$ -labeled antibody-BFCA conjugate relative to $^{177}\text{Lu}/^{\text{nat}}\text{Lu}$ -DTPA was used for determining the average number of BFCA attached per antibody molecule.

3a.3.3. Quality control

Determination of percentage radiochemical purity of the prepared radiolabeled antibody conjugates viz. ^{177}Lu -labeled-*p*-NCS-benzyl-DOTA-Rituximab and ^{177}Lu -labeled-*p*-NCS-benzyl-DOTA-Trastuzumab was carried out using high performance liquid chromatography (HPLC). HPLC elution profile was obtained by using 0.05M phosphate

Chapter 3

buffer with 0.05% NaN₃ as eluting solvent (isocratic mode). Flow rate was maintained at 0.5 mL/min.

3a.3.4. *In vitro* stability studies

In vitro stability of ¹⁷⁷Lu-labeled-*p*-NCS-benzyl-DOTA-Rituximab and ¹⁷⁷Lu-labeled-*p*-NCS-benzyl-DOTA-Trastuzumab complexes was studied by incubating the radiolabeled conjugates at room temperature for 48 h in NH₄OAc buffer medium (*pH* = 7.0). Aliquots of antibody complexes (10 µL) were then injected into HPLC to determine the radiochemical purities and estimate the extent of dissociation of the complexes if any.

3a.3.5. *In vitro* cell binding studies

In vitro cell binding studies were carried out with ¹⁷⁷Lu-labeled-*p*-NCS-benzyl-DOTA-Rituximab in order to determine the specificity of the antibody complex towards binding with cell lines overexpressing CD20 antigen receptors. These studies were carried out in Raji cell lines (human lymphoma cell lines) as they are known to overexpress the CD20 antigen receptors. Inhibition studies were carried out to determine the specificity of binding by using excess (100 µg) of cold (unlabeled) antibody.

3a.3.6. Biodistribution studies

Pharmacokinetic behaviour of ¹⁷⁷Lu-labeled-*p*-NCS-benzyl-DOTA-Rituximab complex was studied by carrying out biodistribution studies in normal Swiss mice. Each animal was injected via the tail vein with 100 µL (~3.7 MBq) of the radiolabeled preparation. The animals were sacrificed by cardiac puncture post-anesthesia at 3 h, 24 h, 48 h and 6 d

Chapter 3

post injection (p.i.). Various organs were excised following sacrifice and the radioactivity associated with each organ/tissue was determined using a flat type NaI(Tl) counter. The percentage of injected activity (% IA) accumulated in various organs/tissue was calculated from the above data. The activity excreted was indirectly determined from the difference between total injected activity and the % IA accounted for in all the organs. The uptake in blood, bone and muscles were calculated based on the assumption that 7%, 10% and 40% of the body weight of the animals are constituted by these organs, respectively.

3a.4. Results and discussion

3a.4.1. Preparation of ^{177}Lu -labeled-*p*-NCS-benzyl-DOTA-Rituximab and ^{177}Lu -labeled-*p*-NCS-benzyl-DOTA-Trastuzumab

The first step of preparation of ^{177}Lu -labeled-*p*-NCS-benzyl-DOTA-Rituximab and ^{177}Lu -labeled-*p*-NCS-benzyl-DOTA-Trastuzumab involved the coupling of these monoclonal antibodies with a BFCA namely, *p*-NCS-benzyl-DOTA. A molar ratio of 10:1 of BFCA and antibody was selected for conjugation instead of 1:20 so as to decrease the probability of binding of BFCA moieties with the variable region (portion of antibody active towards binding with antigen receptor) of the antibody as it may interfere with the binding of antibody conjugate with the antigen receptors. On the other hand, a BFCA:antibody ratio lower than 1:10 may affect the radiochemical yield of the resultant radiolabeled antibody. After coupling reaction, the excess or unreacted BFCA was removed using pre-packed PD-10 columns based on the principle of size exclusion chromatography. After purification, the fraction containing majority of antibody-BFCA conjugate was identified

Chapter 3

from UV-Vis absorption signal observed at $\lambda=280$ nm using HPLC whereas estimation of protein/*p*-NCS-benzyl-DOTA-Rituximab and Trastuzumab concentration in the desired eluted fraction was carried out by Bio Rad protein assay and was found to be ~ 4 mg/mL. Purified *p*-NCS-benzyl-DOTA-Rituximab as well as *p*-NCS-benzyl-DOTA-Trastuzumab were radiolabeled individually with $^{177}\text{LuCl}_3$. The percentage radiochemical purity of the radiolabeled conjugates was determined using HPLC where radiolabeled antibodies eluted first at retention time (R_t) of 15-16 min ($R_t = 15.5$ and 16 min for ^{177}Lu -Rituximab and ^{177}Lu -Trastuzumab respectively) whereas free ^{177}Lu eluted at retention time of 21 min. A RCP of $> 95\%$ was obtained corresponding to ^{177}Lu -labeled-Rituximab and ^{177}Lu -labeled-Trastuzumab (Fig. 3a.2 (a) and (b) respectively).

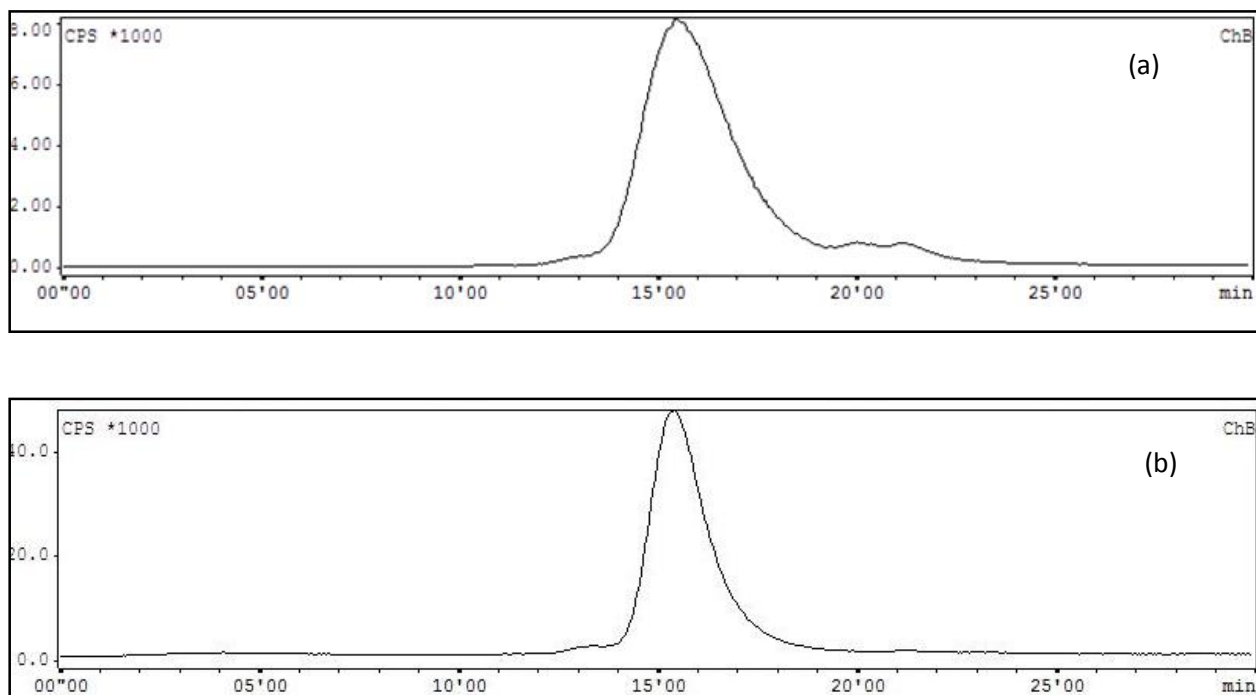


Fig. 3a.2. HPLC profiles of (a) ^{177}Lu -labeled-Rituximab and (b) ^{177}Lu -labeled Trastuzumab

Chapter 3

3a.4.2. Determination of average number of BFCAs per antibody molecule

The average number of BFCAs (*p*-NCS-benzyl-DOTAs) attached per antibody molecule (Rituximab and Trastuzumab) was determined by a reported method and was calculated by determining the areas corresponding to $^{177}\text{Lu}/^{\text{nat}}\text{Lu}$ -labeled-antibody-BFCA conjugate and $^{177}\text{Lu}/^{\text{nat}}\text{Lu}$ -labeled-DTPA peaks obtained in the HPLC chromatogram and were found to be in a ratio of 60:40. With a prior knowledge that Lu and *p*-NCS-benzyl-DOTA forms 1:1 complex and since known amount of $^{\text{nat}}\text{Lu}$ was used for complexation, number of moles of $^{\text{nat}}\text{Lu}$ consumed were related to corresponding moles of *p*-NCS-benzyl-DOTA present in the reaction mixture. A ratio of no. moles of BFCA and antibody was calculated and was found to be $\sim 6.5 \pm 0.5$ for both the antibodies.

3a.4.3. *In vitro* stability studies

^{177}Lu -labeled-Rituximab and Trastuzumab complexes were found to be stable at room temperature in NH_4OAc buffer medium ($\text{pH} = 5.5$) upto 24 h as determined by HPLC ($\text{RCP} > 95\%$). After 48 hour, the percentage radiochemical purity was observed to decrease to $\sim 85\%$.

3a.4.4. *In vitro* cell binding studies

In vitro cell binding studies carried out with ^{177}Lu -Rituximab in Raji cell lines revealed the affinity of the radiolabeled antibody towards these cell lines. A maximum cell binding of $\sim 29\%$ was observed corresponding to 1.25 ng of ^{177}Lu -Rituximab complex. An inhibition of $\sim 80\%$ was obtained in presence of excess of cold Rituximab corresponding to 7.45 ng of ^{177}Lu -Rituximab complex as shown in **Fig.3a.3**.

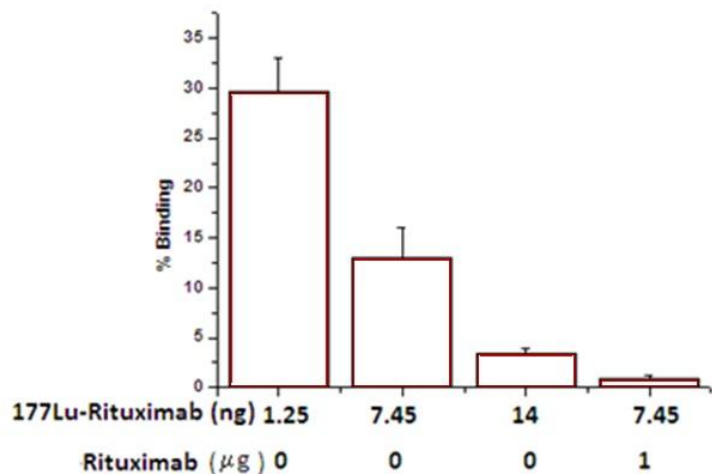


Fig.3a.3. Percent cell binding versus varying amounts of ^{177}Lu -Rituximab complex and effect of excess of cold (100 μg) on % cell binding corresponding to 7.45 ng of ^{177}Lu -Rituximab complex.

3a.4.5. Biodistribution studies

Biodistribution studies carried out in normal Swiss mice revealed high blood uptake (11.64 ± 0.16 % IA/g) at 3 h p.i. which cleared with time (**Table 3a.2**). The observed slow rate of clearance of activity from blood could be attributed to large molecular weight of the ^{177}Lu -antibody complex which leads to longer blood circulation time and slower excretion from the body. Uptake was also observed in other organs such as lungs (3.95 ± 0.54 % IA/g), heart (2.66 ± 0.15 % IA/g), liver (2.81 ± 0.26 % IA/g), GIT (1.18 ± 0.20

Chapter 3

% IA/g) and spleen (1.22 ± 0.02 % IA/g) at 3 h p.i., however it was found to clear away with time. Biodistribution pattern revealed that major activity cleared via renal pathway which probably could be attributed to the presence of multiple hydrophilic BFCAs in antibody backbone which imparted the overall hydrophilic character to the ^{177}Lu -labeled-Rituximab complex

Table 3a.2. Biodistribution pattern of ^{177}Lu -Rituximab in normal Swiss mice at different time points (n=3)

Organ	Injected activity per gram (%IA/g) of organ/tissue			
	3 h	24 h	48 h	6 d
Blood	11.64 ± 0.16	5.44 ± 0.89	4.48 ± 0.77	2.85 ± 0.16
Lung	3.95 ± 0.54	2.32 ± 0.41	2.57 ± 0.10	1.45 ± 0.13
Heart	2.66 ± 0.15	1.48 ± 0.33	1.58 ± 0.23	0.98 ± 0.07
Stomach	0.47 ± 0.21	0.45 ± 0.04	0.45 ± 0.07	0.39 ± 0.26
GIT	1.18 ± 0.20	0.68 ± 0.10	0.64 ± 0.14	0.39 ± 0.05
Liver	2.81 ± 0.26	2.92 ± 0.40	3.01 ± 0.27	2.03 ± 0.39
Spleen	1.22 ± 0.02	1.51 ± 0.41	1.71 ± 0.14	1.84 ± 0.35
Kidney	2.20 ± 0.17	2.25 ± 0.16	1.70 ± 0.23	1.71 ± 0.33
Muscle	0.25 ± 0.04	0.61 ± 0.09	0.47 ± 0.16	0.33 ± 0.13
Bone	4.53 ± 0.20	8.28 ± 0.09	10.01 ± 3.90	7.14 ± 0.87
Excretion	64.12 ± 1.95	70.25 ± 2.11	78.34 ± 1.56	81.23 ± 2.25

Chapter 3

3a.5. Conclusions

Conjugation as well as radiolabeling protocols for preparation of two different ^{177}Lu -labeled monoclonal antibodies i.e. Rituximab and Trastuzumab were optimized. Both the radiolabeled complexes could be prepared with a RCP > 95%. *In vitro* cell binding studies revealed the affinity of ^{177}Lu -labeled-Rituximab towards CD20 antigens in human lymphoma cell lines. Also, an inhibition of ~80% observed in *in vitro* cell studies is indicative of specificity of ^{177}Lu -labeled-Rituximab towards CD20 antigens. *In vivo* pharmacokinetic behaviour of ^{177}Lu -labeled-Rituximab in normal Swiss mice showed that complex exhibited low uptake in vital organs except blood and bone. High residence time in blood, though decreasing with time, is expected and can be attributed to high molecular weight of the antibody (Rituximab) whereas uptake in bone is probably due to decreasing *in vivo* stability of ^{177}Lu -labeled-Rituximab complex at longer p.i. time points.

Chapter 3

3(b) PREPARATION OF ^{99m}TcN -LABELED RGD DERIVATIVE FOR TUMOR IMAGING

3b.1. Peptides and radionuclidic imaging of tumors

Peptides are made up of amino acid monomers linked via peptide bonds (-CONH-). A peptide bond is the one formed by the condensation reaction between a carboxylic acid and an amine. Peptides have the ability to be used as biomarkers owing to their ability to bind or mark specific type of cellular receptors [106-110]. Receptors are protein molecules which are present either on cell surface or on surface of nucleus or in the cytoplasm. Various types of receptors are expressed in the normal cells whereas in tumor cells they are overexpressed. Peptide-based ligands which are specific towards binding with these receptors, can be used as vectors for radiolabeling with suitable isotopes. The radiolabeled peptides thus obtained serve as target-specific radiotracers towards application in imaging as well as therapy of tumors [106-110]. These modalities known as Peptide Receptor Scintigraphy (PRS) or Peptide Receptor Radionuclide Therapy (PRRT) have been used in development of peptide-based imaging and therapy in nuclear medicine and are considered to be one of the most efficient means to target tumor cells. Additionally, they can tolerate harsher reaction conditions for carrying out structural modifications as well as radiolabeling due to lack of complex structure unlike of proteins. Also, being of lower molecular weight as compared to polypeptides and proteins, the smaller peptides or peptide-fragments exhibit fast clearance from blood pool thereby resulting into better target to background ratios. The additional dose exposure to non

Chapter 3

target organs is also prevented [111]. Few peptide based radiolabeled agents for receptor-targeted tumor imaging have been listed in the **Table 3b.1** [106].

Table 3b.1. List of few radiolabeled peptides and the corresponding target receptors

Radiolabeled peptides	Targets/Application
^{99m}Tc -Hynic-TOC	$^{\#}\text{SSTR}$ overexpressing cancer
^{111}In -DOTA-TATE	SSTR overexpressing cancer
^{68}Ga -DOTA-NOC, ^{68}Ga -DOTA-TOC	SSTR overexpressing cancer
^{68}Ga -AMBA	$^{\#}\text{GRP}$ receptor-based imaging of prostate cancer
^{18}F -galacto-RGD	$\alpha_v\beta_3$ targeted imaging of cancer
^{111}In -[DTPA-Pro1,Tyr4]BN	Androgen-dependent BN/GRP receptor imaging in human prostate tumor xenografts
$^{68}\text{Ga}/^{111}\text{In}$ -DOTA-RGD	$\alpha_v\beta_3$ targeted imaging of cancer
$^{\#}\text{GRP}$ (Gastrin releasing peptide), $^{\#}\text{SSTR}$ (Somatostatin receptors)	

Arginine-Glycine-Aspartic acid (RGD) is one such peptide-based ligand which shows high specificity towards integrin $\alpha_v\beta_3$ receptors.

3b.2. $\alpha_v\beta_3$ integrin receptors as angiogenesis marker

‘Angiogenesis’, the sprouting of new blood vessels from the existing vasculature, is well recognized as one of the key occurrences during tumor growth and metastasis

Chapter 3

[112-118]. The angiogenic process depends on vascular endothelial cell migration and invasion, and is regulated by cell-adhesion receptors. The integrin family is a group of transmembrane glycoproteins comprised of 19 α and 8 β subunits and are expressed in over 25 different α/β heterodimeric combinations on the cell surface. At least 24 distinct integrins are formed by a combination of 19 α and 8 β subunits, such as $\alpha_v\beta_3$, $\alpha_v\beta_5$, $\alpha_5\beta_1$ etc. [118-123]. Among these, $\alpha_v\beta_3$ has a crucial role in the regulation of tumor growth and metastasis as it is highly expressed on activated and proliferating endothelial cells during tumor angiogenesis and metastasis. The $\alpha_v\beta_3$ integrin binds to the tripeptide, Arg-Gly-Asp (RGD), containing components of the extracellular matrix like vitronectin and fibronectin. Thus, a variety of linear and mostly cyclic RGD-based probes have been developed for monitoring expression of $\alpha_v\beta_3$ *in vivo*. Integrins play a critical role in several physiologic processes including cell proliferation, wound healing and remodelling of bone. Integrins also contribute to pathological events such as thrombosis, atherosclerosis, tumour invasion, angiogenesis and metastasis. Among the integrin family, $\alpha_v\beta_3$ (vitronectin receptor or VnR) is studied most extensively for its role in tumour growth, progression and angiogenesis [124]. The vitronectin receptor has a common RGD (Arg-Gly-Asp) tripeptide sequence and hence RGD derivatives when radiolabeled are suitable for targeting $\alpha_v\beta_3$ integrin receptors. The cyclic RGD peptide [Leu¹-Glu²-Glu³-Glu⁴-Glu⁵-Glu⁶-Ala⁷-Tyr⁸-Gly⁹-Trp¹⁰-Met¹¹-Asp¹²-Phe¹³-NH₂] and its multimers have been investigated for developing targeting agents to image neoangiogenesis and in this respect ¹⁸F-cRGD has been evaluated in patients with solid tumours [125]. The function of integrins during tumor angiogenesis has been studied

Chapter 3

most extensively for integrin $\alpha_v\beta_3$, which is overexpressed on activated endothelial cells and of the neovasculature as well as on different variety of growing tumors including osteosarcomas, neuroblastomas, glioblastomas, melanomas, lung and breast carcinomas as compared to normal cells, epithelial cells and mature endothelial cells of established blood vessels [126-132]. Therefore integrin $\alpha_v\beta_3$ has been identified as an interesting molecular target for the early diagnosis as well as therapy of rapidly growing and metastatic tumors [133-138].

3b.3. Radiolabeled RGDs for imaging $\alpha_v\beta_3$ overexpression

Over the last decade, a series of radiotracers based on Arg-Gly-Asp (RGD) peptide derivatives have been synthesized and studied for imaging integrin $\alpha_v\beta_3$ expression in tumor by PET or SPECT [139-150]. Among these, [^{18}F]-AH111585 and [^{18}F]-Galacto-RGD are under clinical investigation for noninvasive visualization of integrin expression in cancer patients [151-156]. These ^{18}F -labeled RGD monomer derivatives can specifically bind to integrin $\alpha_v\beta_3$ receptors overexpressed in certain cancer. However, high cost of ^{18}F and lack of preparation modules for the ^{18}F -labeled RGD peptides pose significant challenges for their widespread clinical application [157-159]. Thus, there is a continuing need for designing more efficient integrin $\alpha_v\beta_3$ -targeting radiotracers based on $^{99\text{m}}\text{Tc}$ that can be readily prepared at hospital radiopharmacy and used without further post-labeling purification.

In the present study, the cyclic RGD peptide derivative $\text{G}_3\text{-c(RGDfK)}$ ($\text{G}_3 = \text{Gly-Gly-Gly}$, $\text{f} = \text{Phe}$, $\text{K} = \text{Lys}$) has been chosen as the starting material to synthesize a $^{99\text{m}}\text{Tc}$ -labeled dimeric RGD peptide derivative. Since the natural mode of interactions between

Chapter 3

integrin $\alpha_v\beta_3$ and RGD-containing proteins involve multivalent binding sites, the idea to improve the integrin $\alpha_v\beta_3$ binding affinity with multivalent cyclic RGD peptides could provide more effective antagonists with better targeting capability [160-161]. It is already well documented that with increase in peptide moieties there is an increase in tumor uptake of radiotracer and retention of the resultant radiolabeled RGD multimers. A comparison of biological behavior of radiolabeled RGD monomer, dimer and tetramer revealed that dimers exhibit considerable tumor uptake with best target/non-target ratio and is the most suitable candidate for tumor imaging and therapy [162]. Liu and co-workers have reported [$^{99m}\text{Tc}(\text{HYNIC-3G}_3\text{-dimer})(\text{tricine})(\text{TPPTS})$] ($3\text{G}_3\text{-dimer} = \text{G}_3\text{-E}[\text{G}_3\text{-c(RGDfK)}]_2$, $\text{G}_3 = \text{Gly-Gly-Gly}$, and $\text{TPPTS} = \text{trisodium triphenylphosphine-3,3',3''-trisulfonate}$) as a potential radiotracer for imaging integrin $\alpha_v\beta_3$ expression in athymic nude mice bearing U87MG glioma and MDA-MB-435 breast cancer xenografts [160-162]. Results from the *in vitro* integrin $\alpha_v\beta_3$ binding assay and *ex vivo* biodistribution clearly demonstrate that the G_3 linkers between cyclic RGD motifs are useful for further enhancing the integrin $\alpha_v\beta_3$ binding affinity of dimeric RGD peptides and thereby increasing the ^{99m}Tc radiotracer tumor uptake. It also helped in improving the clearance kinetics of the radiotracer from non-cancerous organs, such as intestine, liver, and kidneys. Similar results were also obtained for $^{64}\text{Cu}(\text{DOTA-3G}_3\text{-dimer})$ ($\text{DOTA} = 1,4,7,10\text{-tetraazacyclo-dodecane-1,4,7,10-tetraacetic acid}$) [160-162].

In recent years, there is a significant interest in the utilization of [^{99m}TcN] $^{2+}$ core for labeling a variety of biomolecules. This is attributable to the increased stability of the nitrido core towards oxidation-reduction reactions and pH variations, in comparison to the

Chapter 3

conventional ^{99m}Tc -oxo core [163-169]. The $[\text{}^{99m}\text{TcN}]^{2+}$ core has been found to complex well with ligands containing sulfur atoms, as in dithiocarbamates and xanthates [163-169]. The complexes formed are symmetrical $^{99m}\text{TcNL}_2$ type with two ligand molecules involved in the complexation.

The present study involves a novel method of dimerization of the dithiocarbamate derivative of cyclic RGD monomer viz. $\text{G}_3\text{-c(RGDfK)}$ using $[\text{}^{99m}\text{TcN}]^{+2}$ core, which can form a tetracoordinated complex involving two RGD monomers. Preliminary biological studies of this new radiotracer have also been carried out in tumor bearing mice.

3b.4. Experimental

3b.4.1. Materials and Method

The cyclic RGD peptide derivative $\text{G}_3\text{-c(RGDfK)}$ was custom synthesized by Ms. Peptide International, Louisville, KY, USA. All other chemicals were of AR grade and procured from reputed chemical manufacturers. Sodium pertechnetate ($\text{Na}^{99m}\text{TcO}_4$) was eluted with saline from a ^{99}Mo - ^{99m}Tc alumina column generator just before use. Whatman chromatography paper (Whatman 3 MM Chr, 20 mm width, Maidstone, England) was used for paper chromatography studies. Flexible silica gel plates used for carrying out preparative thin layer chromatography (TLC) studies were obtained from Bakerflex Chemical Company, Germany. The high performance liquid chromatography (HPLC) system (PU 1580) used was obtained from JASCO, Japan. The elution was monitored by detecting the radioactivity signal using a NaI(Tl) detector system coupled with the HPLC system. All the solvents used for HPLC were degassed and filtered prior to use and were of HPLC grade. Ultra Violet-Visible (UV-Vis) spectra were recorded using JASCO V-

Chapter 3

530 UV/Vis spectrophotometer (Japan). The gradient system consisting of eluting solvents H₂O (solvent A) and acetonitrile (solvent B) with 0.1% trifluoroacetic acid was used (0-28 min, 90% A-10% A; 28-30 min, 10% A; 30-32 min, 10% A-90% A). All other radioactivity measurements were carried out using a well-type NaI(Tl) scintillation counter. Mass spectra were recorded on QTOF micromass instrument using electron spray ionization (ESI) in positive mode.

Scintigraphic images were recorded using a single head digital gamma camera (GE Wipro, USA) with a Low-Energy-High-Resolution (LEHR) collimator. The gamma camera was calibrated for 140 keV gamma photon of ^{99m}Tc with 20% window for acquisition of the images. Xylazine hydrochloride and ketamine hydrochloride, used for anesthetizing the animals prior to recording the scintigraphic images, were purchased from Indian Immunologicals Limited and Themis Medicare Limited (India), respectively. All the animal experiments were carried out in compliance with the relevant national laws as approved by the local committee on the conduct and ethics of animal experimentation.

3b.4.2. *Synthesis of dithiocarbamate derivative of RGD monomer*

To the solution of G₃-c(RGDfK) (10 mg, 11.7 mmol) in pre-cooled aqueous ammonia (2 mL), 0.5 mL solution of CS₂ in ethanol (1:4, v/v) was added slowly at 0°C under constant stirring (**Fig.3b.1**). The resulting solution was stirred at room temperature overnight. After the completion of the reaction, the solution was centrifuged under vacuum at 45°C (3000 rpm, 30 min). The residue thus obtained was separated and characterized by ESI-MS.

Chapter 3

ESI-MS (m/z): (calc.) $C_{35}H_{54}N_{12}O_9S_2$ 850.2; (obs.) (M+H) 851.3 [Fig. 3b.2]

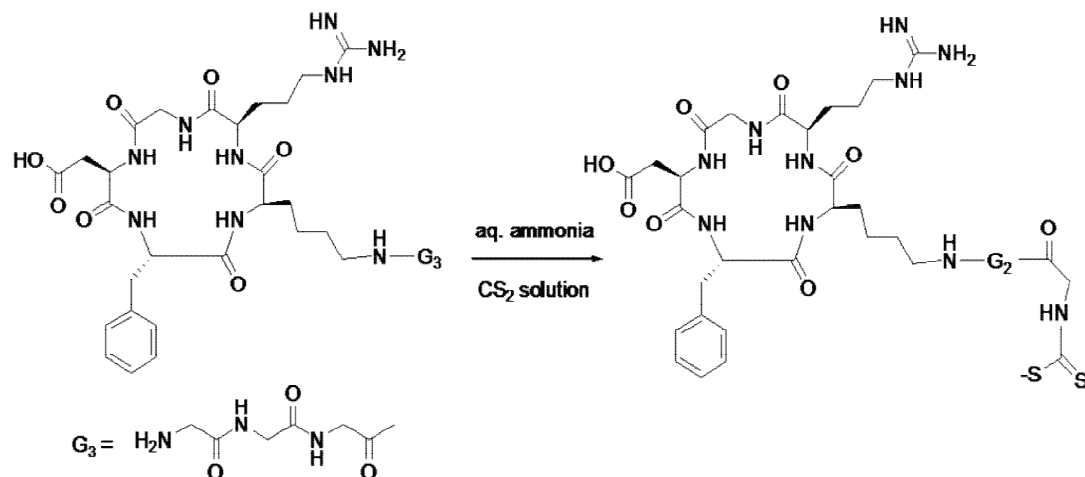


Fig.3b.1. Schematic representation of conversion of G_3 -c(RGDfK) to corresponding dithiocarbamate derivative

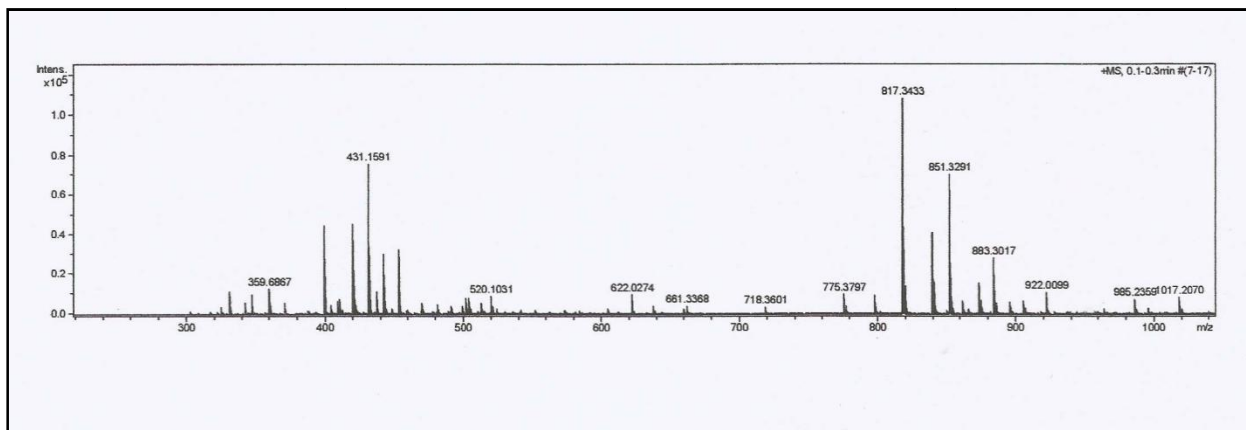


Fig. 3b.2. Mass spectrum of dithiocarbamate derivative of G_3 -c(RGDfK)

3b.4.3. Radiolabeling studies

Chapter 3

3b.4.3.1. Preparation of the [^{99m}TcN] $^{2+}$ core

To a solution of containing 0.05 mg of stannous chloride dihydrate, 5.0 mg of succinic dihydrazide (SDH) and 5.0 mg of propylenediaminetetraacetic acid (PDTA) in 1 mL of phosphate buffered saline (PBS), was added 1 mL of $\text{Na}^{99m}\text{TcO}_4$ (37 MBq of ^{99m}Tc) in normal saline. The mixture was vortexed and kept at room temperature for 20 minutes. The [^{99m}TcN] $^{2+}$ intermediate formed was characterized by radio TLC using ethanol:chloroform:toluene:0.5 M ammonium acetate (6:3:3:0.5 v/v) as the eluting solvent. The [^{99m}TcN] $^{2+}$ intermediate was found to remain near the point of application ($R_f = 0-0.2$), while $^{99m}\text{TcO}_4^-$ exhibits $R_f = 0.4-0.6$ in the same solvent system.

3b.4.3.2. Preparation of ^{99m}TcN -[G₃-c(RGDfK)]₂

For the preparation of ^{99m}Tc complex of the RGD peptide derivative, 0.5 mL solution of freshly prepared [^{99m}TcN] $^{2+}$ intermediate (15 MBq) was added to 0.5 mL of saline containing 25 μg of the ligand (**Fig.3b.3**). The pH of the reaction mixture was adjusted to around 4-5, vortexed for 1 min and subsequently incubated at room temperature for 1 h.

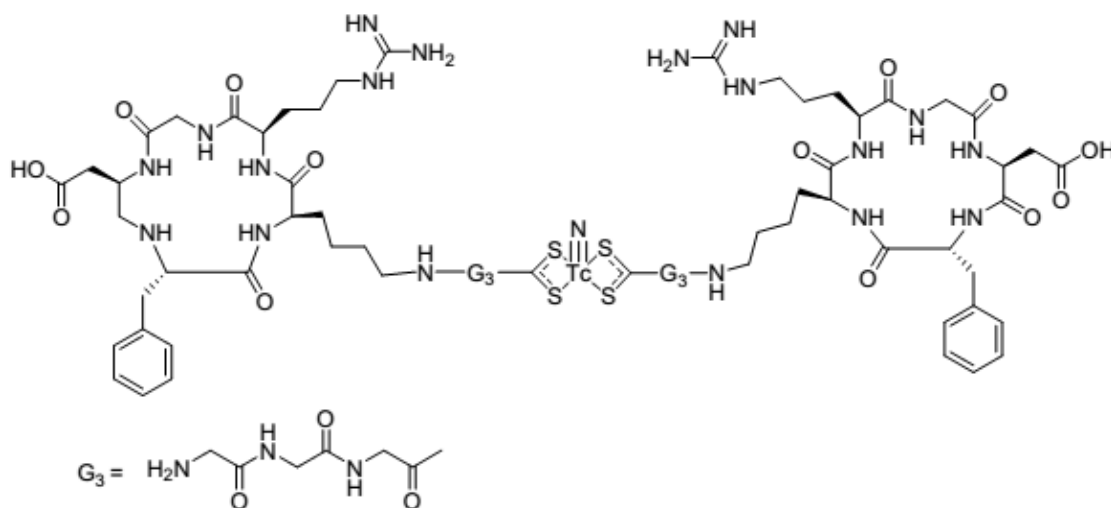


Fig.3b.3. Proposed structure of $^{99\text{m}}\text{TcN}-[\text{G}_3\text{-c(RGDfK)}]_2$

3b.4.4. Quality Control techniques

The $^{99\text{m}}\text{TcN}-[\text{G}_3\text{-c(RGDfK)}]_2$ complex was characterized by HPLC. A dual pump HPLC unit with a C-18 reversed phase column was used. About 25 μL of the test solution was injected into the column and elution was monitored by observing the radioactivity profile using a NaI(Tl) scintillation detector attached to the HPLC system. Water (A) and acetonitrile (B) mixtures with 0.1% trifluoroacetic acid were used as the mobile phase following the gradient elution system mentioned in section **3b.2.1** of this chapter.

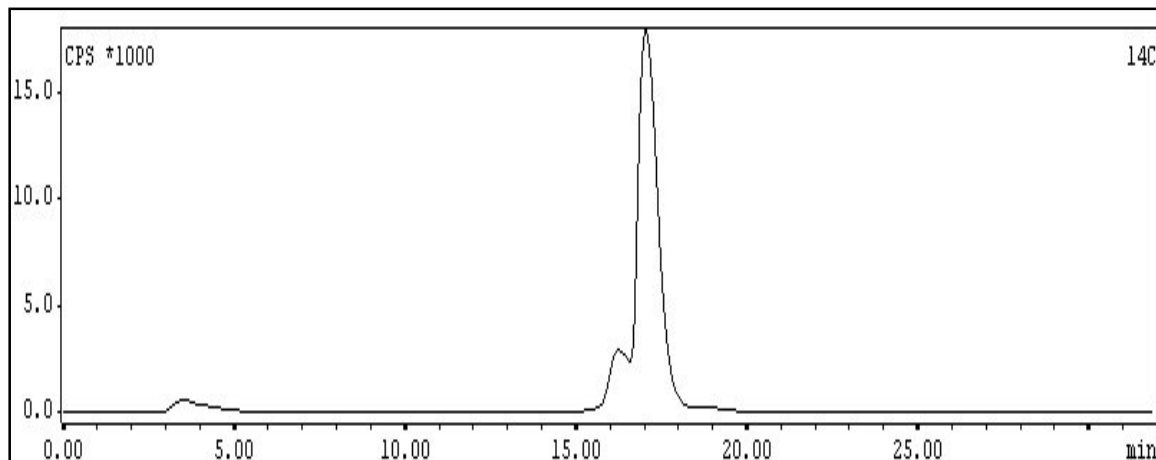


Fig.3b.4. HPLC elution profile of $^{99m}\text{TcN-[G}_3\text{-c(RGDfK)]}_2$

3b.4.5. Determination of partition coefficient (Log $P_{o/w}$)

The Log $P_{o/w}$ of $^{99m}\text{TcN-[G}_3\text{-c(RGDfK)]}_2$ complex was determined using the following protocol. Three different aliquots (25 μL) of the complex prepared under optimized conditions were diluted to 1 mL volume using normal saline. To each of these solutions 1 mL of n-octanol was added and the mixtures stirred vigorously for ~ 10 min. Subsequently, the mixtures were centrifuged at a speed of 3000 rpm for 5 min. Aliquots of 0.1 mL were withdrawn from both water and n-octanol layers and counted for ^{99m}Tc activity using NaI(Tl) counter. The Log $P_{o/w}$ values were determined from these data and reported as an average of three independent measurements.

3b.4.6. Stability Studies

The *in vitro* stability of the $^{99m}\text{TcN-[G}_3\text{-c(RGDfK)]}_2$ complex was studied by incubating the radiolabeled preparation in phosphate buffer saline ($\text{pH} \sim 7.5$) at 37°C and monitoring the radiochemical purity using HPLC. The studies were continued for 6 h.

Chapter 3

3b.4.7. Biological studies

Biological efficacy of the radiotracer was ascertained by carrying out biodistribution as well as scintigraphic imaging studies in C57BL/6 mice bearing melanoma tumors. Melanoma tumors were developed by injecting $\sim 1 \times 10^6$ viable cells suspended in PBS subcutaneously into the right thigh of C57BL/6 mice each weighing 20-25 g. The animals were observed for visibility of tumors and subsequently allowed to grow for about 2 weeks to attain a tumor mass of 0.2-0.4 g. Each animal was injected 100 μL (~ 3.7 MBq) of the radiolabeled preparation via the tail vein. The animals were sacrificed by cardiac puncture post-anesthesia at 30 min, 1 h and 3 h post injection (p.i.). Various organs and tumors were excised following sacrifice and the radioactivity associated with each organ/tissue was determined using a flat type NaI(Tl) counter. The percentage of injected activity (% IA) accumulated in various organs/tissue and tumor was calculated from the above data. The activity excreted was indirectly determined from the difference between total injected activity and the % IA accounted for in all the organs. The uptake in blood, bone and muscles were calculated based on the assumption that 7%, 10% and 40% of the body weight of the animals are constituted by these organs, respectively [165].

For imaging studies tumors were developed in the animals by following the same protocol mentioned above. The radiolabeled conjugate [~ 200 μL , 7.4 MBq] was injected through the tail vein of the animals and serial scintigraphic images were recorded at 30 min and 1 h p.i. using a LEHR collimator. Prior to the acquisition of images, the animals were anesthetized using a combination of xylazine hydrochloride (2 mg/kg of body

Chapter 3

weight) and ketamine hydrochloride (2 mg/kg of body weight). All the images were recorded by acquiring 500 K counts using 256×256 matrix size. All the animal experiments were carried out in strict compliance with the relevant national laws relating to the conduct of animal experimentation.

3b.5. Results and discussion

3b.5.1. Synthesis and characterization

The [G₃-c(RGDfK)]-DTC derivative was prepared by reacting G₃-c(RGDfK) with an equivalent amount of carbon disulfide in ammonium hydroxide solution (**Fig.3b.1**). The compound was characterized by ESI-MS and the data obtained was consistent with the proposed formula (**Fig.3b.2**).

3b.5.2. Radiochemistry

The radiolabeling of [G₃-c(RGDfK)]-DTC derivative with ^{99m}TcN core was carried out at room temperature (**Fig.3b.3**). The radiochemical purity of the complex was checked by HPLC. The HPLC pattern of the radiolabeled conjugate is shown in **Fig.3b.4**. The retention time of the radiolabeled conjugate was found to be 17.1 ± 0.1 min while that of ^{99m}TcN intermediate was 3.2 ± 0.1 min. Parameters such as ligand concentration and reaction time were optimized to obtain maximum complexation yields. It was observed that ~98% complexation could be obtained using 25 µg of ligand in reaction with [^{99m}TcN]²⁺ core at room temperature for 1 h. The water- octanol partition coefficient (Log P_{o/w}) value of ^{99m}TcN-[G₃-c(RGDfK)]₂ was found to be -1.08 ± 0.11 (n=3) suggesting it to be a hydrophilic complex.

Chapter 3

Dithiocarbamates are known to complex with $[^{99m}\text{TcN}]^{2+}$ intermediate leading to neutral complexes of $[^{99m}\text{TcNL}_2]$ type [163] having square pyramidal geometry with an apical $^{99m}\text{Tc}\equiv\text{N}$ bond and two mono anionic dithiocarbamate ligands spanning the four positions in the basal plane and coordinating through the four sulfur atoms. Therefore, it seems reasonable to presume that the $^{99m}\text{TcN}-[\text{G}_3\text{-c(RGDfK)}]_2$ complex prepared would exhibit the similar structure (**Fig.3b.3**).

3b.5.3. *In vitro* stability studies

In vitro stability of the $^{99m}\text{TcN}-[\text{G}_3\text{-c(RGDfK)}]_2$ complex was studied by incubating the complex in phosphate buffer saline (PBS) at 37°C and analyzing its radiochemical purity using HPLC at different time intervals. It was observed that the radiolabeled conjugate retains radiochemical purity to the extent of ~96% after 6 h incubation upto which studies were carried out.

3b.5.4. Biological studies

The uptake of $^{99m}\text{TcN}-[\text{G}_3\text{-c(RGDfK)}]_2$ complex in the different organs/tissue of C57BL/6 mice bearing melanoma tumors expressed as percentage injected activity per gram of organ/tissue (%IA/g) at different post-injection times is shown in **Table 3b.2**. The results of the biodistribution studies revealed significant tumor uptake within 30 min p.i. (4.61 ± 0.04 %IA/g). Initial accumulation of activity was observed in various non-target organs viz. liver, GIT, kidney, lungs etc. However, with the progress of time, the uptake in non-target organs was observed to reduce gradually. The tumor to blood ratio was observed to increase from 1.81 ± 0.21 at 30 min p.i. to 2.82 ± 0.22 at 180 min p.i., while tumor to muscle ratio increased from 4.12 ± 0.44 to 11.62 ± 0.12 respectively,

Chapter 3

between the same time points. The radiolabeled conjugate exhibited predominant urinary excretion, as more than 80% of the injected activity was observed to clear via renal pathway within 60 min p.i.

Table 3b.2. Biodistribution pattern of $^{99m}\text{TcN}-[\text{G}_3\text{-c(RGDfK)}]_2$ conjugate in C57BL/6 mice (n=5) bearing melanoma tumor

Organ	%Injected activity per gram (%IA/g) of organ/tissue		
	30 min	60 min	180 min
Blood	2.50±0.43	1.15±0.26	1.11±0.20
Liver	4.49±0.87	3.12±0.55	3.08±0.43
GIT	4.90±0.23	3.14±0.49	2.14±0.19
Kidney	7.82±1.54	5.66±1.29	4.61±0.78
Stomach	1.80±0.33	1.03±0.08	0.94±0.36
Heart	1.42±0.18	0.95±0.17	1.23±0.14
Lungs	3.23±0.68	2.53±0.73	2.57±0.58
Skeleton	0.35±0.16	0.00±0.00	0.00±0.00
Muscle	1.12±0.47	0.28±0.05	0.27±0.05
Spleen	3.31±1.08	1.42±0.44	1.59±0.24
Tumor	4.61±0.04	2.79±0.27	3.14±0.18
Excretion [#]	68.33±4.66	83.16±2.58	87.80±4.36

[#]Excretion has been calculated by subtracting the activity accounted in all the organs from the total activity injected

Chapter 3

Fig.3b.5 compares the uptake of $^{99m}\text{TcN}-[\text{G}_3\text{-c(RGDfK)}]_2$ in various organ/tissue of C57BL/6 mice bearing melanoma tumors at 30 min p.i. in the absence/presence of excess $\text{G}_3\text{-c(RGDfK)}$. Clearly, co-injection of excess $\text{G}_3\text{-c(RGDfK)}$ almost completely blocked the tumor uptake of $^{99m}\text{TcN}-[\text{G}_3\text{-c(RGDfK)}]_2$ ($0.88 \pm 0.22\%$ ID/g with $\text{G}_3\text{-c(RGDfK)}$ vs. $4.61 \pm 0.04\%$ ID/g without $\text{G}_3\text{-c(RGDfK)}$ at 30 min p.i.). Its uptake in normal organs such as liver, intestine, lungs, kidney and spleen was also significantly blocked by co-injection of excess $\text{G}_3\text{-c(RGDfK)}$ as shown in **Fig.3b.5**. The blockage of radiotracer uptake observed, is suggestive of the localization of the radiotracer in melanoma tumor via a receptor-mediated mode. The partial blockage of uptake in the normal organs as specified above indicates that the accumulation of $^{99m}\text{TcN}-[\text{G}_3\text{-c(RGDfK)}]_2$ in these organs is also via the integrin $\alpha_v\beta_3$ -receptors.

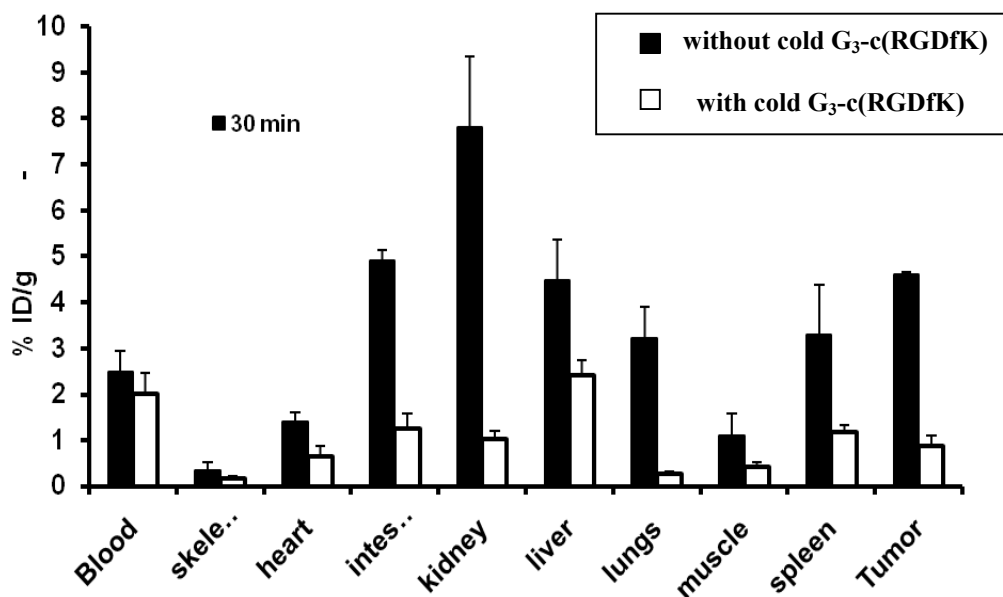


Fig.3b.5. Comparison of uptake of $^{99m}\text{TcN}-[\text{G}_3\text{-c(RGDfK)}]_2$ in various organ/tissue of C57BL/6 mice bearing melanoma tumors at 30 min p.i. in the absence/presence of excess $\text{G}_3\text{-c(RGDfK)}$

The whole-body scintigraphic images of the C57BL/6 mice bearing melanoma tumors recorded at 30min and 60 min post-administration of $^{99m}\text{TcN}-[\text{G}_3\text{-c(RGDfK)}]_2$ are shown in **Fig.3b.6**. It is evident that the melanoma tumor could be clearly visualized within 30 min post-administration of the conjugate.

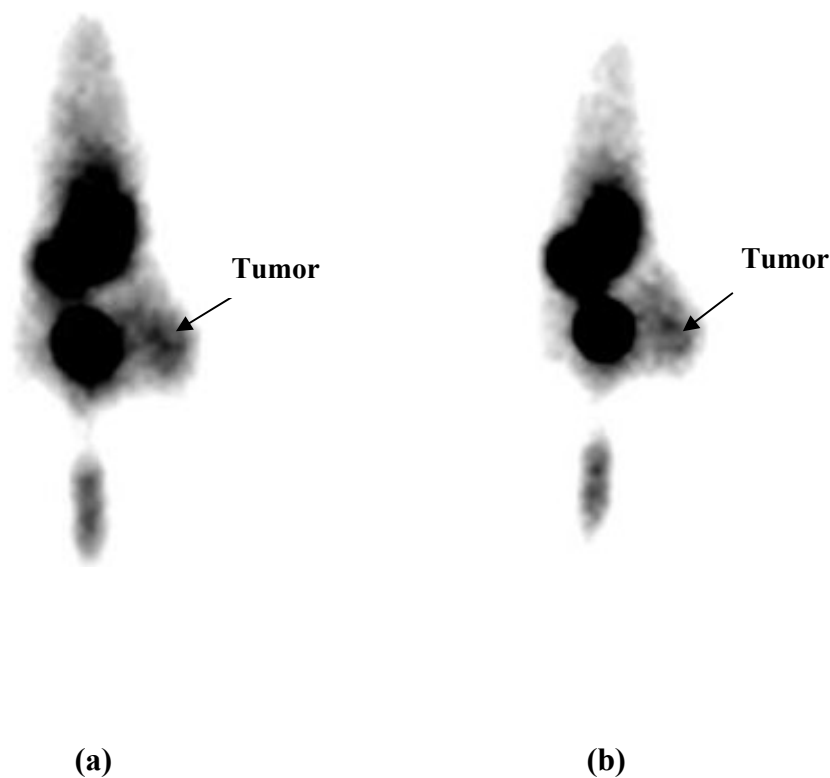


Fig.3b.6. Whole-body scintigraphic images of C57BL/6 mice bearing melanoma tumors recorded at (a) 30 min and (b) 60 min post-administration of $^{99m}\text{TcN}[\text{G}_3\text{-c(RGDfK)}]_2$

3b.6. Conclusions

The work described in this section constitutes the synthesis of a novel ^{99m}Tc labeled dimeric RGD peptide derivative using $[\text{}^{99m}\text{TcN}]^{+2}$ intermediate. Towards this, the dithiocarbamate derivative of cyclic RGD monomer, $\text{G}_3\text{-c(RGDfK)}$ was prepared and radiolabeled using $[\text{}^{99m}\text{TcN}]^{+2}$ intermediate to form the $^{99m}\text{TcN}[\text{G}_3\text{-c(RGDfK)}]_2$ complex in high yield. The radiochemical purity of the complex was more than 98% as determined

Chapter 3

by high performance liquid chromatography (HPLC). The octanol-water partition coefficient value determined for the complex indicated that the radiolabeled conjugate is hydrophilic. Biological properties of the synthesized radiotracer were studied in C57BL/6 mice bearing melanoma tumors. Results of biodistribution studies showed specific uptake of radiotracer in melanoma tumor [4.61 ± 0.04 % IA/g at 30 min post-injection (p.i.)]. The complex exhibited favorable tumor/blood and tumor/muscle ratios (1.84 ± 0.21 and $4.12 \pm$ at 30 min p.i., respectively). Fast clearance of the activity was observed from non-target organs/tissue through renal route. Imaging studies also showed visible accumulation of activity in the tumor with appreciable target to background ratio. These preliminary studies indicate the potential of the developed radiotracer in tumor imaging.

Chapter 4

PREPARATION OF NEUTRAL $^{99m}\text{Tc}(\text{CO})_3$ -COMPLEXES OF “CLICKED”NITROIMIDAZOLE LIGANDS FOR IMAGING OF TUMOR HYPOXIA

Chapter 4

4.1. Introduction

Chapter 4 describes the use of differently substituted nitroimidazole derivatives as tumor targeting molecules for development of ^{99m}Tc -based radiotracers for hypoxia. The role of nitroimidazoles in targeting tumor hypoxia, mechanism of localization, preparation and evaluation of ^{99m}Tc -labeled neutral complexes of different nitroimidazole derivatives viz. 2-, 4- and 5-nitroimidazole have been discussed. The study described in this chapter makes use of the property of nitroimidazole derivatives, (in the present study, the nitroimidazole-based radiotracer) to enter tumor tissue by passive diffusion, followed by selective cell entrapment in hypoxic regions of the tumor.

4.1.1. Hypoxia

Hypoxia is a pathological condition that arises in organs or tissue in the body due to inadequate oxygen level. Medical conditions such as cancers, cardiovascular disease, cerebrovascular disease, diabetes, infection and wound healing are few of the several causes for tissue hypoxia. [170,171]

In tumors hypoxic condition arises when fast multiplication of the tumor cells outgrows the rate of blood supply to the tumor. This results in leaving portions of the tumor where the oxygen concentration is significantly lower than that in healthy tissues. Hypoxic microenvironments in solid tumors arise due to available oxygen being consumed within 70 to 150 μm of tumour vasculature by rapidly proliferating tumor cells thus limiting the amount of oxygen available to diffuse further into the tumor tissue. [172,173]. The negative influence of hypoxia in the clinical management of cancer is well documented [174-181]. Presence of hypoxic regions makes tumors resistant towards

Chapter 4

treatment modalities such as chemotherapy and radiotherapy and have direct implications on the prognosis and therapeutic outcome of the disease [171,172,175-178, 182,183].

The resistance of hypoxic cells to radiation therapy and chemotherapy was discovered in 1953, when well oxygenated tumor cells were found to exhibit three-fold greater response to radiotherapy compared to anoxic cells [179]. The problems posed by hypoxia in treatment of cancerous lesions have been extensively reviewed [179,180] and have prompted the clinical oncologists to assess the hypoxic status of the cancerous lesions so that appropriate modifications can be made in planning the therapeutic strategy. Assessment of the hypoxic status of cancer in patients enables the physicians to delineate patients who would be benefited from hypoxia-directed treatment from the other group of patients. These factors adequately substantiate the significance of detection of hypoxia in cancer and the relevance of development of efficient techniques to achieve this objective.

There are several methods to detect and quantify hypoxia in tumor which can be broadly classified into invasive and non-invasive categories. Since invasive techniques have several drawbacks and most of them are applicable only to superficial tumors, [181,184] non-invasive techniques are a preferred choice.

Currently, two non-invasive modalities available for the detection and quantification of hypoxia. These are imaging using radiopharmaceuticals and Magnetic Resonance Imaging (MRI). While MRI combines morphological imaging with limited functional imaging, the spatial resolution of the images obtained using MRI technique is high. The sensitivity is low and, it often requires appreciable quantity of contrast agents, which may be toxic to the body, to obtain images of acceptable quality. On the other

Chapter 4

hand, radiopharmaceuticals with their high sensitivity and ability to provide functional information of organs/tissue are considered superior to that of MRI [184].

4.1.2. Nitroimidazoles as the targeting vectors for tumor hypoxia

Nitroimidazoles which show selective accumulation in hypoxic cells are the most widely explored molecules for delineating hypoxic tumor cells from normoxic cells [185]. Nitroimidazoles are substituted imidazoles which are planar and pi-electron rich heteroaromatic compounds. 2-nitroimidazole (azomycin) was the first nitroimidazole isolated from a natural source. 4- and 5-nitroimidazoles are positional isomers of 2-nitroimidazole and differ only with respect to the position of the nitro group. Nitroimidazoles have been found to be able to delineate normal cells from hypoxic ones. This ability could be attributed to an interesting mechanism whose initial step involves an enzyme-mediated (nitro-reductase) single electron reduction of nitroimidazole to the corresponding radical anion. This reduction step is reversible in normal cells due to presence of sufficient oxygen which oxidizes the radical anion and promotes its clearance out of the cell. Whereas in hypoxic cells, the nitroimidazole radical anion gets reduced further and corresponding metabolites get trapped within the cells (**Fig. 4.1**) [172,173,186].

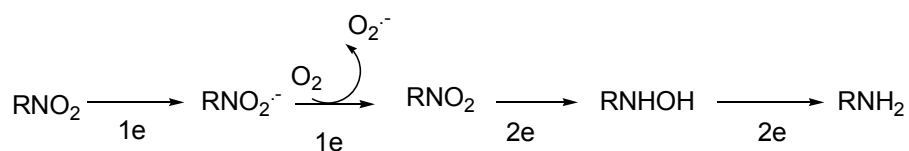


Fig. 4.1. Schematic representation of reduction of nitroimidazole

Chapter 4

4.1.3. Radiopharmaceuticals for hypoxia

Detection of hypoxia by a radiopharmaceutical is based on a principle governed by the oxygen-dependent chemical change of the radiotracer internalized in the tumor tissue. It will therefore be different in normoxic and hypoxic tissue thereby enabling the detection and delineation of these two tissue types from each other. Majority of radiopharmaceuticals developed and evaluated for the detection of hypoxia are based on nitroimidazoles. The two prominent non-nitroimidazole radiopharmaceuticals are $^{62/64}\text{Cu}$ -ATSM [187-189].

Several nitroimidazole based radiopharmaceuticals labeled with PET as well as SPECT isotopes have been reported [190-205]. Presently, [^{18}F]fluoromisonidazole ([^{18}F]FMISO), a 2-nitroimidazole-radiotracer, is the radiopharmaceutical of choice for clinical imaging of tumor hypoxia [206]. However, owing to optimal decay characteristics, easy availability and low cost of $^{99\text{m}}\text{Tc}$, a nitroimidazole radiopharmaceutical based on this isotope is expected to find wider applicability. Though, several $^{99\text{m}}\text{Tc}$ -labeled nitroimidazole radiopharmaceuticals are evaluated for their potential in detecting tumor hypoxia, $^{99\text{m}}\text{Tc}$ -BRU59-21 is, probably, the only complexone that have reached the stage of phase-I clinical trials [207]. Other complexes evaluated so far have not shown suitable pharmacokinetics for hypoxia-detecting applications in a clinical setup. This aspect has provided the impetus for the development of new nitroimidazole radiopharmaceuticals labeled with $^{99\text{m}}\text{Tc}$ for targeting tumor hypoxia. It has been observed from experience with various nitroimidazole based radiopharmaceuticals that, apart from suitable SERP (single electron reduction potential),

Chapter 4

overall lipophilicity and charge of the radiolabeled complex are equally important parameters in governing the uptake in hypoxic regions of the solid tumors. A suitable SERP is an essential feature for any hypoxia-targeting agent as it decides how readily it will get reduced in the hypoxic environment and be subsequently retained therein. Lipophilicity plays an important role in promoting the intracellular accumulation of the radiolabeled agents via passive diffusion pathway as more lipophilic complexes will have greater affinity for lipid bilayer of the cell membrane. The overall charge of the complex (positive, negative and neutral) on the other hand will be the determining factor for the overall pharmacokinetic behavior of the radiopharmaceutical [201,203,208].

4.1.4. Choice of ^{99m}Tc as the radioisotope

Detection of tumor hypoxia by imaging techniques with radiolabeled 2-nitroimidazoles was proposed by Chapman in 1979 [209]. Since then, a number of nitroimidazole derivatives have been radiolabeled and proposed for their use as SPECT and PET imaging of hypoxic tumors. ^{18}F FMISO (^{18}F fluoromisonidazole) is the most widely used nitroimidazole-based PET radiopharmaceutical used for hypoxia imaging [206]. Apart from ^{18}F FMISO, various other ^{18}F -labeled agents which have been evaluated clinically are [^{18}F]FAZA [^{18}F]fluoroazomycin arabinofuranoside), [^{18}F]FETNIM ([^{18}F]fluoroerythronitroimidazole), [^{18}F]FETA (^{18}F fluoroetanidazole) etc. [192,210,211]. Among the ^{99m}Tc -based radiotracers ^{99m}Tc -labeled 2-metronidazole (BMS181321) is the first agent to be used in diagnosis of hypoxia. BRU59-21 is another similar kind of second-generation hypoxia imaging agent. However, both of these agents

Chapter 4

were highly lipophilic and exhibited poor target to non target ratio when tested in vivo (Fig. 4.2) [212].

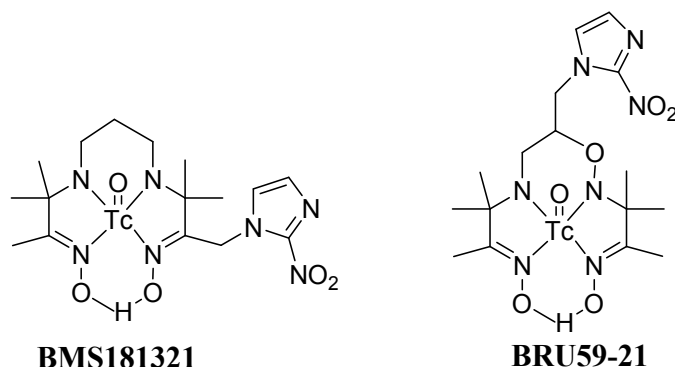


Fig. 4.2. Structures of two clinically evaluated ^{99m}Tc-labeled nitroimidazole based hypoxia imaging agents.

Until recently, no ^{99m}Tc based radiopharmaceutical has been able to replace the widely used ¹⁸[F]FMISO considered to be the gold standard in diagnosis of hypoxia [206]. The main limiting factor on the use of ¹⁸[F]FMISO is the availability of ¹⁸F. Fluorine-18 is a cyclotron produced isotope with a half-life of 110 minutes which poses logistic restriction towards its availability in distant centres away from the location of the cyclotron. Another factor is the availability of number of PET cameras which are fewer in comparison to SPECT cameras. All these factors add to the manufacturing cost of this imaging agent. A SPECT based hypoxia imaging agent can circumvent all these issues, particularly, in the current scenario with the advent of improved SPECT cameras which provide better resolution, Technetium-99m therefore becomes the ideal choice for developing a SPECT based hypoxia imaging agent owing to its excellent nuclear decay characteristics, low cost of production, availability from a ⁹⁹Mo-^{99m}Tc generator which

Chapter 4

overcomes the problem of distribution to places far away from production site. Additionally, introduction of unconventional ^{99m}Tc -cores, such as $[\text{}^{99m}\text{TcN}]^{+2}$ core and $[\text{}^{99m}\text{Tc}(\text{CO})_3]^+$ core, for radiolabeling biomolecules have alleviated the problems associated with the usage of the conventional ^{99m}Tc -oxo or ^{99m}Tc -dioxo cores to a great extent. The $[\text{}^{99m}\text{TcN}]^{+2}$ core and $[\text{}^{99m}\text{Tc}(\text{CO})_3]^+$ core are easy to prepare and stable over a wide range of pH conditions. The $[\text{}^{99m}\text{Tc}(\text{CO})_3(\text{H}_2\text{O})_3]^+$ precursor complex, introduced by Alberto et al [213], is especially attractive for radiolabeling small bio-molecules and peptides. Three labile water molecules in $[\text{}^{99m}\text{Tc}(\text{CO})_3(\text{H}_2\text{O})_3]^+$ precursor complex permits radiolabeling with a suitable tridentate ligand resulting in the formation of a stable pseudo-octahedral complex [214].

In the present work, the concept of ‘click chemistry’ was employed to prepare triazole derivatives of three differently substituted nitroimidazoles viz. 2-, 4- and 5-nitroimidazole, for radiolabeling with $[\text{}^{99m}\text{Tc}(\text{CO})_3]^+$ core [204-206]. 2-, 4- and 5-nitroimidazole are three position isomers of nitroimidazole molecule and exhibit different SERP (single electron reduction potential) values viz. -418 mV, -527 mV and -450 mV, respectively (**Fig. 4.3**). Triazole ligands form neutral pseudo-octahedral complex with $[\text{}^{99m}\text{Tc}(\text{CO})_3(\text{H}_2\text{O})_3]^+$ precursor complex [202]. The three, differently substituted, neutral, nitroimidazole-triazole complexes prepared were subsequently evaluated in Swiss mice bearing fibrosarcoma tumor. The biodistribution results obtained are thoroughly analyzed and compared with clinically used hypoxia imaging agent $[\text{}^{18}\text{F}]\text{FMISO}$.

Chapter 4

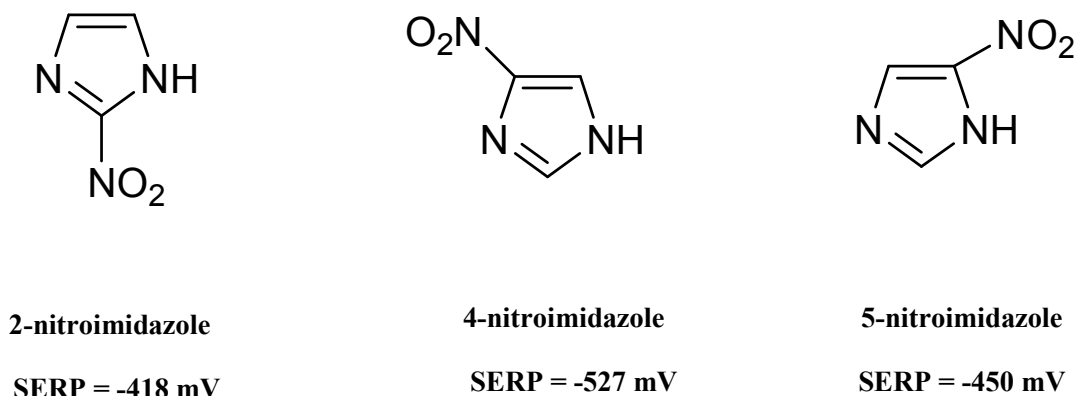


Fig. 4.3. Structural representation of 2-, 4- and 5-nitroimidazoles with respective SERP values

4.2. Experimental

4.2.1. Materials and methods

2-Nitroimidazole, 4-nitroimidazole, 1,3-dibromopropane, anhydrous potassium carbonate and L-propargyl glycine were procured from M/s. Fluka, Germany. Copper sulphate, sodium azide, ascorbic acid and sodium carbonate were purchased from S.D. Fine Chemicals, Mumbai, India. Flexible silica gel plates used for thin layer chromatography (TLC) were obtained from Bakerflex Chemical Company, Germany. The HPLC analyses were performed on a JASCO PU 2080 Plus dual pump HPLC system, Japan, with a JASCO 2075 Plus tunable absorption detector and a Gina Star radiometric detector system, using a C-18 reversed phase HiQ Sil column (5 μ m, 4 x 250 mm). All the solvents used for HPLC were degassed and filtered prior to use and were of HPLC grade. IR spectra of the synthesized compounds were recorded on JASCO-FT/IR-420 spectrometer, Japan. ^1H -NMR spectra were recorded using 300MHz Bruker Avance

Chapter 4

II, spectrometer, Germany. Mass spectra were recorded on QTOF Micromass Instrument using electron spray ionization (ESI) in positive mode.

4.2.2. Synthesis

4.2.2.1. Synthesis of 1-(3-bromopropyl)-2-nitro-1H-imidazole (**4a**)

Compound **4a** was prepared from 2-nitroimidazole (0.11 g, 1 mmol) and 1, 3-dibromopropane (0.59 g, 10 mmol) in presence of crushed anhydrous K_2CO_3 in acetonitrile (10 mL) [196]. The reaction mixture was stirred overnight at room temperature. Upon completion of the reaction (cf. TLC), solvent was removed under vacuum and the residue was dissolved in water (30 mL). The aqueous layer was extracted with chloroform (15 mL x 3). Combined organic layer was washed with brine and dried over anhydrous sodium sulphate. The dried organic layer was concentrated and purified by silica gel column chromatography to obtain compound **4a** (0.19 g, 80%). R_f (diethylether) = 0.22. IR (neat, cm^{-1}) 3121(m); 2918(w); 2853(w); 1545(s); 1406(s); 1044(s); 656(s). 1H -NMR (δ ppm, $CDCl_3$) 2.41 (m, 2H, $-CH_2CH_2CH_2Br$), 3.38 (t, 2H, $J = 7.35$ Hz, $-CH_2CH_2CH_2Br$), 4.63 (t, 2H, $J = 7.35$ Hz, $-CH_2CH_2CH_2Br$), 7.22 (s, 1H, 2-nitroimidazole-C5-H), 7.27 (s, 1H, 2-nitroimidazole-C4-H).

4.2.2.2. Synthesis of 1-(3-bromopropyl)-4-nitro-1H-imidazole and 1-(3-bromopropyl)-5-nitro-1H-imidazole (**4b** & **4c**)

Compounds **4b** and **4c** were prepared in a one-pot reaction between 4-nitroimidazole (0.5 g, 4.4 mmol) and 1, 3-dibromopropane (2.6 g, 44 mmol) in presence of crushed anhydrous K_2CO_3 as base in acetonitrile (10 mL) [200]. The reaction mixture

Chapter 4

was kept stirring overnight at room temperature. Upon completion of the reaction (cf. TLC), the mixture was worked-up following a procedure similar to the one described for compound **4a**. Compound **4b** and **4c** were separated by silica gel column chromatography using diethyl ether. Yield of compound **4b** was 75% (0.77 g) and that of compound **4c** was 11% (0.11 g).

Compound 4b: R_f (diethylether) = 0.3. IR (neat, cm^{-1}) 3121(m); 2918(w); 2853(w); 1545(s); 1406(s); 1044(s); 656(s). $^1\text{H-NMR}$ (δ ppm, CDCl_3) 2.36 (m, 2H, - $\text{CH}_2\text{CH}_2\text{CH}_2\text{Br}$), 3.36 (t, 2H, $J = 5.73$ Hz, - $\text{CH}_2\text{CH}_2\text{CH}_2\text{Br}$), 4.27 (t, 2H, $J = 6.51$ Hz, - $\text{CH}_2\text{CH}_2\text{CH}_2\text{Br}$), 7.52 (s, 1H, 4-nitroimidazole-C2-H), 7.84 (s, 1H, 4-nitroimidazole-C5-H) [Fig. 4.4]

Compound 4c: R_f (diethylether) = 0.4. IR (neat, cm^{-1}) 3114(w); 2969(w); 1529(s); 1371(s); 1121(s); 741(s); 650(w). $^1\text{H-NMR}$ (δ ppm, CDCl_3) 2.39 (m, 2H, - $\text{CH}_2\text{CH}_2\text{CH}_2\text{Br}$), 3.36 (t, 2H, $J = 6.24$ Hz, - $\text{CH}_2\text{CH}_2\text{CH}_2\text{Br}$), 4.59 (t, 2H, $J = 7.02$ Hz, - $\text{CH}_2\text{CH}_2\text{CH}_2\text{Br}$), 7.74 (s, 1H, 5-nitroimidazole-C2-H), 8.03 (s, 1H, 5-nitroimidazole-C4-H)

4.2.2.3. General procedure for synthesis of nitroimidazole azides

Bromide derivatives of different nitroimidazoles were converted into corresponding azides by reacting with NaN_3 in dimethylformamide [204]. Upon completion of the reaction the solvent was removed using rotary evaporator. The residue was dissolved in water (30 mL) and extracted with chloroform (15 mL x 3). Combined

Chapter 4

organic layer was washed with brine, concentrated and purified by silica gel column chromatography to obtain corresponding nitroimidazole azide.

4.2.2.4. Synthesis of 1-(3-azidopropyl)-2-nitro-1H-imidazole (**4d**)

Compound **4d** was prepared from compound **4a** (0.15 g, 0.64 mmol) and NaN₃ (0.04 g, 0.64 mmol) following the general procedure described above. Yield 75% (0.09 g). R_f(chloroform) = 0.28. IR (neat, cm⁻¹) 3114(m); 2936(w); 2873(w); 2099(s); 1537(s); 835(s). ¹H-NMR (δ ppm, CDCl₃) 2.12 (m, 2H, -CH₂CH₂CH₂N₃), 3.38 (t, 2H, J = 6.18 Hz, -CH₂CH₂CH₂N₃), 4.51 (t, 2H, J = 6.69 Hz, -CH₂CH₂CH₂N₃), 7.14 (s, 1H, 2-nitroimidazole-C5-H), 7.15 (s, 1H, 2-nitroimidazole-C4-H).

4.2.2.5. Synthesis of 1-(3-azidopropyl)-4-nitro-1H-imidazole (**4e**)

Compound **4e** was prepared by reaction of compound **4b** (0.5 g, 2.13 mmol) with NaN₃ (0.14 g, 2.13 mmol) following the general procedure described above. The yield of the reaction was 75% (0.32 g). R_f(chloroform) = 0.21. IR (neat, cm⁻¹) 3126(m); 2921(w); 2099(s); 1541(s); 1126(s); 831(s). ¹H-NMR (δ ppm, CDCl₃) 2.09 (m, 2H, -CH₂CH₂CH₂N₃), 3.38 (t, 2H, J = 6.69 Hz, -CH₂CH₂CH₂N₃), 4.16 (t, 2H, J = 8.04 Hz, -CH₂CH₂CH₂N₃), 7.49 (s, 1H, 4-nitroimidazole-C2-H), 7.83 (s, 1H, 4-nitroimidazole-C5-H) [Fig. 4.5].

4.2.2.6. Synthesis of 1-(3-azidopropyl)-5-nitro-1H-imidazole (**4f**)

Compound **4f** was prepared by reaction of compound **4c** (0.05 g, 0.21 mmol) with NaN₃ (0.02 g, 0.21 mmol) following the general procedure stated above. The yield of the

Chapter 4

reaction was 60% (0.025 g). R_f (chloroform) = 0.25. IR (neat, cm^{-1}) 3119(m); 2926(w); 2881(w); 2100(s); 1523(s); 1125(s); 824(s); 648(vs). $^1\text{H-NMR}$ (δ ppm, CDCl_3) 2.08 (m, 2H, $-\text{CH}_2\text{CH}_2\text{CH}_2\text{N}_3$), 3.38 (t, 2H, $J = 10.11$ Hz, $-\text{CH}_2\text{CH}_2\text{CH}_2\text{N}_3$), 4.51 (t, 2H, $J = 13.47$ Hz, $-\text{CH}_2\text{CH}_2\text{CH}_2\text{N}_3$), 7.68 (s, 1H, 5-nitroimidazole-C2-H), 8.03 (s, 1H, 5-nitroimidazole-C4-H).

4.2.2.7. General procedure for synthesis of triazole from azide

Different terminal nitroimidazole azides were converted into corresponding triazoles via “click reaction” with L-propargyl glycine in presence of sodium ascorbate and copper sulphate in water [204]. The reaction mixture was kept stirring at room temperature for 36 h. It was subsequently washed with dichloromethane to remove excess nitroimidazole azide.

4.2.2.8. Synthesis of 2-amino-3-(1-(3-(2-nitro-1H-imidazol-1-yl)propyl)-1H-1,2,3-triazol-4-yl)propanoic acid (**4g**)

Compound **4d** (50 mg, 0.26 mmol), L-propargyl glycine (30 mg, 0.26 mmol), ascorbic acid (20 mg, 40 mol%) and $\text{CuSO}_4 \cdot 2\text{H}_2\text{O}$ (10 mg, 20 mol%) were dissolved in 3 mL of double distilled water. The reaction was carried out following general procedure stated above. Overall yield of **4g** was 40 % (30 mg). IR (KBr, cm^{-1}) 3407(m); 2949(w); 1773(s); 1626(s); 1486(s); 1359(m); 1285(m); 1111(s); 832(s); 616(s). ESI-MS (m/z): $\text{C}_{11}\text{H}_5\text{N}_7\text{O}_4$ MS (ESI^+): 309.2(M) $^+$.

4.2.2.9. Synthesis of 2-amino-3-(1-(3-(4-nitro-1H-imidazol-1-yl)propyl)-1H-1,2,3-triazol-4-yl)propanoic acid (**4h**)

Chapter 4

Compound **4e** (0.02 g, 0.10 mmol), L-propargyl glycine (0.08 g, 0.74 mmol), ascorbic acid (0.06 g, 40 mol%) and CuSO₄·2H₂O (0.04 g, 20 mol%) were dissolved in 3 mL of double distilled water. The reaction was carried out following general procedure stated above. Overall yield of **4h** was 47 % (0.11 g). IR (KBr, cm⁻¹) 3426(m); 2956(w); 1640(s); 1486(m); 1404(m); 1290(s); 1219(m); 1124(s); 1060(s); 825(s). ESI-MS (m/z): C₁₁H₅N₇O₄ MS (ESI⁺): 309.1 (M)⁺ [Fig. 4.6].

4.2.2.10. Synthesis of 2-amino-3-(1-(3-(5-nitro-1H-imidazol-1-yl)propyl)-1H-1,2,3-triazol-4-yl)propanoic acid (**4i**)

Compound **6** (0.12 g, 0.61 mmol) with L-propargyl glycine (0.07 g, 0.61 mmol), ascorbic acid (0.05 g, 40 mol%) and CuSO₄·2H₂O (0.03 g, 20 mol%) were dissolved in 3 mL of double distilled water. The reaction was carried out following general procedure stated above. Overall yield of **9** was 44 % (0.08 g). IR (KBr, cm⁻¹) 3439(m); 2924(m); 1735(s); 1633(s); 1398(v); 1305(m); 1226(m); 1131(s); 533(m); 616(s). ESI-MS (m/z): C₁₁H₅N₇O₄ MS (ESI⁺): 309.1(M)⁺.

4.2.2.11. Preparation of 4-nitroimidazole-triazole-Re(CO)₃ complex (**4m**)

The rhenium analogue of 4-nitroimidazole-triazole-[^{99m}Tc(CO)₃] was prepared by refluxing a mixture of 4-nitroimidazole-triazole (0.170 g, 0.55 mmol) and bis(tetraethylammonium)-*fac*-tribromotricarbonylrhenate (0.422 g, 0.55 mmol) in 5 mL water for 15 h [204]. The compound bis(tetraethylammonium)-*fac*-tribromotricarbonylrhenate was prepared following a procedure reported by Alberto et al [215]. After refluxing, reaction mixture was allowed to cool down followed by the

Chapter 4

filtration. The filtrate was evaporated under vacuum to yield the 4-nitroimidazole-triazole-Re(CO)₃ complex as tetraethylammonium salt (0.152 g, 48%). ESI-MS (m/z): C₁₄H₁₄N₇O₇Re MS (ESI⁺): 601.8 (M+Na)⁺ [Fig. 4.7].

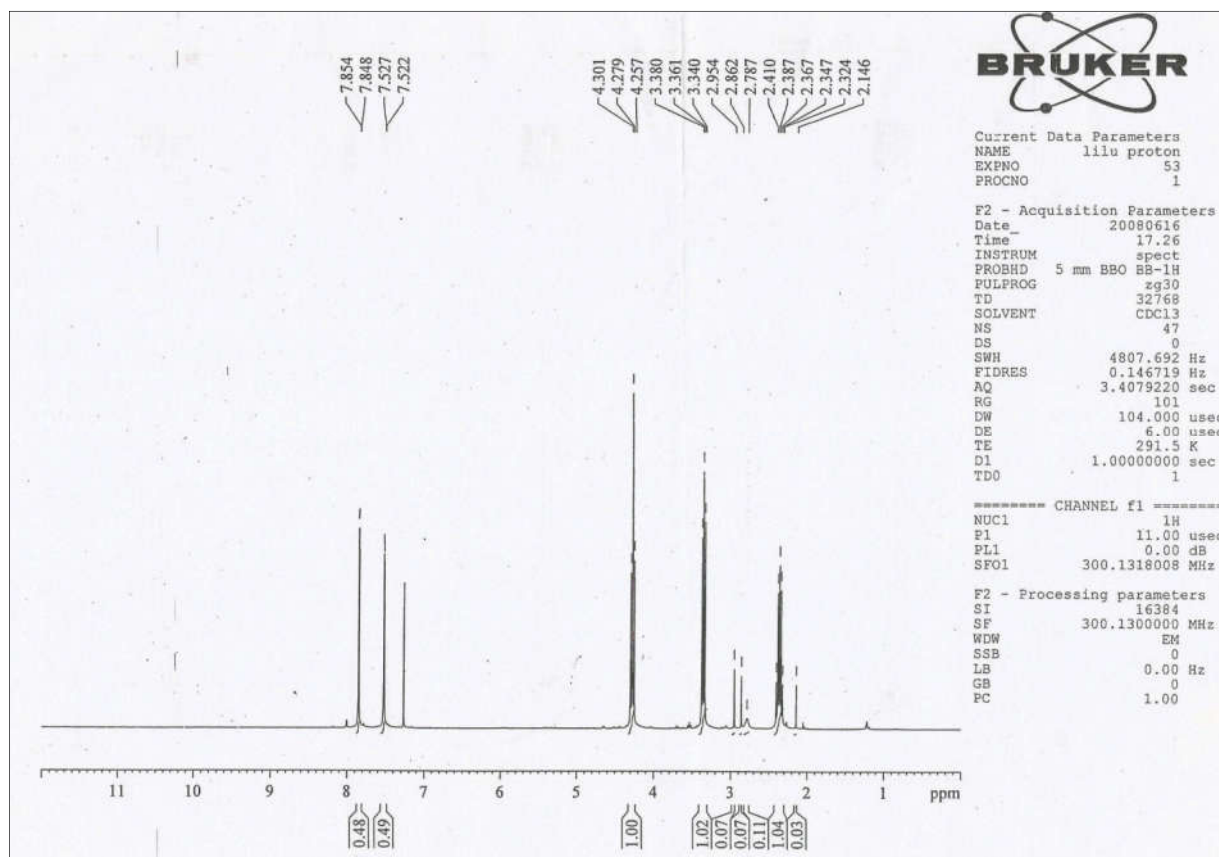


Fig. 4.4. ¹H-NMR of 1-(3-bromopropyl)-4-nitro-1H-imidazole (**4b**)

Chapter 4

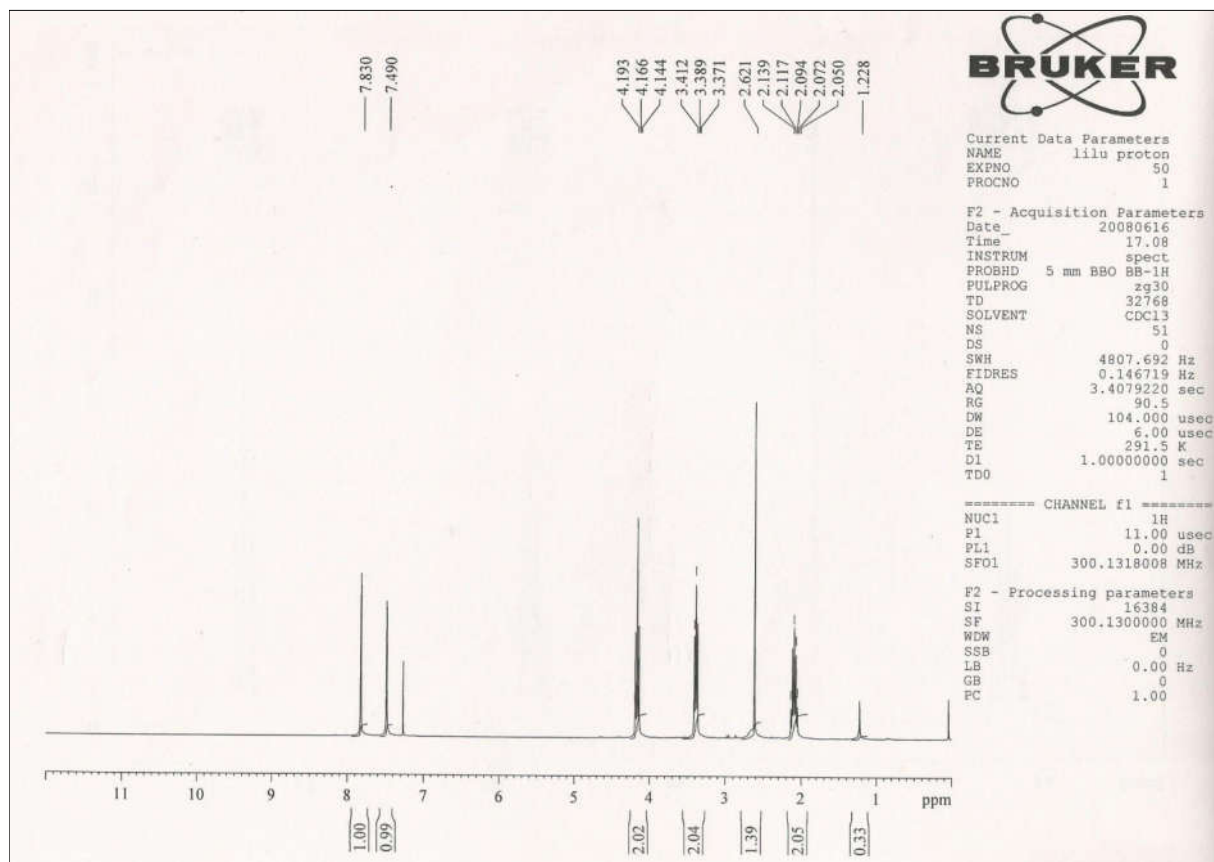


Fig. 4.5. ^1H -NMR of 1-(3-azidopropyl)-4-nitro-1H-imidazole (**4e**)

Chapter 4

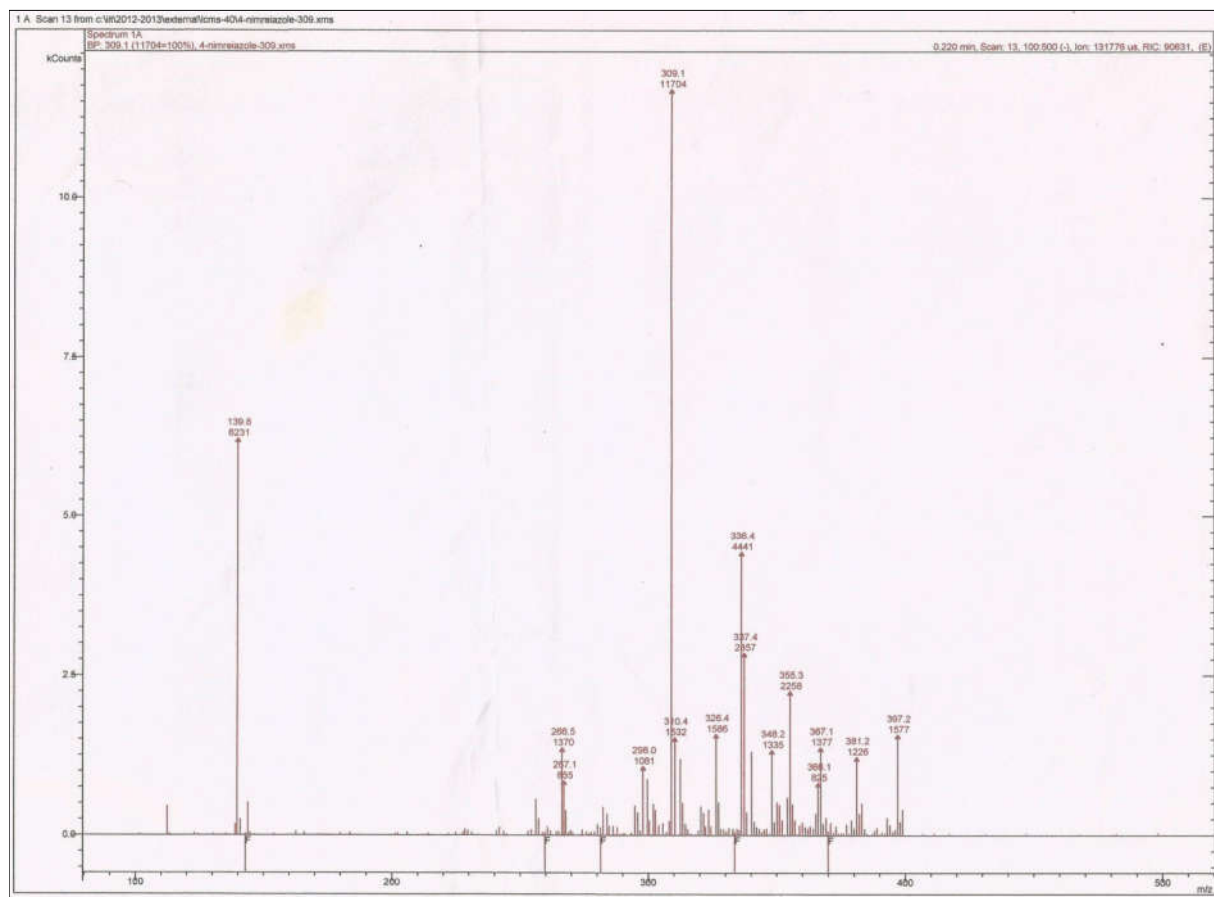


Fig. 4.6. ESI-MS of 2-amino-3-(1-(3-(4-nitro-1H-imidazol-1-yl)propyl)-1H-1,2,3-triazol-4-yl)propanoic acid (**4h**)

Chapter 4

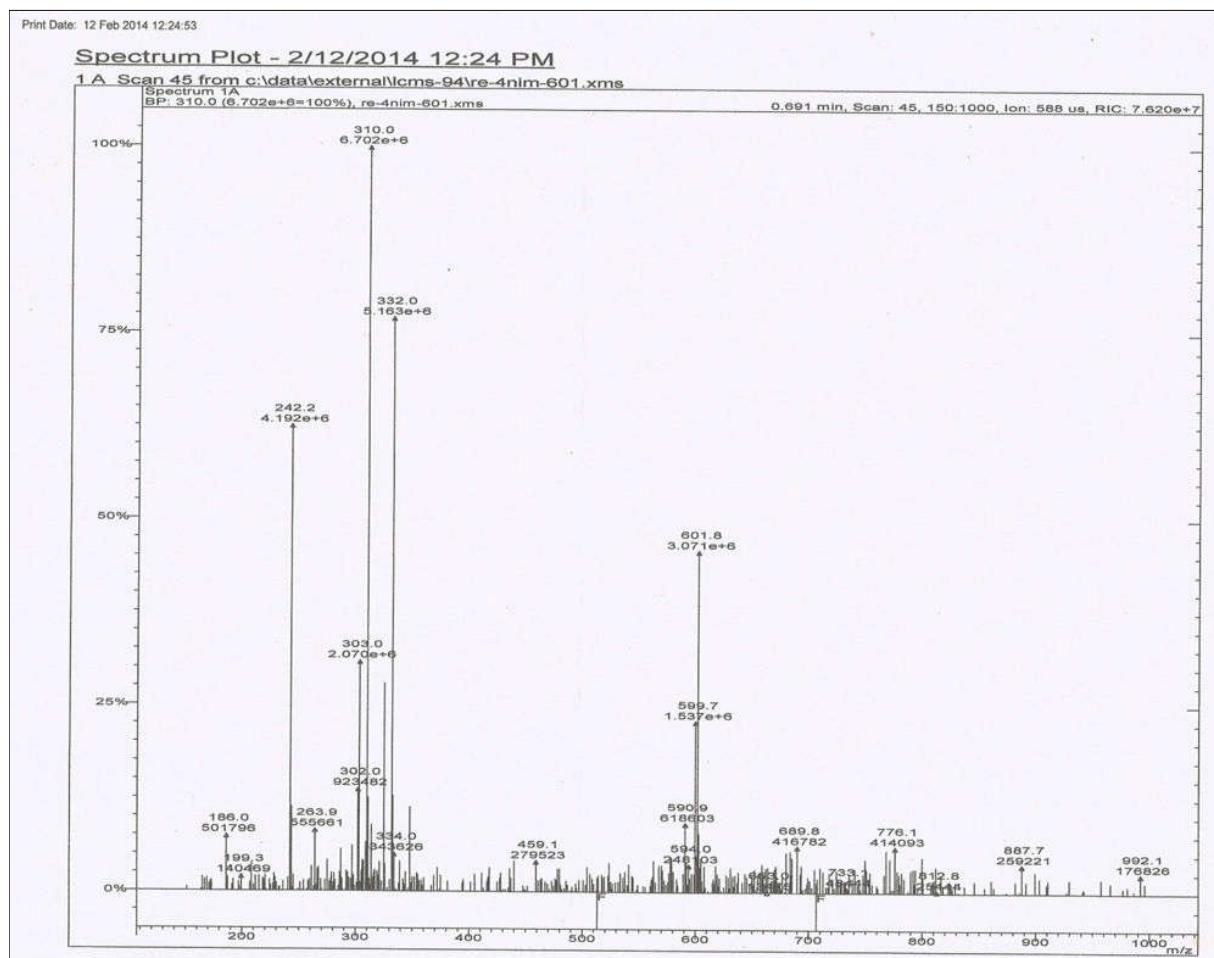


Fig. 4.7. ESI-MS of $\text{Re}(\text{CO})_3$ complex of compound 4h (**4m**)

4.2.3. Radiolabeling

4.2.3.1. Preparation of $[\text{}^{99\text{m}}\text{Tc}(\text{CO})_3(\text{H}_2\text{O})_3]^+$ precursor complex

The $[\text{}^{99\text{m}}\text{Tc}(\text{CO})_3(\text{H}_2\text{O})_3]^+$ precursor complex was prepared following the procedure reported by Alberto et al [213]. An aqueous solution of NaBH_4 (5.5 mg), Na_2CO_3 (4 mg) and Na/K tartrate (15 mg) in 0.5 mL double distilled water in a sealed 10 mL vial was purged with carbon monoxide gas for 5 minutes. To this solution freshly

Chapter 4

eluted $\text{Na}^{99\text{m}}\text{TcO}_4$ (1 mL, ~ 37 MBq) was added and the mixture was heated at 80°C for 15 min. The reaction mixture was then cooled on an ice bath for 5 min. The pH of the reaction mixture was adjusted to 7 using 0.5 M phosphate buffer (pH 7.5): 1 M HCl (1:3 v/v) and subsequently characterized by HPLC.

4.2.3.2. General procedure for the radiolabeling of nitroimidazole triazole derivatives (4g, 4h & 4i) with $[\text{}^{99\text{m}}\text{Tc}(\text{CO})_3(\text{H}_2\text{O})_3]^+$ precursor to prepare $^{99\text{m}}\text{Tc}(\text{CO})_3$ complexes of 2-, 4- and 5-nitroimidazoles (4j, 4k, 4l)

To 900 μL of 10^{-3} M solution of respective nitroimidazole triazole ligand in saline, 100 μL of freshly prepared $[\text{}^{99\text{m}}\text{Tc}(\text{CO})_3(\text{H}_2\text{O})_3]^+$ precursor complex was added and the radioactive solution incubated at 80°C for 45 min. The solution was then cooled to room temperature and the complex obtained was characterized using HPLC.

4.2.4. Quality control

4.2.4.1. HPLC

The radiochemical purity (RCP) of $[\text{}^{99\text{m}}\text{Tc}(\text{CO})_3(\text{H}_2\text{O})_3]^+$ precursor complex as well as different nitroimidazole- $^{99\text{m}}\text{Tc}(\text{CO})_3$ complexes (**4j**, **4k**, **4l**) was assessed by HPLC with a C18 reversed phase column. About 15 μL of the test solution (~ 0.37 MBq) was injected into the column and elution was monitored by observing the radioactivity profile. Aqueous 0.05M triethylammonium phosphate (TEAP) buffer, pH = 2.5 (Solvent A) and methanol (Solvent B) were used as the mobile phase. Both the solvents were filtered through 0.22 μ filter. The elution started with 100% A from 0 to 6 min. At 6 min the eluent switched to 75% A and 25% B and at 9 min to 66% A and 34% B followed by

Chapter 4

a linear gradient 66% A/34% B to 100% B from 9 to 20 min. Up to 30 min the eluent remained at 100% B before switching back to the initial condition. Flow rate was maintained at 1 mL/min.

4.2.4.2. Determination of octanol-water partition coefficient ($\text{Log } P_{\text{o/w}}$)

The radiolabeled compound (0.1 mL) was mixed with double distilled water (0.9 mL) and *n*-octanol (1 mL) on a vortex mixer for about 3 min and then centrifuged at 3500 g for 5 min to effect clear separation of the two layers. The *n*-octanol layer (0.8 mL) was withdrawn and equal volume of fresh double distilled water was added. The mixture was vortexed and then centrifuged as described above. Equal aliquots of the two layers were withdrawn and measured for the radioactivity. The readings thus obtained were used to calculate the $\text{Log } P_{\text{o/w}}$ value of the complex.

4.2.4.3. In vitro serum stability and protein binding studies

About 50 μL of the labeled complex (**4j**, **4k** or **4l**) was added to 0.45 mL of human serum and this solution was incubated at 37°C. After 3 h, ethanol (0.5 mL) was added to this solution to precipitate serum proteins. The mixture was centrifuged (at how many g) and the supernatant was analyzed by HPLC to assess the stability of the complex in serum. The activity associated with protein pellet was determined in a well-type NaI(Tl) detector. The ratio of activity associated with the protein pellet to the activity initially added to serum gives a measure of activity bound to serum protein.

4.2.5. Biological studies

Chapter 4

All procedures performed herein were in strict compliance with the national laws governing the conduct of animal experiments. Solid tumor was developed in Swiss mice by implantation of HSDM1C1 murine fibrosarcoma. About 10^6 cells in 100 μL volume were injected subcutaneously on the dorsum of each animal. The tumors were allowed to grow till they were approximately 10 mm in diameter after which the animals were used for the experiment. For the biodistribution studies, the radioactive preparation (~ 0.37 MBq per animal in 100 μL volume) was administered intravenously through the lateral tail vein. Individual sets of animals ($n=3$) were utilized for studying the biodistribution at different time points (30 min, 60 min, and 180 min). At the end of the respective time periods, the animals were sacrificed and the relevant organs excised for measurement of retained activity. The organs were weighed and the activity associated with them was measured in a flat-bed type NaI(Tl) counter with suitable energy window for $^{99\text{m}}\text{Tc}$. The activity retained in each organ/tissue was expressed as percentage injected dose per gram (%ID/g).

4.2.6. Statistical analysis

Statistical analysis of relevant data was performed by one-way analysis of variance (ANOVA). Confidence level of 95% ($p<0.05$) was taken for statistical significance.

Chapter 4

4.3. Results and discussion

Appropriate terminal azides when ‘clicked’ with L-propargyl glycine form tridentate triazole ligands suitable for preparing neutral $^{99m}\text{Tc}(\text{CO})_3$ complexes in high RCP and in vivo stability. This strategy was adopted to convert 2-, 4- and 5-nitroimidazole azide derivatives into corresponding tridentate triazole ligands (**4g-4i**) as shown in **Fig. 4.8**. All intermediates were characterized by appropriate spectroscopic techniques. Mass spectrometric analysis confirmed the identity of target compounds **4g-4i**.

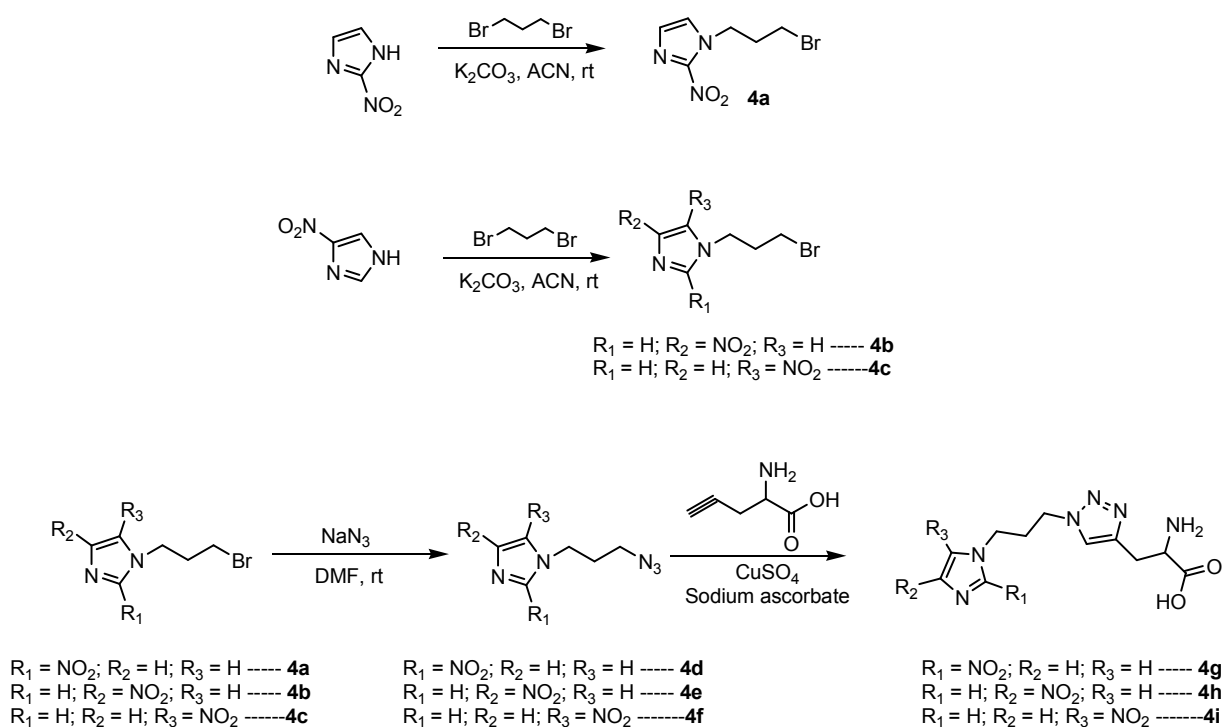


Fig. 4.8. Synthesis of triazole derivatives of 2-, 4- and 5-nitroimidazoles

Chapter 4

Following the optimized protocol, the nitroimidazole triazole derivatives (**4g-4i**) were radiolabeled using freshly prepared $[^{99m}\text{Tc}(\text{CO})_3(\text{H}_2\text{O})_3]^+$ precursor complex (**Fig. 4.9**).

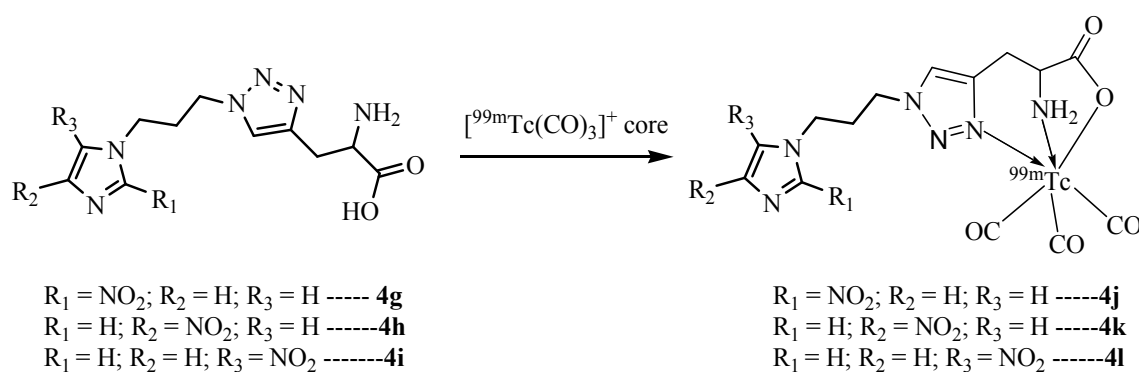


Fig. 4.9. Radiolabeling of 2-, 4- and 5-nitroimidazole triazole derivatives with $[^{99m}\text{Tc}(\text{CO})_3(\text{H}_2\text{O})_3]^+$ precursor complex

The $[^{99m}\text{Tc}(\text{CO})_3(\text{H}_2\text{O})_3]^+$ precursor complex as well as the $^{99m}\text{Tc}(\text{CO})_3$ complexes of 2-, 4-, and 5-nitroimidazole triazole (**4j**, **4k**, **4l**) were analyzed by reversed phase HPLC following the gradient elution program described in the experimental section. The HPLC retention time observed for the three nitroimidazole-triazole- $^{99m}\text{Tc}(\text{CO})_3$ complexes is summarized in **Table 4.1**. Typical HPLC profiles of $[^{99m}\text{Tc}(\text{CO})_3(\text{H}_2\text{O})_3]^+$ precursor complex and three nitroimidazole triazole complexes (**4j-4l**) are shown in **Fig. 4.10**. The HPLC peak area measurements showed that RCP of all the complexes were >90%.

Chapter 4

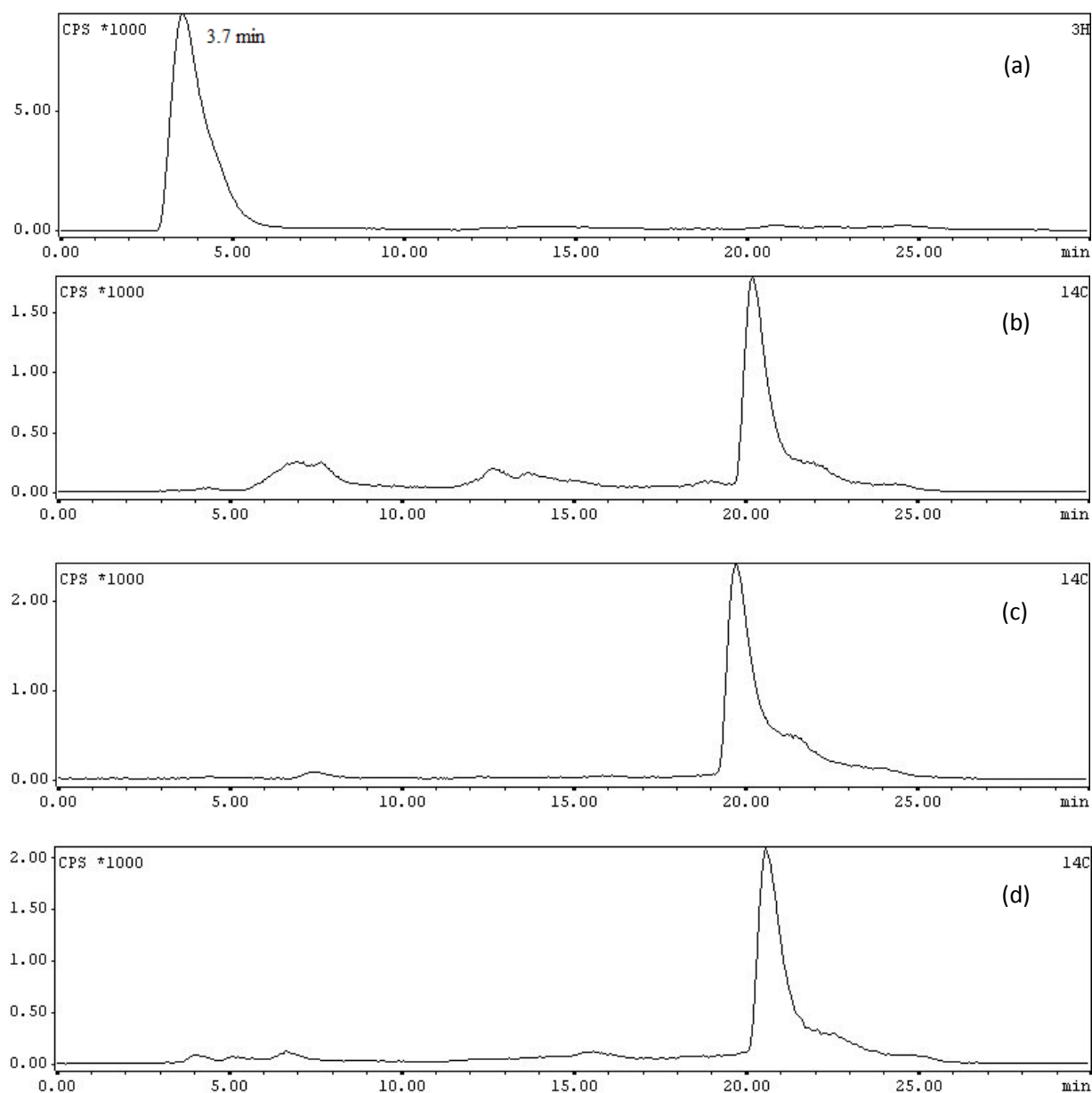


Fig. 4.10. HPLC elution profile of (a) $[^{99m}\text{Tc}(\text{CO})_3(\text{H}_2\text{O})_3]^+$ precursor complex and (b) 2-nitroimidazole triazole- $^{99m}\text{Tc}(\text{CO})_3$ complex (c) 4-nitroimidazole triazole- $^{99m}\text{Tc}(\text{CO})_3$ complex (d) 5-nitroimidazole triazole- $^{99m}\text{Tc}(\text{CO})_3$ complex

Lipophilicity ($\text{LogP}_{\text{o/w}}$) of the complexes was determined following a reported procedure (Table 4.1) [36]. Serum stability studies showed that all the complexes (**4j-4l**) were stable in human serum when incubated at 37°C for 3 h. Serum protein binding studies of the

Chapter 4

complexes (**4j-4l**) showed that about 30–35 % activity was associated with the serum proteins upon incubation in the human serum at 37°C for 3 h (**Table 4.1**). To obtain evidence for the structure of $^{99m}\text{Tc}(\text{CO})_3$ -complexes prepared at the tracer level, a 4-nitroimidazole triazole- $\text{Re}(\text{CO})_3$ complex was prepared in macroscopic level. Matching HPLC elution profile of 4-nitroimidazole triazole- $\text{Re}(\text{CO})_3$ complex and corresponding $^{99m}\text{Tc}(\text{CO})_3$ complex prepared at the tracer

level indicated the formation of structurally similar complexes (**Table 4.1**). A $(\text{M}+\text{Na})^+$ ion peak at m/z 601.8 in the mass spectrum provided another confirmatory evidence for the formation of the expected 4-nitroimidazole triazole- $\text{Re}(\text{CO})_3$ complex.

Table 4.1. Log $P_{o/w}$ values and other quality control parameters of different nitroimidazole triazole- $^{99m}\text{Tc}(\text{CO})_3$ complexes

	Log $P_{o/w}$	Retention time in HPLC (in min)	%RCP	Specific activity $\mu\text{Ci}/\mu\text{mol}$ ligand)	%Activity (in of associated with serum proteins
$[^{99m}\text{Tc}(\text{CO})_3(\text{H}_2\text{O})_3]^+$ precursor complex	-	3.7±0.2	-	-	-
2-nitroimidazole triazole- $^{99m}\text{Tc}(\text{CO})_3$ complex	- 0.32±0.02	20.5±0.1	95.0±1.00	105.55±1.11	32.8±1.35
4-nitroimidazole triazole- $^{99m}\text{Tc}(\text{CO})_3$ complex	- 0.52±0.01	20.0±0.2	96.3±0.57	107.03±0.64	30.1±1.06
5-nitroimidazole triazole- $^{99m}\text{Tc}(\text{CO})_3$ complex	- 0.03±0.01	21.0±0.1	97.0±1.00	107.77±1.11	35.4±0.96
4-nitroimidazole triazole $\text{Re}(\text{CO})_3$	-	19.5±0.2	-	-	-

Chapter 4

Biological evaluations of all the three nitroimidazole-triazole- $^{99m}\text{Tc}(\text{CO})_3$ complexes (**4j-4l**) were carried out in Swiss mice bearing fibrosarcoma tumor. Though the hypoxic status of the fibrosarcoma tumor used for the present study was not determined, a systematic study by Markus et al. on a number of murine tumors, including a fibrosarcoma tumor, had shown that these tumors are hypoxic [216]. Additionally, biodistribution of [^{18}F]FMISO carried out earlier in the fibrosarcoma tumor model being used in the present study had shown significant tumor uptake which provided an indirect evidence for the hypoxic nature of the tumor [203].

Biodistribution of the complexes (**4j-4l**) was studied at three time points viz. 30 min, 1 h and 3 h. Tumor uptake observed with the three nitroimidazole complexes is shown in **Table 4.2**. For comparison, tumor uptake observed with [^{18}F]FMISO is also shown in **Table 4.2**. Similar to our earlier observations, all the complexes showed relatively fast clearance from tumor between 30 min and 1 h post injection (p.i.), which could be attributed to the clearance of unbound nitroimidazole complex from the tumor. Slow clearance of tumor activity observed after 1 h p.i. is attributed to the hypoxia specific reduction and trapping of the radiotracer in tumor [Mallia MB Nuc Med Biol 41:600-610].

Chapter 4

Table 4.2. Activity of different nitroimidazole-triazole-^{99m}Tc(CO)₃ complexes and [¹⁸F]FMISO observed in tumor and blood at different time points (n=5)

		4j	4k	4l	[¹⁸F]FMISO[*]
Tumor	30 min	1.41±0.08	0.63±0.09	2.03±0.32	4.65±0.86
%ID/g (s.d) [#]	60 min	0.97±0.06	0.56±0.05	1.45±0.08	3.70±0.09
	180 min	0.75±0.14	0.26±0.02	0.81±0.06	2.04±0.14
Blood	30 min	0.95±0.05	0.73±0.08	1.91±0.14	3.95±0.31
%ID/g (s.d) [#]	60 min	0.62±0.12	0.37±0.02	1.31±0.11	2.38±0.42
	180 min	0.43±0.06	0.35±0.04	0.77±0.04	0.53±0.07

[#]%ID/g – Percentage injected dose per gram; s.d. – standard deviation; ^{*} Ref. [203]

The effectiveness of a nitroimidazole complex to detect hypoxic tumor cells depend on factors such as its single electron reduction potential (SERP), ease with which the nitroimidazole complex enters the hypoxic cells and the time nitroimidazole complex spends in hypoxic cells. Ease of reduction of nitroimidazole complex in hypoxic tumor cells is determined by its SERP. SERP depends on the position of nitro-group in the imidazole ring. Reported SERP value of unsubstituted 2-, 4- and 5-nitroimidazole in aqueous solution is -418 mV, -527 mV and -450 mV, respectively, with respect to standard hydrogen electrode (SHE) [217]. Though modification at N1-nitrogen of nitroimidazole ring, as done in the present work, can potentially alter the SERP values of

Chapter 4

the nitroimidazole derivative, previous studies have shown that such variations are not significant [218]. Among the different nitroimidazole triazole derivatives, we expected that 2-nitroimidazole derivative with highest SERP value will show the highest tumor uptake. However, contrary to our expectations, the 5-nitroimidazole complex showed higher tumor uptake than the 2-nitroimidazole counterpart at all the time points (**Table 4.2**). Statistical analysis showed that tumor uptake observed with 5-nitroimidazole-triazole complex is significantly higher ($p < 0.05$) than the 2-nitroimidazole counterpart at 30 min and 60 min p.i. However, at 3 h p.i., the difference in tumor uptake was found to be insignificant ($p > 0.05$). Tumor uptake of 4-nitroimidazole-triazole complex was lowest among the three triazole complexes at all the time points. This is not surprising, since SERP of 4-nitroimidazole is lowest among 2-, 4- and 5-nitroimidazole. In comparison, [^{18}F]FMISO with a SERP of -389 mV (with respect to SHE) showed significantly higher uptake than any of the nitroimidazole-triazole complexes at all the time points (**Table 4.2**). It is clear from the above discussion that SERP value alone cannot explain the difference in tumor uptake between 2- and 5-nitroimidazole triazole complexes.

A possible explanation for this observation can be proposed considering the lipophilicity ($\text{LogP}_{\text{o/w}}$) (**Table 4.1**) and blood clearance of the three nitroimidazole triazole complexes (**Table 4.2**). Lipophilicity is important for smooth entry of the complex in tumor cells by passive diffusion. It could also be noted that blood clearance pattern of nitroimidazole complexes (**Table 4.2**) correlated well with their $\text{LogP}_{\text{o/w}}$ values (**Table 4.1**) and 5-nitroimidazole complex having the highest $\text{LogP}_{\text{o/w}}$ value showed the slowest blood clearance. Slow blood clearance provides more time for the radiotracer to

Chapter 4

distribute in tumor by passive diffusion. It also allows the radiotracer to spend more time in tumor cells by maintaining a positive concentration gradient between the blood pool and the tumor tissue, thus facilitating hypoxia specific reduction. We speculate that due to relatively fast blood clearance, the effective distribution and time spent by 2-nitroimidazole complex in tumor may be lower compared to the 5-nitroimidazole counterpart. This could have resulted in lower tumor uptake of the former despite having a better SERP. Blood clearance of 4-nitroimidazole complex was fastest among the three triazole complexes (**Table 4.2**) and combined with the low SERP value, this complex showed the lowest tumor uptake among the three nitroimidazole triazole complexes evaluated.

On the other hand, at 30 min p.i., activity of [^{18}F]FMISO in blood was higher than any other nitroimidazole-triazole complex (**Table 4.2**). This must have facilitated better diffusion ($\text{LogP}_{\text{o/w}}$ of [^{18}F]FMISO - 0.41 [185] and distribution of [^{18}F]FMISO in tumor compared to other nitroimidazole complexes. A careful look at the blood clearance pattern (**Table 4.2**) will reveal that blood clearance of [^{18}F]FMISO was the slowest among the four nitroimidazole radiotracers till 1 h p.i. Consequently, [^{18}F]FMISO could be anticipated to spend more time in tumor cells than any other nitroimidazole-triazole complex. All these favorable factors resulted in higher tumor uptake by [^{18}F]FMISO.

It is worth mentioning here that a metronidazole triazole- $^{99\text{m}}\text{Tc}(\text{CO})_3$ complex, similar to the 5-nitroimidazole-triazole- $^{99\text{m}}\text{Tc}(\text{CO})_3$ complex evaluated herein, has been reported [204]. The difference between the two complexes is in the linker used to couple the nitroimidazole and the triazole moiety. The metronidazole triazole- $^{99\text{m}}\text{Tc}(\text{CO})_3$

Chapter 4

complex, reported earlier, was less lipophilic than the 5-nitroimidazole triazole- ^{99m}Tc $(\text{CO})_3$ complex evaluated in the present study. Its clearance from blood was faster and tumor uptake lower when compared to 5-nitroimidazole triazole- $^{99m}\text{Tc}(\text{CO})_3$ complex (**4I**). This is similar to the observations made in the present study, where complexes with faster blood clearance show lower tumor uptake.

Table 4.3 shows the distribution of nitroimidazole-triazole complexes in other organs at different time points. It could be noted that major clearance of activity of all the complexes is through hepatobiliary route, indicated by presence of significant level of activity in liver and gastrointestinal tract. Activity observed in other vital organs like lung, heart, spleen and kidney gradually cleared with time.

Chapter 4

Table 4.3. Biodistribution of various nitroimidazole triazole- $^{99m}\text{Tc}(\text{CO})_3$ complexes (**4j**, **4k** & **4l**) (%ID/gram) in Swiss mice bearing fibrosarcoma tumor (n=5) at three different time points

Organ	2-nitroimidazole complex			4-nitroimidazole complex			5-nitroimidazole complex		
	30 min	1 h	3 h	30 min	1 h	3 h	30 min	1 h	3 h
Lung	1.55±0.38	0.99±0.04	0.77±0.04	1.18±0.20	0.68±0.10	0.47±0.07	2.09±0.27	1.48±0.19	0.84±0.20
Heart	1.42±0.19	0.84±0.01	0.57±0.01	0.56±0.03	0.41±0.02	0.21±0.03	0.74±0.06	0.65±0.03	0.51±0.02
Intestine	9.32±0.97	10.29±0.89	10.54±2.33	19.64±2.97	21.19±0.80	21.78±1.21	6.42±1.24	9.06±0.26	8.72±0.64
Liver	8.79±0.38	6.81±0.99	5.29±1.15	8.51±0.73	5.68±1.12	3.65±0.40	11.62±1.00	7.96±0.34	6.29±0.41
Spleen	0.70±0.04	0.58±0.13	0.49±0.07	0.66±0.07	0.64±0.12	0.19±0.05	0.58±0.11	1.33±0.13	0.35±0.05
Kidney	4.69±0.52	2.77±0.40	2.35±0.38	2.41±0.23	1.09±0.10	0.87±0.06	8.47±1.12	6.64±0.72	4.67±0.26
Muscle	0.48±0.08	0.37±0.03	0.33±0.03	0.36±0.04	0.18±0.01	0.10±0.01	0.25±0.02	0.37±0.03	0.15±0.01
T/B*	1.48±0.13	1.59±0.35	1.80±0.50	0.87±0.19	1.53±0.15	0.78±0.14	1.06±0.16	1.11±0.13	1.05±0.03
T/M*	2.99±0.50	2.59±0.27	2.33±0.60	1.78±0.43	3.20±0.22	2.56±0.38	8.15±1.42	3.92±0.23	5.39±0.53

*T/B – Tumor to Blood ratio; T/M – Tumor to Muscle ratio

The tumor to blood and tumor to muscle ratio obtained with the three nitroimidazole complexes are also shown in **Table 4.3**. All the three nitroimidazole complexes showed tumor to blood ratio ranging from 1 to 1.8 and tumor to muscle ratio between 2 to 5. Major clearance of all complexes was observed through hepatobiliary route, as is evident from the presence of significant level of activity in liver and intestine.

4.4. Conclusions

The present study reports an unexpected result wherein a 5-nitroimidazole- $^{99m}\text{Tc}(\text{CO})_3$ complex showed better tumor uptake than the 2-nitroimidazole counterpart.

Chapter 4

A possible reason for this observation was attributed to the slower blood clearance of the radiotracer. The study also highlights the necessity of evaluating nitroimidazole complexes other than 2-nitroimidazole in order to exclude the possibility of overlooking potential nitroimidazole radiotracers other than 2-nitroimidazole for hypoxia detecting applications.

SUMMARY

Summary

The work carried out in present thesis describes the preparation of different radiolabeled agents for use as targeted radiotracers in different applications and their preliminary bioevaluation in suitable animal models. Biomolecules which were utilized in the present study include porphyrin derivatives, monoclonal antibodies, peptide and nitroimidazoles. Each of these biomolecules is used for targeting tumor lesions by use of independent and unique mechanism. The aim of this work was to design specific radiotracers for different tumors making use of different carrier molecules as targeted vectors and also to demonstrate their tumor targeting abilities in diagnostic or therapeutic applications. This thesis has been divided into four chapters and the respective contents of each chapter are summarized below.

Chapter one gives a brief overview of radiopharmaceuticals and their usage in nuclear medicine. General methods of production of radioisotopes with their merits and inadequacies for a particular application are described with an emphasis on the generator-produced radioisotopes (^{99m}Tc , ^{68}Ga and ^{90}Y) and reactor produced isotope (^{177}Lu). The various mechanisms which govern the uptake of radiopharmaceuticals in a specific target have been discussed. Radiolabeling methodologies for preparation of ^{99m}Tc -labeled radiotracers and the advantages of using preformed ^{99m}Tc cores/radiosynthons viz. $[\text{}^{99m}\text{TcN}]^{2+}$, $[\text{}^{99m}\text{Tc}(\text{CO})_3]^+$ etc. over the conventionally used method involving the Tc (V) route have been described. For radiolabeling with ^{177}Lu and ^{90}Y the suitability of macrocyclic ligands as BFCA to give stable complexes in high yield has been discussed.

Chapter two describes the use of porphyrins in designing radiolabeled agents for targeting tumor, the mechanisms involved, details of synthesis of different derivatives of

Summary

porphyrin, their radiolabeling with suitable radionuclides (^{68}Ga , ^{177}Lu and ^{90}Y) and preliminary evaluations in suitable animal tumor models. Since the macrocyclic tetrapyrrolic ring of the porphyrin imparts the lipophilicity to the molecule, appropriate modification of the meso and peripheral substituents are made in order to tailor the properties of the molecule with the aim of achieving the desired pharmacokinetic behavior in the *in vivo* distribution studies. Taking three different porphyrin derivatives with variable lipophilicities viz. 5-(*p*-aminopropyleneoxyphenyl)-10,15,20-tris(*p*-carboxymethyleneoxyphenyl) porphyrin (**I**), 5,10,15,20-tetra(*p*-N-methylpyridyl) porphyrin (**II**) and 5-carboxymethyleneoxyphenyl-10, 15, 20-tri(*p*-N-methylpyridyl) porphyrin (**III**) were synthesized. Radiolabeling of compound **I** and **III** was carried out using radiolanthanides viz. ^{177}Lu and ^{90}Y via a macrocyclic bifunctional chelating agent (BFCA) namely, *p*-NCS-benzyl-DOTA (*p*-isothiocyanatobenzyl-1,4,7,10-tetraazacyclododecane-1,4,7,10-tetraacetic acid) as direct radiolabeling in the porphyrin core is not feasible while envisaging the radiolanthanides $^{177}\text{Lu}^{+3}$ and $^{90}\text{Y}^{+3}$ due to the mismatch of the porphyrin core size and that of the ionic radii of these radiometals. The *p*-NCS-benzyl-DOTA conjugate of compound **I** was radiolabeled with ^{90}Y and ^{177}Lu whereas compound **III** was radiolabeled with ^{177}Lu in good radiolabeling yields. Biodistribution studies performed in Swiss mice bearing fibrosarcoma tumors revealed high tumor uptake corresponding to ^{90}Y and ^{177}Lu -labeled compound **I**. The complexes exhibited favorable tumor to blood and tumor to muscle ratios at various post-administration time points. Scintigraphic imaging performed in Swiss mice bearing fibrosarcoma tumors after intravenous administration of ^{177}Lu -labeled-compound **I** also

Summary

corroborated the results obtained in biodistribution studies indicating the selective accumulation of activity in the tumor. Bioevaluation of ^{177}Lu -labeled-compound **III** carried out in the same tumor model revealed only the early accumulation of the radiolabeled agent in the tumor with fast clearance with time. The non target uptake was very low and that too cleared away rapidly with time. This behavior could probably be attributed to a combination of charged substituents and hydrophilic BFCA that led to an increase in the hydrophilicity beyond the optimum level. Radiolabeling of compound **II** was carried out using ^{68}Ga directly in the porphyrin core owing to the suitable ionic radius (62 pm) of ^{68}Ga (III). Tumor targeting potential of the ^{68}Ga labeled compound **II** was evaluated by biodistribution studies in Swiss mice bearing fibrosarcoma tumor. The studies revealed high uptake of the radiotracer in the tumor within 30 min post-injection (6.47 ± 0.87 % of the injected activity) and retention therein till 2 h post-administration (4.48 ± 1.11 % of the injected activity) up to which the study was continued.

In **Chapter three**, targeting receptor over expression in specific tumors, using two different types of molecular vectors such as monoclonal antibodies (mAbs) and RGD peptide is discussed under two sub-headings viz. 3A and 3B.

Section 3A describes the preparation of ^{177}Lu -labeled monoclonal antibodies Rituximab and Trastuzumab and their preclinical evaluation. Rituximab is chimeric mAb having specificity towards CD20 antigen receptors overexpressed in Non-Hodgkins' Lymphoma whereas Trastuzumab is a humanized IgG1 monoclonal antibody and is used in the treatment of breast cancer where the targets on the cancer are HER2 receptors. The procedure used for preparation of radiolabeled mAbs involved three steps. As ^{177}Lu

Summary

cannot be introduced directly in the antibody structure, mAb is first conjugated with a BFCA namely, *p*-NCS-benzyl-DOTA for complexation with ^{177}Lu , second step involves the purification of the antibody-BFCA conjugate and third step is the radiolabeling of the purified antibody-BFCA conjugate with ^{177}Lu . The radiochemical purity (RCP) of the radiolabeled mAbs was evaluated by HPLC indicating the formation of ^{177}Lu -labeled Rituximab and Trastuzumab with radiochemical purities of $> 95\%$. Initial studies for optimizing the method of conjugation and also the radiolabeling parameters were carried out with a readily available mAb namely, immunoglobulin G (IgG) owing to its ready availability and low cost. In subsequent efforts, the radiolabeled mAbs i.e. Rituximab as well as Trastuzumab were prepared and evaluated *in vitro* using cell lines viz. Raji and BT 474 known to over express antigen receptors, CD20 and HER2 respectively. This study indicated the specificity and binding of the radiolabeled mAb conjugates with these antigen receptors.

Section 3B describes the preparation of $^{99\text{m}}\text{TcN}$ -labeled RGD derivative for tumor imaging. Arginine-Glycine-Aspartic acid (RGD) is a tripeptide which shows high specificity towards integrin $\alpha_v\beta_3$ receptors. Integrin $\alpha_v\beta_3$ plays a significant role in tumor angiogenesis and considered to be an important target for molecular imaging as well as *in vivo* targeted therapy using radiolabeled agents. Efficacy of cyclic RGD dimer in targeting more number of integrin $\alpha_v\beta_3$ receptors overexpressed in specific tumors as compared to the corresponding monomer has been reported. Taking this into account, an attempt was made to radiolabel a cyclic RGD monomer with $^{99\text{m}}\text{Tc}$ using $[\text{}^{99\text{m}}\text{TcN}]^{2+}$ core whereby the resultant complex can be envisaged to possess two monomeric units and

Summary

could possibly mimic as dimeric species of RGD. The work outlined in this chapter is preparation of a dimeric $^{99m}\text{TcN}[\text{G}_3\text{-c(RGDfk)}]_2$ complex and its bioevaluation as a potential agent for early detection of malignant tumor by SPECT imaging. The dithiocarbamate derivative of cyclic RGD monomer $\text{G}_3\text{-c(RGDfK)}$ was prepared as two such dithiocarbamate units are required for complexation with $[\text{}^{99m}\text{TcN}]^{2+}$ core of ^{99m}Tc to form the $^{99m}\text{TcN}[\text{G}_3\text{-c(RGDfk)}]_2$ dimeric complex in high yield. A radiochemical purity >95% was obtained. Results of biodistribution studies carried out in C57BL/6 mice bearing melanoma tumors showed good tumor uptake accompanied by favorable tumor/blood and tumor/muscle ratios. Scintigraphic studies in tumor bearing mice were also carried out and visible accumulation of activity in the tumor was observed with appreciable target to background ratio.

Chapter four describes the preparation of neutral $^{99m}\text{Tc}(\text{CO})_3$ -complexes of three nitroimidazole isomers for imaging of tumor hypoxia. Hypoxia is a common feature of most of the solid tumors and has prognostic as well as therapeutic implication due its resistance towards chemotherapy and radiation therapy. Nitroimidazoles, which show selective accumulation in hypoxic cells, are the most widely explored molecules for delineating hypoxic tumor cells from normoxic cells. This ability could be attributed to an interesting mechanism whose initial step involves an enzyme-mediated (nitro-reductase) single electron reduction of nitroimidazole to corresponding radical anion. This reduction step is reversible in normal cells due to presence of sufficient oxygen which oxidizes the radical anion and promotes its clearance out of the cell. On the other hand, in hypoxic cells, nitroimidazole radical anion gets reduced further and corresponding metabolites get

Summary

trapped in such cells. In the present work, three neutral $^{99m}\text{Tc}(\text{CO})_3$ complexes of nitroimidazole were synthesized and their potential to detect hypoxia in tumor was evaluated *in vivo*. The ligands synthesized were characterized and subsequently radiolabeled using $[^{99m}\text{Tc}(\text{CO})_3(\text{H}_2\text{O})_3]^+$ precursor complex to obtain corresponding neutral $^{99m}\text{Tc}(\text{CO})_3$ complexes. All the complexes could be prepared in >90% radiochemical purity (RCP). The complexes were subsequently evaluated in Swiss mice bearing fibrosarcoma tumor. Biodistribution studies showed uptake and retention of all the complexes in tumor with 5-nitroimidazole complex showing relatively better tumor uptake than the 2-nitroimidazole and 4-nitroimidazole counterparts. A notable observation in the present study was the atypical tumor uptake of a 5-nitroimidazole complex. Though a conclusive inference could not be provided in support of this observation, the importance of evaluating nitroimidazole radiotracers other than the 2-nitroimidazole for detecting tissue hypoxia was evidenced.

From the work carried out in this thesis, the following insights are obtained which provide guidelines for carrying out future studies:

Of the different molecules used in the present study to design radiotracers for specific accumulation in tumors, porphyrins are found to exhibit significant tumor localization. In this respect, ^{177}Lu -labeled porphyrins showing high uptake as well as long retention in tumor can be further studied in evaluation of tumor regression.

The potential of radiolabeled cationic porphyrins show considerable promise as radiotracers for intercalation in double stranded DNA. This concept can be extrapolated

Summary

in studying their efficacy in tumor DNA both with respect to imaging as well as therapeutic application. The study using nitroimidazole-based radiotracers indicate that an optimum hypoxia detecting agent should distribute quickly throughout the tumor mass, exhibit optimum residence therein for undergoing hypoxia specific reduction, and subsequently clear from blood and other non-target organs such that an image with acceptable level of contrast between the target and non-target tissue could be achieved. These parameters can be achieved by trials. However, a logical starting point towards this is to aim at mimicking the blood clearance pattern of [^{18}F]FMISO, by appropriate modification of the lipophilicity and charge of the radiotracer. The results obtained in the present study employing clicked-nitroimidazoles in preparation of $^{99\text{m}}\text{Tc}(\text{CO})_3$ -labeled radiotracers could provide insights for further modifications to envisage an optimum radiotracer for diagnostic applications for tumor hypoxia.

The preclinical optimization studies in the development of ^{177}Lu -labeled Rituximab and Trastuzumab as potential radiopharmaceuticals in Radio-immuno-targeting of specific cancers, will be utilized in arriving at a freeze-dried kit formulation for radiolabeling with ^{177}Lu in the hospital radiopharmacy prior to injection in cancer patients.

References

References

1. Jurisson S, Berning D, Jia W, Ma D. *Chem Rev*, **1993**, 93, 1137-1156.
2. Berman DS, Kiat HS, Van Train KF, Germano G, Maddahi J, Friedman JD. *J Nucl Med*, **1994**, 35, 681-688.
3. Taylor AT. *J Nucl Med*, **2014**, 55, 1–8.
4. Saha GB, MacIntyre WJ, Go RT. *Seminars in Nuclear Medicine*, **1994**, 24, 324–34.
5. Firestone R. *John Wiley and Sons Inc*, **1996**, 8th edition.
6. Lauridsen B. *Riso National Laboratory, Roskilde, Denmark*, **1982**.
7. Urruticoechea A, Alemany R, Balart J, Villanueva A, Viñals F, Capellá G. *Current Pharmaceutical Design*, **2010**, 16, 3-10.
8. Phelps ME. *J Nucl Med*, **2000**, 41, 661-681.
9. *IAEA-TECDOC*, **2008**, 1597, 1.
10. https://en.wikipedia.org/wiki/Molecular_imaging.
11. Casey ME, Nutt R. *IEEE Trans Nucl Sci*, **1986**, NS33, 460-463.
12. Rahmima A, Zaidib H. *Nucl Med Commun*, **2008**, 29,193-207.
13. Liu S, Edwards DS. *Chem Rev*, **1999**, 2235-2268.
14. Loberg MD, Corder EH, Fields AT, Callery PS. *J Nucl Med*, **1979**, 20, 1181-1188.
15. Chen L, Li F, Zhuang H. et al. *J Nucl Med*, 2009, 5, 397-400.
16. A. Kurtaran. *Nuclear oncology*, Springer-Verlag, New York, **1999**, 333-343.
17. Duatti A. *Nucleus N°*, **2012**, 52, 41-49
18. Alberto R, Ortner K, Wheatly N, Schibli R, Schubiger AP. *J Am Chem Soc*, **2001**, 123, 3135.

References

19. Alberto R, Pak JK, van Staveren D, et al. *Biopolymers*, **2004**, 76, 324-333.
20. Zoller F, Riss PJ, Montforts FP, et al. *Nucl Med Biol*, **2013**, 40, 280-288.
21. Velikyan I. *Theranostics*, **2014**, 4, 47-80.
22. Shetty D, Lee YS, Jeong JM. *Nucl Med Mol Imaging*, **2010**, 44 233-240.
23. Fazaeli Y, Jalilian AR, Amini MM, et al. *Nucl Med Mol Imaging*, **2012**, 46, 20-26.
24. Huang HJ, Lo JM. *Tamkang Journal of Science and Engineering*, **2003**, 6, 19-30.
25. Wadas TJ, Wong EH, Weisman GR, Anderson CJ. *Chem Rev*, **2010**, 110, 2858–2902.
26. Vallabhajosula S1, Kuji I, Hamacher KA, Konishi S, Kostakoglu L, Kothari PA, Milowski MI, Nanus DM, Bander NH, Goldsmith SJ. *J Nucl Med*, **2005**, 46, 634-641.
27. Chakravarty R, Pandeya U, Manolkara RB, Dasha A, Venkatesha M, Pillai MRA. *Nucl Med Biol*, **2008**, 35, 245–253.
28. Shuang Liu. *Adv Drug Deliv Rev*, **2008**, 60, 1347-1370.
29. Das T, Chakraborty S, Sarma HD, Banerjee S, Venakatesh M. *Nucl Med Biol*, **2010**, 37, 655–663.
30. Liu S, Edwards DS. *Bioconjug Chem*, **2001**, 12, 7–34.
31. Byegard J, Scarnemark G, SKalberg M. *J Radioanal Nucl Chem*, **1999**, 241, 281-290.
32. G.B. Saha. *Fundamentals of nuclear pharmacy. 3rd edition, Springer-Verlag, New York*, **2000**, 143-167.
33. Briner WI. *Radioactive pharmaceuticals, US AEC, Symposium Series, Oak-Ridge, Tennessee, USA*, **1965**, 93-111.
34. Bhelose AA, Mehra KS, Raju A *Radiopharmaceuticals and hospital radiopharmacy practices. Department of Atomic Energy, Government of India, Mumbai*, **2000**, 72-82.

References

35. Pauwels EKJ, Feitsma RIJ. *Eur J Nucl Med*, **1977**, 2, 97-102.
36. Troutner DE, Volkert WA, Hoffman TJ, et al. *Int J Appl Radiat Isot*, **1984**, 35, 467-470.
37. Král V, Králová J, Kaplánek R, et al. *Physiol Res*, **2006**, 55, S3-S26.
38. Ormond AB, Freeman HS. *Materials*, **2013**, 6, 817-840.
39. Policard A. *C R Soc Biol*, **1924**, 91, 14-32.
40. Shirasu N, Nam SO, Kuroki M. *Anticancer Research*, **2013**, 33, 2823-2832.
41. Huang Z. *Technol Cancer Res Treat*, **2005**, 4, 283-293.
42. Vedachalam S, Choi BH, Pasunooti KK, et al. *Med Chem Commun*, **2011**, 2, 371-377.
43. Sarma HD, Das T, Banerjee S, et al. *Cancer Biother Radiopharm*, **2010**, 25, 47-54.
44. Banerjee S, Das T, Samuel G, et al. *Nucl Med Commun*, **2001**, 22, 1101-1107.
45. Mittal S, Bhadwal M, Das T, et al. *Cancer Biother Radiopharm*, **2013**, 28, 651-656.
46. Bhadwal M, Das T, Sarma HD, et al. *Mol Imag Boil*, **2014**, 17, 111-118.
47. Gelfusoa GM, Gratieria T, Souzaa JG, et al. *Eur J Pharm Biopharm*, **2011**, 77, 249–256.
48. Kral V, Kralova J. *Physiol Res*, **2006**, 55, S3-S26.
49. Aviezer D, Cotton S, David M, et al. *Cancer Res*, **2000**, 60, 2973-2980.
50. Volkert WA, Goeckeler WF, Ehrhardt GJ, et al. *J Nucl Med*, **1991**, 32, 174–185.
51. Volkert WA, Hoffman TJ. *Chem Rev*, **1999**, 99, 2269–2292.
52. Srivastava SC, Dadachova E. *Semin Nucl Med*, **2001**, 31, 330–341.
53. Jhu H, Jain RK, Baxter LT. *J Nucl Med*, **1998**, 39, 65–76.
54. Meredith RF, Partridge EE, Alvarez RD. *J Nucl Med*, **1996**, 37, 1491–1496.

References

55. Wessels BW, Rogus RD. *Med Phys*, **1984**, 11, 638–645.
56. Fritzberg AR, Gustavson LM, Hylarides MD. *CRC Press, Boca Raton. FL*, **1995**, 125.
57. Hamblin MR, Newman EL. *J Photochem Photobiol B: Biol*, **1994**, 23, 3-8.
58. Moan J, Berg K. *Photochem Photobiol*, **1992**, 55, 931-948.
59. Gianferrara T, Bergamo A, Bratos I, et al. *J Med Chem*, **2010**, 53, 4678-4690.
60. Vicente MGH. *Curr Med Chem Anticancer Agents*, **2001**, 1, 175-194.
61. Zhiyun J, Houfu D, Manfei P. *Nucl Med Biol*, **2007**, 34, 643–649.
62. Winkelman J, Slater G, Grossman J. *Cancer Res*, **1967**, 27, 2060-2064.
63. Murugesan S, Shetty SJ, Srivastava TS, et al. *J Porphyr Phthalocyanines*, **2001**, 5, 824-828.
64. Chatterjee SR, Murugesan S, Kamat JP, et al. *Arch Biochem Biophys*, **1997**, 339, 242-249.
65. Riccheli F. *J Photochem Photobiol B: Biol*, **1995**, 29, 109.
66. Banfi S, Caruso E, Caprioli S, et al. *Bioorg Med Chem*, **2004**, 12, 4853-4860.
67. Samaroo D, Vinodu M, Chen X, et al. *J Comb Chem*, **2007**, 9, 998-1011.
68. Rusin O, Hub M, Kral V. *Mater Sci Eng C*, **2001**, 18, 135–140.
69. Sibrian-Vazquez M, Jensen TJ, Vicente MG. *J Photochem Photobiol B*, **2007**, 86, 9–21.
70. Shetty SJ, Murugesan S, Chatterjee SR, et al. *J label compds radiopham*, **1996**, 38, 411–418.
71. Das T, Chakraborty S, Sarma HD et al. *Radiochim Acta*, **2008**, 96, 427–433.
72. Marion de Jon. *J Nucl Med*, **2005**, 46, 13S-17S.

References

73. Pillai MRA, Chakraborty S, Das T, et al. *Appl Radiat Isot*, **2003**, 59, 109–118.
74. Firestone R. *8th edition New York: John Wiley and Sons*; 1996.
75. Gonsalves AMdR, Varejso JMTB, Pereira MMOL. *J Het Chem*, **1991**, 28, 635-640.
76. Baell JB, Duggan PJ, Forsyth SA, et al. *Bioorg Med Chem*, **2004**, 12, 4025–4037.
77. Kulkarni HR, Baum RP. *J Postgraduate Med*, **2013**, 47, 47-53.
78. Lazzeri D, Durantini EN. *ARKIVOC*, **2003**, 10, 227-239.
79. Driaf K, Granet R, Krausz P, et al. *Can J Chem*, **1996**, 74, 1550-1563.
80. Biron E, Voyer N. *Chem Comm*, **2005**, 37, 4652-4654.
81. Br̃iza T, Kralova J, Kigler P, et al. *Bioorg Med Chem Lett*, **2012**, 22, 82-84.
82. Schwach G, Thamyongkit P, Reith LM, et al. *Bioorg Chem*, **2012**, 40, 108-113.
83. Gantchev TG, Ali H, van Lier JE. *Eur J Biochem*, **1993**, 217, 371-376.
84. Izbicka E, Wheelhouse RT, Raymond E, et al. *Cancer Res*, **1999**, 59, 639-644.
85. Sehlstedt U, Kim SK, Carter P, et al. *Biochemistry*, **1994**, 33, 417-426.
86. Sari MA, Battioni JP, Dupre D, et al. *Biochemistry*, **1990**, 29, 4205-4215.
87. Mironov AF. *Russ Chem Rev*, **2013**, 82, 333-351.
88. Alder A, Longo FR, Finarelli JO, et al. *J Org Chem*, 1967, 132, 476.
89. <http://en.wikipedia.org/wiki/antibody>
90. <http://pathmicro.med.sc.edu/mayer/igstruct2000.html>
91. Wang S. *Antibody Technology Journal*, **2011**, 1, 1–4.
92. Strebhardt K, Ullrich A. *Nat Rev Cancer*, **2008**, 8, 473-480.
93. Koehler G, Milstein C. *Nature*, **1975**, 256, 495-497.
94. Schlom, J. *Cancer Res*, **1986**, 46, 3225-3238.

References

95. Goldenberg DM. *CRC Press: Boca Raton, Florida*, **1995**.
96. Hauptrock B, Hess G. *Biologics: Targets & Therapy*, **2008**, 2, 619–633.
97. Forrer F, Chen J, Fani M et al. *Eur J Nucl Med Mol Imaging*, **2009**, 36, 1443–1452.
98. Forrer F, Oechsli-Oberholzer C, Campana B, et al. *J Nucl Med*, **2013**, 54, 1045–1052.
99. Audicio PF, Castellano G, Tassano MR, et al. *Appl Radiat Isotopes*, **2011**, 69, 924–928.
100. Banerjee S, Pillai MRA, Knapp FF. *Chem Rev*, **2015**, 115, 2934–2974.
101. Meares CF, McCall MJ, Reardan, DT. *Anal Biochem*, **1984**, 142, 68–78.
102. Dadachova E, Chappell LL, Brechbiel MW. *Nucl Med Biol*, **1999**, 26, 977–982.
103. Geoffrey LR, Baidoo KE, Keller LMM, et al. *Pharmaceuticals*, **2012**, 5, 1–15.
104. Rasaneha S., Hossein Rajabia H., Babaeib M. H., Dahab F. J. *Nucl Med Biol*, **2010**, 37, 949–955.
105. Bradford MM. *Anal Bio Chem*, **1976**, 72, 248–254.
106. Fani M, Maecke HR, Okarvi SM. *Theranostics*, **2012**, 2, 481–501.
107. Rufini V, Calcagni ML, Baum RP. *Semin Nucl Med*, **2006**, 36, 228–247.
108. Ambrosini V, Fani M, Fanti S, et al. *J Nucl Med*, **2011**, 52, 42S–55S.
109. Kaltsas GA, Papadogias D, Makras P, et al. *Endocr Relat Cancer*, **2005**, 12, 683–699.
110. Bodei L, Paganelli G, Mariani G. *J Nucl Med*, **2006**, 47, 375–377.
111. Lozza C, Navarro-Teulon I, Pèlegri A, et al. *Front Oncol*, 2013, 247.
112. Folkman J. *Nat Med*, **1995**, 1, 27–31.
113. Mousa SA. *Drugs Future*, **1998**, 23, 51–60.

References

114. Mousa SA. *Emerging Ther Targets*, **2000**, 4, 143-153.
115. Carmeliet, P. *Nat Med*, **2000**, 6, 389-395.
116. BÖgler O, Mikkelsen T. *Cancer J*, **2003**, 9, 205-213.
117. Folkman J. *Semin Oncol*, **2002**, 29, 15-18.
118. Hwang R, Varner JV. *Hematol Oncol Clin North Am*, **2004**, 18, 991-1006.
119. Van der Flier A, Sonnenberg A. *Cell and Tissue Research*, **2001**, 305, 285.
120. Jin H, Varner J. *Br J Cancer*, **2004**, 90, 561-565.
121. Kumar C. *Curr Drug Targets*, **2003**, 4, 123-131.
122. Brooks PC, Clark RAF, Cheresch DA. *Science*, **1994**, 264, 569-571.
123. Ruoslahti E, Pierschbacher MD. *Science*, **1987**, 238, 491-497.
124. Harris TD, Cheesman E, Harris AR et al. *Bioconjug Chem*, **2007**, 18, 1266-1279.
125. Chen X, Park R, Shahinian AH, et al. *Nucl Med Biol*, **2004**, 31, 179.
126. Meitar D, Crawford SE Rademaker AW, et al. *J Clin Oncol*, **1996**, 14, 405-414.
127. Gasparini G, Brooks PC, Biganzoli E, et al. *Clin Cancer Res*, **1998**, 4, 2625-2634.
128. Albelda SM, Mette SA, Elder DE, et al. *Cancer Res*, **1990**, 50, 6757-6764.
129. Falcioni R, Cimino L, Gentilsechi MP, et al. *Exp Cell Res*, **1994**, 210, 113-122.
130. Sengupta S, Chattopahyay N, Mitra A, et al. *J Exp Clin Cancer Res*, **2001**, 20, 585-590.
131. Felding-Habermann B, Mueller BM, Romerdahl CA, et al. *J Clin Invest*, **1992**, 89, 2018-2022.
132. Zitzmann S, Ehemann V, Schwab M. *Cancer Res*, **2002**, 62, 5139-5143.
133. Weber WA, Haubner R, Vabulienė E, et al. *Q J Nucl Med*, **2001**, 45, 179-182.

References

134. Costouros NG, Diehn FE, Libutti SK. *J Cell Biol*, **2002**, 39, 72-78.
135. van de Wiele C, Oltenfreiter R, De Winter O, et al. *Eur J Nucl Med*, **2002**, 29, 699-709.
136. Liu S, Robinson SP, Edwards DS. *Drugs Future*, **2003**, 28, 551-564.
137. Liu S, Robinson SP, Edwards DS. *Top Curr Chem*, **2005**, 252, 117-153.
138. Haubner R, Wester HR. *Curr Pharm Des*, **2004**, 10, 1439-1455.
139. Van Hagen PM, Breeman WAP, Bernard HF, et al. *Int J Cancer Radiat Oncol Invest* **2000**, 90, 186-198.
140. Sivolapenko GB, Skarlos D, Pectasides D, et al. *Eur J Nucl Med*, **1998**, 25, 1383-1389.
141. Haubner R, Wester HJ, Senekowitsch-Schmidtke R, et al. *J Label Compd Radiopharm*, **1997**, 40, 383-385.
142. Haubner R, Wester HJ, Reuning U, et al. *J Nucl Med*, **1999**, 40, 1061-1071.
143. Haubner R, Wester HJ, Weber WA, et al. *Cancer Res*, **2001**, 61, 1781-1785.
144. Haubner R, Wester HJ, Burkhart F, et al. *J Nucl Med*, **2001**, 42, 326-336.
145. Thumshirn G, Hersel U, Goodman SL, et al. *Chem Eur J*, **2003**, 9, 2717-2725.
146. Poethko T, Schottelius M, Thumshirn G, et al. *J Nucl Med*, **2004**, 45, 892-902.
147. Haubner R, Kuhnast B, Mang C, et al. *Bioconj Chem*, **2004**, 15, 61-69.
148. Alves S, Correia JDG, Gano L, et al. *Bioconj Chem*, **2007**, 18, 530-537.
149. Wang JJ, Kim YS, He ZJ, et al. *Bioconj Chem*, **2008**, 19, 634-642.
150. Liu S, Hsieh WY, Jiang Y, et al. *Bioconj Chem*, **2007**, 18, 438-446.
151. Morrison MS, Ricketts SA, Barnett J, et al. *J Nucl Med*, **2009**, 50, 116-122.

References

152. Kenny LM, Coombes RC, Oulie I. *J Nucl Med*, **2008**, 49, 879-886.
153. Beer AJ, Haubner R, Goebel M, et al. *J Nucl Med*, **2005**, 46, 1333-1341.
154. Haubner R, Weber WA, Beer AJ, et al. *PLoS Med*, **2005**, 2, e70.
155. Beer AJ, Grosu AL, Carlsen J, et al. *Clin Cancer Res*, **2007**, 13, 6610-6616.
156. Beer AJ, Niemeyer M, Carlsen J, et al. *J Nucl Med*, **2008**, 49, 255-259.
157. Mammen M, Choi SK, Whitesides GM. *Angew Chem Int Ed Engl*, **1998**, 37, 2755-2794.
158. Chen, XY, Liu S, Hou Y, et al. *Mol Imaging Biol*, **2004**, 6, 350-359.
159. Jansen, ML, Oyen WJG, Dijkgraaf I, et al. *Cancer Res*, **2002**, 62, 6146-6151.
160. Shi J, Wang L, Kim YS, et al. *J Med Chem*, **2008**, 51, 7980–7990.
161. Wang L, Kim YS, Shi J, et al. *Mol Pharm*, **2009**, 6, 231–245.
162. Shi J, Wang L, Kim YS, et al. *Bioconj Chem*, **2009**, 20, 750–759
163. Zhang S, Zhang W, Wang Y, et al. *Bioconjugate Chem*, **2011**, 22, 369–37.
164. Zhang J, Lin Y, Sheng X, et al. *Appl Radiat Isotopes*, 2009, 67, 79-82.
165. Mathur A, Mallia MB, Subramanian S, et al. *J Labelled Comp Radiopharm*, **2006**, 49, 1053-1060.
166. Mathur A, Mallia MB, Subramanian S, et al. *Appl Radiat Isotopes*, **2006**, 64, 3, 663-667.
167. Pasqualini R, Duatti A, Bellande E, et al. *J Nucl Med*, **1994**, 35, 334–341.
168. Zhang J, Wang X, Li CY. *Appl Radiat Isot*, **2002**, 56, 857–861.
169. Baldas, J, Bonnyman J, Pojer PM, et al. *J Chem Soc Dalton Trans*, **1981**, 1798–1801.
170. Hockel M, Vaupel P. *J Natl Cancer Inst*, **2001**, 93, 266.

References

171. Weibe LI, Machulla HJ. *Imaging Hypoxia*, Kluwer Academic Publishers, Netherlands, **1999**, 1.
172. Gilles Mees G, Dierckx R, Vangeste C, et al. *Eur J Nucl Med Mol Imaging*, **2009** 36, 1674–1686.
173. Splith K, Bergmann R, Pietzsch J, et al. *ChemMedChem*, **2012**, 7, 57–61.
174. Mees G, Dierckx R, Vangestel C, et al. *Eur J Nucl Med Mol Imaging*, **2009**, 36, 1674-1686.
175. Gray LH, Conger AD, Ebert MB. *J Radiol*, **1953**, 26, 638-648.
176. Höckel M, Schlenger K, Aral B, et al. *Cancer Res*, **1996**, 56, 4509-4515.
177. Fyles AW, Milosevic M, Wong R, et al. *Radiother Oncol*, **1998**, 48, 149-156.
178. Nordsmark M, Overgaard M, Overgaard J. *J Radiother Oncol*, **1996**, 41, 31-39.
179. Brizel DM, Sibley GS, Prosnitz LR, et al. *J Radiat Oncol Biol Phys*, **1997**, 38, 285-289
180. Nordsmark M, Bentzen SM, Rudat V. *J Radiother Oncol*, **2005**, 77, 18-24.
181. Duffy JP, Eibl G, Reber HA, et al. *J Mol Cancer*, **2003**, 2, 12.
182. Brizel DM, Scully SP, Harrelson JM, et al. *Cancer Res*, **1996**, 56, 941-943.
183. Vaupel P, Harrison L. *The Oncologist*, **2004**, 9(suppl 5), 4-9.
184. <http://www.hbni.ac.in/phdthesis/chem/CHEM01200604036.pdf>
185. Krohn KA, Link JM, Mason RP Molecular imaging of hypoxia. *J Nucl Med*, **2008**, 2, 129S-148S.
186. Nunn A, Linder K, Strauss HW, *Eur J Nucl Med*, **1995**, 22, 265-280.
187. Fujibayashi Y, Taniuchi H, Yonekura Y, et al. *J Nucl Med*, **1997**, 38, 1155-1160.

References

188. Dearling JLD, Lewis JS, Mullen GED, et al. *Eur J Nucl Med*, **1998**, 25, 788-792.
189. Honess DJ, Hill SA, Collingridge DR, et al. *J Int J Radiat Oncol Biol Phys*, **1998**, 42,731-735.
190. Sorger D, Patt M, Kumar P, et al. *Nucl Med Biol*, **2003**, 30, 17-26.
191. Komar G, Seppänen M, Eskola O, et al. *J Nucl Med*, **2008**, 49, 1944-1951.
192. Rasey JS, Hofstrand PD, Chin LK, et al. *J Nucl Med*, **1999**, 40, 1072-1079.
193. Lewis JS, McCarthy DW, McCarthy TJ, et al. *J Nucl Med*, **1999**, 40, 177-183.
194. Bonnitcho PD, Bayly SR, Theobald MB, et al. *J Inorg Biochem*, **2010**, 104, 126-135.
195. Grunbaum Z, Freauuff SJ, Krohn KA, et al. *J Nucl Med*, **1987**, 28, 68-75.
196. Evans SM, Kachur AV, Shiue CY, et al. *J Nucl Med*, **2000**, 41, 327-336.
197. Zha Z, Zhu L, Liu Y, et al. *Nucl Med Biol*, **2011**, 38, 501-508.
198. Tatum JL, Kelloff GJ, Gillies RJ, et al. *Int J Radiat Biol*, **2006**, 82, 699-757.
199. Ballinger JR. *Semin Nucl Med*, **2001**, 31:321-329.
200. Mallia MB, Subramanian S, Mathur A, et al. *J Label Compd Radiopharm*, **2010**, 53, 535-542.
201. Mallia MB, Kumar C, Mathur A, et al. *Nucl Med Biol*, **2012**, 39, 1236-1242.
202. Mallia MB, Subramanian S, Mathur A, et al. *Bioorg Med Chem Lett*, **2008**, 18, 5233-5237.
203. Mallia MB, Subramanian S, Mathur A, et al. *Nuc Med Biol*, **2014**, 41, 600-610.
204. Fernández S, Giglio J, Rey AM, et al. *Bioorg Med Chem*, **2012**, 20, 4040-4048.
205. Giglio J, Dematteis S, Fernández S, et al. *J Label Compd Radiopharm*, **2014**, 57, 403-409.

References

206. Lee ST, Scott AM. *Semin Nucl Med*, **2007**, 37, 451-461.
207. Hoebers FJP, Janssen HLK, Olmos RAV, et al. *Eur J Nucl Med Mol Imaging* **2002**, 29, 1206-1211.
208. Mallia MB, Subramanian S, Mathur A, et al. *J Label Compd Radiopharm*, **2008**, 51, 308-313.
209. Chapman, JD, Franko AJ, Sharplin J. *Brit J Cancer*, **1981**, 43, 546-550.
210. Piert M, Machulla HJ, Picchio M, et al. *J Nucl Med*, **2005**, 46, 106-113.
211. Yang D J, Wallace S, Cherif A, et al. *Radiology*, **1995**, 194, 795-800.
212. Melo T, Duncan J, Ballinger JR, et al. *J Nucl Med*, **2000**, 41, 169-176.
213. Alberto R, Schibli R, Egli A, et al. *J Am Chem Soc*, **1998**, 120, 7987-7988.
214. Alberto R, Schibli R, Schubiger PA. *Polyhedron*, **1996**, 15, 1079-1089.
215. Alberto R, Egli A, Abram U et al. *J Chem Soc Dalton Trans*, **1994**, 1, 2815–2820.
216. Adams MF, Dorie MJ, Brown JM. *Int J Radiat Oncol Biol Phys*, **1999**, 45, 171-180.
217. Wardman P. *J Phys Chem*, **1989**, 18, 1637-1755.
218. Adams GE, Cooke MS. *Int J Radiat Biol Relat Stud Phys Chem Med*, **1969**, 15, 457–471.